CHAPTER 6

Linear Stability of Combustor Dynamics

All problems of unsteady motion in combustion systems can be divided into the two classes: linearized and nonlinear. From the earliest discoveries of their transient behavior until the late 1950s, 'combustion instabilities' implied small amplitude unsteady (and unwanted) motions growing out of a condition of linear instability. Even with the expanding awareness that the nonlinear properties must be understood as well, linear behavior always remained an essential part of understanding all aspects of combustion instabilities, including the consequences of nonlinear processes.

The literature of linear combustion instabilities contains many papers dealing with special problems. There seems often to be a tendency to regard the results as somehow disconnected. However, apparent differences arise chiefly from the differences in the processes accounted for and in the choices of models for those processes. So long as the problems are dominated by oscillating behavior in combustors, probably most, if not practically all, of the results can be obtained in equivalent forms by suitable applications of the methods explained here. That statement is not as outrageous as it may seem, following as it does from the generality of the expansion procedures and the method of averaging covered in Chapter 4.

6.1. Historical Background of Linear Stability [1]

Among the earliest interpretations of combustion instabilities was the idea of unstable disturbances having small amplitude. That idea lies behind the characterization of small oscillations and is commonly assumed to explain the initial stage, and hence the origin, of an oscillation in a combustion chamber. In fact it is a widely observed motion in solid rockets, but the cases in other systems are often not so clearly defined. The latter are often regarded as 'nonlinear' in some sense. Of the wide range of possible behavior, linear motions are most easily and rigorously described, and form the context within which the greater part of understanding combustion instabilities has been developed. We will examine some important aspects of nonlinear behavior in Chapter 7.

Although there were earlier considerations of oscillations in solid propellant rockets, the first analysis of a combustion instability seems to be that worked out by Grad (1949). At the suggestion of E.W. Price (private communication), Grad considered the problem of unsteady motions in a solid propellant rocket. Although he did not ignore the average flow entirely, he managed to avoid treating the details of the velocity field within the chamber away from the burning surface. He used an approximation to the mean flow based on a separate analysis. Eventually Grad worked out simple formulas for perturbations of the wavenumber. However, the calculations are difficult to follow and, so far as this writer knows, the results have never been checked against observations. A natural result of the analysis is that high frequency oscillations are possible. Grad closed his paper with the footnote that "high frequency oscillations have actually been observed recently in experiments performed at Inyokern, California." That place was the Naval Ordnance Test Station (NOTS) which became the Naval Weapons Center (NWC) and is now the Naval Air Warfare Center (NAWC). Researchers at China

[1] A more thorough account of early developments of linear stability is given in Chapter 2.

Lake have had remarkable influence on the fields of steady and unsteady combustion of solid propellants continuously since the beginnings during World War II.

Grad's analysis and interpretation of his results were largely ignored, perhaps because combustion instabilities in such a well-developed form did not constitute a pressing problem and because accurate data were lacking. Moreover, when troublesome instabilities were encountered in solid rockets, they were eliminated or reduced by making changes in the system.[2] The situation changed markedly in the late 1950s. Apparently the development of large motors was the main stimulus. The need to develop theoretical, computational, and experimental methods then became clear. In the U.S. a very substantial effort grew, widespread but well-coordinated. A particularly important outgrowth of the coordination was the organization that in 1963 became JANAF and subsequently the JANNAF (Joint Army/Navy/NASA/Air Force) Sub-Committee. Apparently the initial efforts in JANAF were largely exerted by the solid rocket community, which we will tend to first here.

In the period covering the late 1950s to the middle 1960s, the special *ad hoc* group, "The Technical Panel on Solid Propellant Instability of Combustion", accomplished much in urging and coordinating research on instabilities in solid rockets. A useful collection of papers "Scientific Papers 1960–1963" produced by the panel gives a quite complete coverage of work by the group which included participants from Canada and Europe. The titles of the papers correctly suggest that they truly covered the field and set the agenda for much of the research carried out in the following decades.

The dominant group in theoretical developments during this period was that at the Johns Hopkins Applied Physics (JHU) Laboratory, mainly McClure, Hart, Bird and Cantrell. Although they treated unsteady erosive burning (McClure, Bird and Hart 1960b and McClure, Hart and Bird 1962), their results were not extensive; the subject has still not advanced very far. That is practically the only nonlinear subject that they treated deeply enough to obtain results, limited though they were. Thus, almost all the theoretical work dealt with linear stability. One of their most important accomplishments—which may not seem so impressive now—was to gain universal recognition of the admittance function of a burning surface as possibly the most important quantity to know accurately as an essential part of the basis for determining the stability of a motor. That is a consequence of the thorough fashion in which the JHU group formulated the general problem. In fact, that approach to the overall problem had considerable impact on the development of the theoretical aspects as well as on the general understanding of the field.

A large boost was given activity in the field of instabilities in solid propellant rockets. when a problem arose with the ballistic missile Minuteman II, an instability in the third stage (see Section 1.3). From its first use in the late 1950s (Price and Sofferis 1958) the T-burner had become generally accepted as the test device for giving data on the admittance or response function for a burning surface. The Minuteman problem led to a great deal of effort based on the device in the late 1960s and in the 1970s. Many important research programs devoted to the T-burner and to other subjects were sponsored by the Air Force Rocket Propulsion Laboratory (AFRPL).[3] Simultaneously, work on all aspects of instabilities in solid rockets was actively pursued at the Naval Weapons Center, China Lake. It was during this period that work was begun to develop 'standard stability prediction' programs.

[2]E.W. Price (1992) has given the best historical account of oscillatory combustion in solid propellant rockets in the U.S. from the beginning (c. 1948) to 1991. Apparently no comparable document exists for experiences in other countries although there are scattered brief descriptions.

[3]The author is particularly indebted to AFRPL for supporting programs under which the method of nonlinear analysis described in this book was largely developed. Much of the work, especially in the early stages, was accomplished at Hercules, Inc. where the author served as consultant to a group headed by Dr. Merrill Beckstead. The methods were initiated largely under the sponsorship of the Air Force and the Navy, especially with the encouragement and support of E.W. Price.

The growth of understanding and theory of instabilities in liquid propellant rockets followed a path virtually independent of the work on solid propellant rockets in the U.S.[4] After the early experimental work reported by Gunder and Friant (1950), discussed also by Yachter (1950), and by Summerfield (1950) who first used a time lag following the suggestion of von Karman, Crocco (1951)a, b developed the idea of the time lag for low-frequency oscillations. 'Low' means here that the propagation of disturbances within the chamber was ignored. Higher frequency instabilities, those which are close to normal acoustic modes of the chamber being studied, were then investigated by Crocco and Cheng (1956). They treated only one-dimensional motions in that work.

In his second paper referenced above, Crocco (1951)b essentially formulated the problem subsequently analyzed at great length by the Princeton group, the last published paper on the subject apparently being that by Zinn (1968). Figure 6.1 is a sketch of the situation. During the nearly two decades of work, the method of analyzing the unsteady flow field changed considerably but the prescription of the unsteady injection processes remained virtually unaltered, taking only two or three different forms. Because the injection of mass is restricted to the planar interface at the head end, the 'injector plane', the influx of material imposes a boundary condition on the flow of gases within the chamber. That condition is quite simply related to the velocity or mass flux which, following Crocco, is expressed in terms of the time lag. The reasoning has been summarized in Section 2.3.2, leading to a formula (2.88) for the source of mass w_ℓ containing two unknown quantities, the time lag τ and the 'pressure index' n:

$$w_\ell = \bar{w}_\ell \left(1 - \frac{d\tau}{dt}\right) \tag{6.1}$$

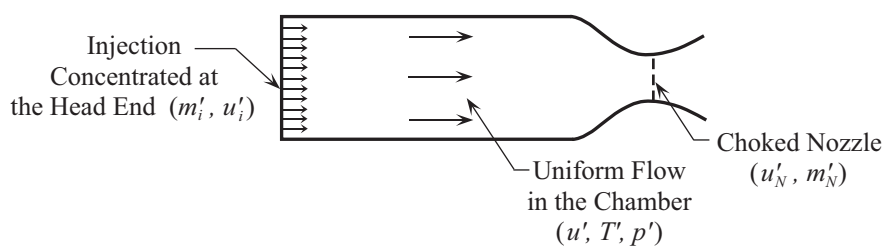

FIGURE 6.1. Basic physical model of a liquid rocket used in the Princeton theoretical work (1950–1968).

As explained in Section 2.3.2, this formula is used for the fluctuation of the mass source in the equation for conservation of mass. When the equations are linearized and written in terms of complex quantities, the real and imaginary parts of the equations effectively serve as two formal conditions determining n and τ as functions of the other variables in the problem.

The first extended theoretical account of linearized combustion instabilities was given in the book by Crocco and Cheng (1956) partly covered in previous papers by the authors. For the most part, the work is really a lengthy discussion and analysis of the linearized formulation of the situation sketched in Figure 6.1. Because the governing equations are not spatially averaged, for simplicity only one-dimensional problems are treated. The text contains an informative extended discussion of the time lag formulation and its linearized form. Appendix B of the book is a calculation of the admittance for a choked nozzle, an elaboration of the works by Tsien (1952) and Crocco (1953).

[4] I have been unable to locate any survey reports from the USSR during this or earlier times. See Natanzon (1999) for brief mention of early work on instabilities in the Soviet Union, and for a good summary of the principal Russian work available, including nonlinear analysis and experimental work. The recent book by Dranovsky (2006) covers test methods and results very thoroughly, but contains no theory dealing with fundamental dynamical processes.

In 1961 Culick (1961, 1963) worked out the first analysis of combustion instabilities using a Green's function and spatial averaging; the analysis was carried out for liquid rockets. That formulation allowed easy handling of linear three-dimensional problems, requiring calculation of the corresponding admittance function for the nozzle. More complete results for the admittance were later reported by Crocco and Sirignano (1967). Three-dimensional oscillations with the approximations shown in Figure 6.1 were analyzed by Scala (1955); Reardon (1961); Crocco, Reardon, and Harrje (1962); and Reardon, Crocco and Harrje (1963). The latter two papers contain limited experimental results.

Probably the greatest motivation for working so diligently to develop theory and prediction methods for solid rockets is the intrinsic limitation of single, short firing times. Thus, much effort has traditionally been devoted to transient behavior, particularly the growth of the amplitude during an unstable firing. The situation is quite different for liquid rockets, and especially for airbreathing systems that present opportunities for relatively long controllable test runs. It is perhaps, therefore, understandable that less attention has been paid to certain details of transient behavior in liquid-fueled systems.[5] An exception to that practice was the early work by Crocco and co-workers, developed especially in the book written with Cheng. The text was devoted almost entirely to linear unstable motions including transients, and had much useful influence in the subject of instabilities in liquid rockets.[6] Subsequently there were many papers published on linear instabilities in various systems.

In the 1980s there was renewed strong interest, both in the U.S. and in Europe, in small vehicles using dump combustors as the basic internal configuration for ramjets. As a result, active research programs were conducted to examine theoretical and experimental problems flowing largely from this simple configuration. The kinds of problems considered were, however, somewhat different from most of those traditionally studied as they were presented for solid and liquid rockets. Probably the most significant difference was that largely nonlinear motions were important,[7] in respects not previously encountered in rocket engines. This characteristic had the far-reaching consequence that computational fluid dynamics became an essential part of progress. One of the first analyses using CFD was the interesting work by Jou and Menon (1986, 1990). Now CFD is widely used to study internal flows, although its practical use is only in early development. The subject is mentioned only briefly in this book.

Despite the rapid growth, broad applications, and truly fundamental importance of numerical methods for internal flows, the approximate literal analysis of internal flows remains an extremely important basis for understanding and designing propulsion systems. Together, this and the following chapter cover the most important practical aspects of the analytical method developed in this book. All results obtained are based on application of the method of spatial averaging.

6.2. Zero-Dimensional Instability of a Bulk Mode

Oscillations characterized by nearly uniform amplitude and phase in a chamber have arisen in practically every type of combustion system. Because the pressure oscillation is nearly independent of position, the velocity fluctuation is approximately zero. These oscillations occur at relatively low frequencies and are often caused by processes confined to the surface of the chamber, or to openings permitting flow. The most familiar related example is the sound produced when one blows past the opening of a bottle. In that case, the term 'Helmholtz mode' is often used to identify the origin of the tone; in discussions of combustion systems, one often finds the descriptive name 'bulk mode', and for solid propellant rockets the special name

[5] I believe that relatively less attention to the fine points of true transient behavior, while no doubt motivated by practical concerns, is responsible for a tendency to acquire less understanding of the behavior of disturbances in liquid-fueled systems.

[6] As a personal note, the author is forever indebted to Professor Crocco, for that work motivated his thesis work (Culick 1960).

[7] An exception enjoying several useful applications was the elementary linear analysis by Culick and Rogers (1981), which included a simple analysis of the choked inlet duct to determine its admittance function.

'L^* instability' is applied. It is the last we treat here in some detail, although in simplified form, to introduce some of the basic ideas of computing linear instability.

Akiba and Tanno (1959) adapted the analysis by Crocco and Cheng (1956, Chapter 2) of a low frequency instability in liquid rockets[8] to the corresponding problem in solid rockets. The main difference between applications to the two classes of systems is in the models used for unsteady combustion. In the limit of linear behavior there are really no basic distinctions, another example of the practical value to be gained from studying systems other than that of immediate concern.

Although Akiba and Tanno apparently had no concern with particular problems in motors, Sehgal and Strand (1964) worked at the Jet Propulsion Laboratory (later officially named JPL) and were involved with development of motors for space vehicles. Because of operations at low pressures requiring lower structure weights, L^* instability became an important problem. The first published concern with the behavior, particularly its connection to intermittent extinction, was documented by Anderson, Strehlow, and Strand (1963). While the subsequent analysis by Sehgal and Strand differed only in certain details from Akiba and Tanno's, their lasting contribution was the first comparison of theory and experiment, shown here in Figure 6.2. The two theoretical lines arise from details of the analysis which produces two intersections of curves defined in the specification of the boundary of the stable and unstable regions of operations. No reason was given that one of the theoretical curves is favored by the experimental results. The definitions of the dimensionless critical time constant $(\tau_n)_{cr}$ and characteristic chamber length L^* are

$$(\tau_n)_{cr} = \tau_{cr}\frac{\bar{r}^2}{4\kappa} \tag{6.2}$$

$$L^* = \frac{4\kappa c_D R T_f (\tau_n)_{cr}}{a^2}\bar{p}_c^{-2n} \tag{6.3}$$

where κ is the thermal diffusivity; c_D is the discharge coefficient; T_f is the flame temperature; and a is the constant in the linear burning rate law. Equation (6.3) therefore predicts quite well the behavior $L^* \sim p^{-2n}$ shown in Figure 6.2, prepared using the properties of the propellant tested, JPL-534.

The two analyses just mentioned differed mainly in their representations of unsteady burning of a solid propellant. Akiba and Tanno drew on Green's model (See Section 2.1.2), while Sehgal and Strand worked out their own analysis of the combustion response, an incomplete[9] form of Denison and Baum's earlier approximate theory (Section 2.2.2). Both treatments followed Tsien's lead in application of a form of Nyquist's theorem (Annex G and Chapter Nine) to study the stability of the system. Tsien used a modification of the theorem suggested by Satche (1949) to handle an exponential necessarily accompanying introduction of a (constant) time lag in the combustion process.[10] Although neither treatment required a time lag in the same way followed by Tsien, both used Satche's modification of Nyquist's theorem. That is an unnecessary complication as Beckstead, Ryan, and Baer (1966) and the next paper by Coates, Cohen and Harvill (1967) implicitly showed.

Following previous authors, Coates *et al.* began their analysis with the transfer function G_m for the motor

$$\frac{\delta m_0}{\delta m_i} = G_m = \frac{G_c}{1 - G_p G_c} \tag{6.4}$$

which follows directly from the block diagram drawn in Figure 6.3.

[8]The discussion by Crocco and Cheng is an extension and elaboration of the original paper by Tsien (1953), based on essentially the same ideas. Tsien also proposed possible use of feedback control; see Chapter Nine.

[9]One consequence of the incompleteness is failure to reach the correct limit for zero frequency; see equation (12) and accompanying comment, in Coates *et al.* (1967).

[10]The analyses by Tsien; Crocco and Cheng; Akiba and Tanno; and by Sehgal and Strand were based on Laplace transforms, applied, naturally, to linear problems. Hence the presence of a constant time lag τ in the coupling between, for example, the heat or mass sources, and the pressure fluctuations, produces exponentals, $e^{-s\tau}$, in the characteristic equation.

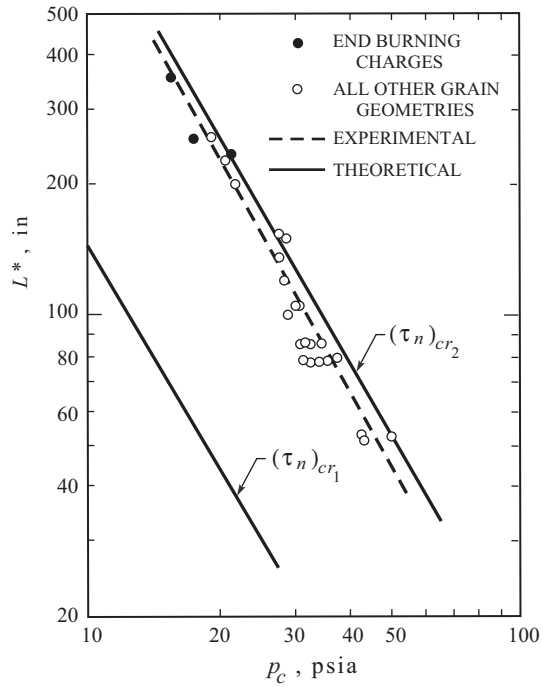

FIGURE 6.2. L^* versus chamber pressure, showing the stability limit for oscillations (Sehgal and Strand 1964).

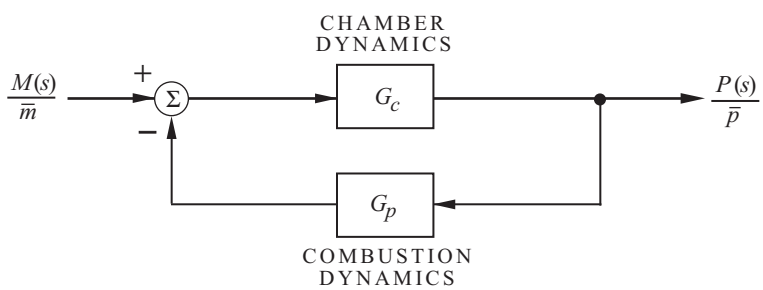

FIGURE 6.3. Block diagram of the system, adapted from Figure 1 of Coates, Cohen, and Harvill (1967).

The transfer function G_p for the combustion dynamics is given by Denison and Baum's result, (2.67) here; G_c is the transfer function for the chamber dynamics. For the model of the L^* burner used in the works cited, and explained in the next section, the equation for the unsteady chamber pressure is,

$$\tau_c \frac{d}{dt}\left(\frac{p'}{\bar{p}}\right) + \frac{p'}{\bar{p}} = \frac{m'}{\bar{m}} \ . \tag{6.5}$$

The Laplace transform is

$$(1 + s\tau_c)\frac{P(s)}{\bar{p}} = \frac{M(s)}{\bar{m}} \tag{6.6}$$

so

$$G_c = \frac{1}{1 + s\tau_c} \ . \tag{6.7}$$

Denison and Baum's result, (2.67), gives G_p, completing the basis for the calculation discussed by Coates, Cohen, and Harvill. Figure 6.4 reproduces two results the authors found in support of their calculations. The solid lines are computed from this result

$$\frac{1}{L^*} = \frac{1}{\kappa\Gamma^2 c^*}\frac{\bar{r}^2}{(\tau_n)_{cr}} \tag{6.8}$$

where $(\tau_n)_{cn} = (\tau_c\bar{r}^2/\kappa)_{cr}$. Beckstead (1965) obtained the data for Utah TF propellent.

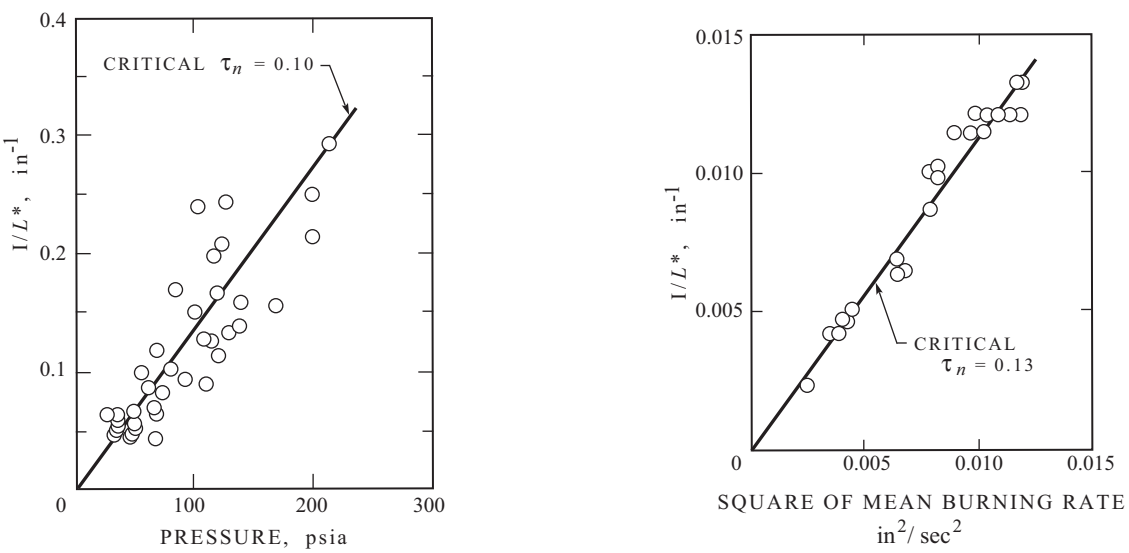

FIGURE 6.4. L^* instability data for two propellants (a) Utah TF (University of Utah) and (b) JPL-534 (Jet Propulsion Laboratory) (Coates, Cohen, and Harvill 1967).

Besides having very low frequencies and nearly uniform but sinusoidal (i.e., pulsating) pressure fields when oscillations are excited, instabilities of the bulk mode often lead to intermittent unsteady behavior commonly referred to as 'chuffing.' Figure 6.5 shows both types of behavior leading to extinction of combustion. Identifying the stability boundary unambiguously, given that loss of stability does not necessarily mean growth of an oscillation out of noise, presents problems under these conditions. The difficulties are both experimental and interpretive, treated at some length in the references. We will not discuss the subject here except to note that whatever the precursor behavior, the limit of stability seems to define a sufficiently narrow band of values, L^* and pressure or burning rate, that a line is a reasonable approximation, Figures 6.2 and 6.4. Put simply, it makes sense to speak of the 'L^* stability limit.'

Chuffing was not a new phenomenon, discovered quite early as one aspect of L^* instability. The earliest written record seems to have been prepared by Crawford *et al.* (1945) although earlier informal reports have been suggested on several occasions. Some early British experiences were discussed by Huffington (1954). An indication of the problem's practical persistence is conveyed by the session on "Nonacoustic Combustion Instability" included in the AIAA Solid Propellant Rocket Conference, January 1964. Eisel *et al.* (1964) reported results of tests with an L^* burner and a very long 'acoustic' burner having adjustable length as long as sixty (!) feet. Several records of chuffing at low frequency instabilities from the paper by Yount and Angelus (1964) are reproduced in Figure 6.6 showing well the intermittent behavior sometimes observed.

Oberg (1968) addressed the problem displayed by Figure 6.5 which had led to the idea of 'nonacoustic' instabilities in contrast to 'acoustic' instabilities of the sort described in Chapter One. It was his correct contention that 'acoustic' and 'nonacoustic' instabilities are in fact closely related. Of those working in the

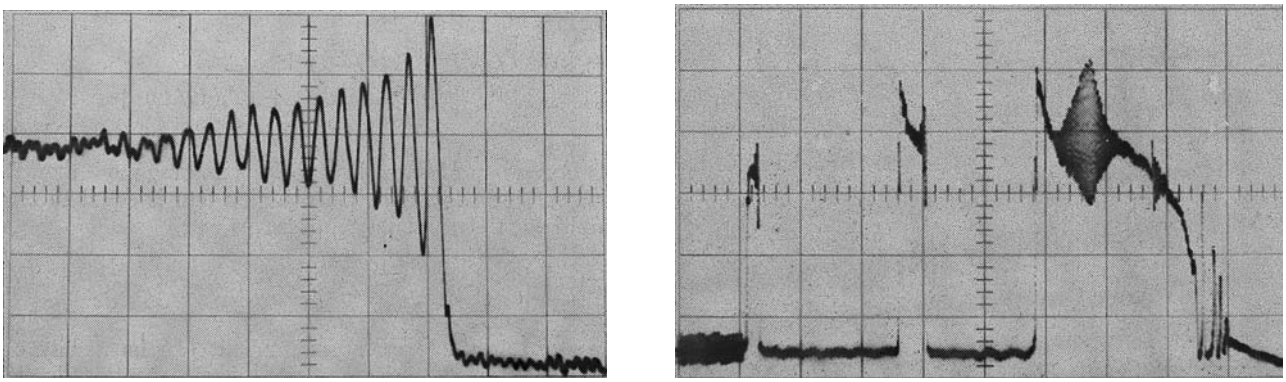

FIGURE 6.5. Two examples of natural cessation of L^* instabilities (a), growth of oscillations ending in extinction; (b) chuffing, leaking to extinction (Beckstead, Ryan, and Baer, 1966).

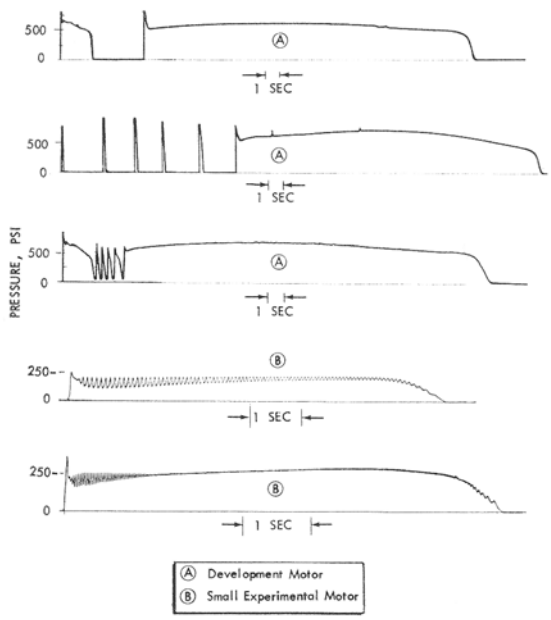

FIGURE 6.6. Five pressure records of chuffing (A) and low frequency instabilities (B) (Yount and Angelus 1964).

field, he was first to recognize that an L^* instability is the limit, as the frequency tends to zero, of the wave or acoustical modes. Oberg showed the result explicitly for longitudinal motions; Culick (1968) subsequently proved that the conclusion holds generally, with a calculation repeated here in Section 6.6.

A straightforward description of the bulk mode or L^* instability is based on the assumption that the frequency is so low that all processes respond essentially instantaneously. This requires that the travel time of a small disturbance in the chamber, and in the nozzle, be much less than the period of the oscillation. The pressure then remains sensibly uniform throughout and pulsates in time.

With this assumption, all variations in space are ignored, and in particular the conservation of momentum need not be considered. Mainly one is concerned with the conservation of mass. Let S_b be the area of burning surface S_t the area of the nozzle throat, V the volume, and c^* the usual characteristic velocity. The total

mass of gas in the volume is ρV at any instant; its rate of change must equal the difference between the rate at which mass enters, and the rate at which it leaves,

$$\frac{d}{dt}(\rho V) = mS_b - S_t \frac{p}{c^*} \tag{6.9}$$

where $m = \rho_s r$ is the mass flux at the burning surface. The relation defining c^* as the ratio of $S_t p$ to the total mass flux out the nozzle $c^* = S_t p/m = \sqrt{RT/\Gamma}$, with $\Gamma^2 = \gamma\left(\frac{2}{\gamma+1}\right)^{\frac{\gamma+1}{\gamma-1}}$ is strictly valid only in steady flow (Altman *et al.* 1960). Its use here is justified by the assumption that the transit time of a fluid element through the nozzle is much less than the period of oscillation. This is sometimes referred to as the "zero-length" approximation to the time-dependent behavior of a nozzle. Note that (6.9) applies to any geometry; it is not restricted to end burners.

We assume that the thermodynamic state of the gases is uniform in the chamber, and that combustion occurs only in a thin zone near the propellant surface; residual combustion is ignored. Further, it is assumed that the gases can be described by the equation of state for a perfect gas, $p = \rho RT$. Thus we have two equations in three variables (p, ρ, T) because the mass flux from the surface m is assumed to be a function of pressure only. The principle of conservation of energy provides a third relation, but it will be handled shortly in a simplified manner.

Now we form a linearized problem in familiar fashion by writing $p = \bar{p} + p' \ldots$ etc. and by ignoring squares and higher order terms. Then the linearized equation of state is

$$\frac{p'}{\bar{p}} = \frac{\rho'}{\bar{\rho}} + \frac{T'}{\bar{T}} \tag{6.10}$$

Similarly, equation (6.9) can be expanded as follows:

$$\bar{\rho}V\frac{d}{dt}\left(\frac{\rho'}{\bar{\rho}} - \frac{T'}{\bar{T}}\right) = (\bar{m}S_b)\frac{m'}{\bar{m}} - \frac{S_t\bar{p}}{\bar{c}^*}\left(\frac{p'}{\bar{p}} - \frac{c^{*\prime}}{\bar{c}^*}\right) \tag{6.11}$$

Because $c^* \sim \sqrt{T}, c^{*\prime}/\bar{c}^* = T'/2\bar{T}$ and the last equation can be written

$$\frac{\bar{\rho}V}{S_t\bar{p}}\bar{c}^*\frac{d}{dt}\left(\frac{p'}{\bar{p}}\right) = \left[\frac{\bar{m}S_b}{\frac{S_t\bar{p}}{\bar{c}^*}}\right]\frac{m'}{\bar{m}} - \frac{p'}{\bar{p}} + \frac{\bar{\rho}V\bar{c}^*}{S_t\bar{p}}\frac{d}{dt}\left(\frac{T'}{\bar{T}}\right) + \frac{1}{2}\frac{T'}{\bar{T}} \tag{6.12}$$

In steady flow, conservation of mass requires

$$\bar{m}_b S_b = S_t\bar{p}/\bar{c}^* \tag{6.13}$$

and with the equation of state, we find the characteristic time τ_c,

$$\frac{\bar{\rho}V\bar{c}^*}{S_t\bar{p}} = \frac{V}{S_t}\frac{\bar{c}^*}{R\bar{T}} = \frac{L^*\bar{c}^*}{R\bar{T}} = \tau_c \tag{6.14}$$

where the conventional definition of L^* is

$$L^* = V/S_t \tag{6.15}$$

Thus the equation for the pressure fluctuation is

$$\tau_c\frac{d}{dt}\left(\frac{p'}{\bar{p}}\right) = \frac{m'}{\bar{m}} - \frac{p'}{\bar{p}} + \left[\tau_c\frac{d}{dt}\left(\frac{T'}{\bar{T}}\right) + \frac{1}{2}\frac{T'}{\bar{T}}\right] \tag{6.16}$$

To simplify the discussion further, consider the extreme case in which the oscillations are so slow, and mixing is so thorough, that the temperature is not only uniform in the chamber but also constant, so $T' = 0$. Then the last equation is

$$\tau_c\frac{d}{dt}\left(\frac{p'}{\bar{p}}\right) = \frac{m'}{\bar{m}} - \frac{p'}{\bar{p}} \tag{6.17}$$

With $m = \rho_s r, m'/\bar{m} = r'/\bar{r}$, and if the burning always responded instantaneously to a change of pressure, $r \sim p^n$, one could write

$$\frac{r'}{\bar{r}} = n\frac{p'}{\bar{p}} \tag{6.18}$$

and (6.17) would become

$$\tau_c \frac{d}{dt}\left(\frac{p'}{\bar{p}}\right) = (n-1)\frac{p'}{\bar{p}} \tag{6.19}$$

The solution to this equation is immediate:

$$\frac{p}{\bar{p}} = \left(\frac{p'}{\bar{p}}\right)_0 e^{\left(\frac{n-1}{\tau_c}\right)t} \tag{6.20}$$

where $(p'/\bar{p})_0$ is the fluctuation at $t = 0$. Thus, if $n > 1$, a small disturbance will grow without limit. This is well-known behavior: motors using propellants with n close to unity are very sensitive to small changes in pressure and if n is positive, the system is unstable. That is the first criterion established for stability if combustion in a solid[11] propellant rocket, found by Malina (Karman and Malina, 1940).

The relation (6.18) is valid only in the limit of very low frequencies. In general, the burning rate of a propellant exposed to a sinusoidal pressure oscillation will vary sinusoidally also, but not in phase with the pressure, as shown in Section 2.2.2, equation (2.66), for the simplest realistic case. That behavior is represented by the response function R_b,

$$\frac{m'}{\bar{m}} = R_p \frac{p'}{\bar{p}} = \left[R_p^{(r)} + iR_p^{(i)}\right]\frac{p'}{\bar{p}} \tag{6.21}$$

The response function is a complex function of frequency, and can be written as

$$R_p = R_p^{(r)} + iR_p^{(i)} = |R_p|(\cos\phi + i\sin\phi) \tag{6.22}$$

For harmonic motions,

$$\begin{aligned} \frac{p'}{\bar{p}} &= Pe^{-i(\omega+i\alpha)t} \\ &= Pe^{\alpha t}e^{-i\omega t} \end{aligned} \tag{6.23}$$

If the growth constant α is positive, then the oscillation is unstable and grows exponentially in time. In all problems of linear stability, the principal task is to compute the growth constant. Substitution of (6.21) and (6.23) into (6.17) leads to

$$\tau_c(\alpha + i\omega)P = [R_p^{(r)} + iR_p^{(i)}]P - P \tag{6.24}$$

The amplitude P is a common factor, and the real and imaginary parts of (6.20) give the two equations

$$\text{Real Part} \qquad \alpha\tau_c = R_p^{(r)} - 1 \tag{6.25}$$

$$\text{Imaginary Part} \qquad \omega\tau_c = R_p^{(i)} \tag{6.26}$$

The response function is a fundamental quantity in all problems of combustion instability in solid propellant rockets. It is a dynamical property of the propellant, summarizing all the linear behavior for unsteady-burning. There is presently no way to calculate the response function for a real propellant. As we have emphasized in Chapter 2, the most important current experimental problem is its measurement.

[11] With only minor changes of definitions and interpretation, the same result follows for liquid or gaseous propellant rockets.

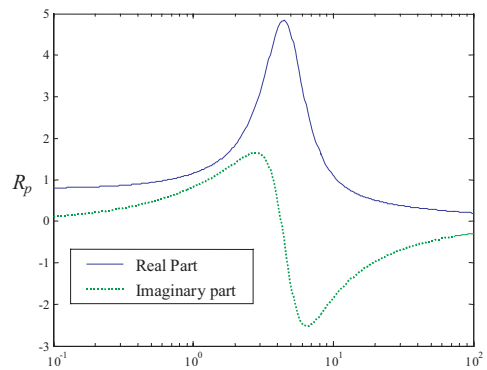

FIGURE 6.7. Real and Imaginary parts of a simple response function (see the same result, Figure 2.14).

Equation (6.25) shows that a sinusoidal oscillation is unstable if the real part of the response function is greater than unity. The frequency of an unstable oscillation is then given by (6.26); obviously $R_p^{(i)}$ must be positive for this relation to make sense.

There have been many attempts to compute the response function. Many of these actually produce the same result,[12] discussed in Section 2.2. The main feature is that the response function depends on two parameters (called A and B) and is a function of the dimensionless frequency

$$\Omega = \frac{\omega\kappa}{\bar{r}^2} \tag{6.27}$$

where κ is the thermal diffusivity of the propellant. The real and imaginary parts of R_b have the form shown in Figure 6.7, a repeat of Figure 2.14. In this case, according to (6.26), a bulk-mode instability can occur only for frequencies such that the dimensionless frequency is below the value Ω_0 at which $R_p^{(i)}$ passes through zero. Let Ω^* be the value of Ω at which $R_b^{(r)} = 1$, so $\alpha = 0$. Then a sinusoidal fluctuation is unstable if Ω lies in the range

$$\Omega^* < \Omega < \Omega_p \ . \tag{6.28}$$

Equation (6.26) becomes

$$\left(\frac{\bar{r}^2}{\kappa}\right)\frac{\omega\kappa}{\bar{r}^2}\tau_c \equiv \frac{\bar{r}^2}{\kappa}\Omega\tau_c = R_p^{(i)} \tag{6.29}$$

On the stability boundary, when $\Omega = \Omega^*$,

$$\bar{r}^2\tau_c = \frac{\kappa}{\Omega^*}R_p^{(i)}(\Omega^*) \tag{6.30}$$

With $\bar{r} = a\bar{p}^n$, and $\tau_c = L^*\bar{c}^*/R\bar{T}$, this relation gives

$$L^* = \left[\frac{\kappa R\bar{T}}{\bar{c}^* a^2}\ \frac{R_p^{(i)}(\Omega^*)}{\Omega^*}\right]\frac{1}{\bar{p}^{2n}} \tag{6.31}$$

The group in brackets is almost independent of pressure, so equation (6.31) gives the result that on the stability boundary, $L^* \sim \bar{p}^{-2n}$. This result has been verified by experimental results such as those given in Figure 6.2 and 6.4.

[12] In the past 10–15 years, efforts have been reported to formulate more realistic forms. The broad characteristics and roles of the real and imaginary parts of the response function remain. That's a useful mnemonic aid. See, however, Section 6.9.3.

For $\alpha \neq 0$, (6.26) again gives (6.31), but with $\Omega > \Omega^*$; dividing the two results one finds

$$\frac{(L^*)_{\alpha>0}}{(L^*)_{\alpha=0}} = \left[\frac{R_b^{(i)}(\Omega)}{R_b^{(i)}(\Omega^*)}\right]\left(\frac{\Omega^*}{\Omega}\right) \tag{6.32}$$

The right-hand side is less than unity, so the unstable region in the plot L^* versus $\bar{p}$ lies below the stability boundary as shown in Figure 6.2.

Equations (6.25) and (6.26) for steady sinusoidal motions follow from the simple model of the combustion dynamics used as the basis of equation (6.17) for general (but linear) time-dependent behavior. Experimental results first confirmed that the picture was correct. For practical applications, and especially as part of the effort to determine the transient behavior of burning propellants at higher frequencies, there was much interest in obtaining firm results for the response function over broad frequency ranges. A reasonable beginning is to determine the extent to which L^* instability may be used to distinguished quantitative differences among propellants.

To do so requires correlating data with the complex equation (6.24) which produces the two real equations (6.25) and (6.26). The two equations allow determination of two parameters. It is a lucky result that Denison and Baum's results (2.66) contains only two parameters, A and B. Then the question is—can A and B be determined from experiments, uniquely for each propellant? Put another way, will the parameters A and B define the dynamical behavior of solid propellants? To answer the question, we must determine how well this theory explains observed behavior.

It is easy to solve (6.25) and (6.26) for A and B to find

$$A = \Omega\frac{\beta_1 h_2 + \beta_2 h_1}{\alpha_1\beta_2 - \alpha_2\beta_1} \tag{6.33}$$

$$B = -\frac{\alpha_1 h_2 + \alpha_1 h_1}{\beta_1 h_2 + \beta_2 h_1} \tag{6.34}$$

where $h_1 = 1 + \alpha\tau_c$, $h_2 = \omega\tau_c$ and

$$\begin{aligned} \alpha_1 &= h_2(1-\lambda_r) + h_1\lambda_i \\ \alpha_2 &= h_1(1-\lambda_r) - h_2\lambda_i \\ \beta_1 &= (h_2 - n)\lambda_r - h_1\lambda_i \\ \beta_2 &= (h_2 - n)\lambda_i + h_1\lambda_r \end{aligned} \tag{6.35)a,b,c,d}$$

function λ of dimensionless frequency was defined by equation (2.26)a,b;

$$\begin{aligned} \lambda_r &= \tfrac{1}{2}\left\{1 + \tfrac{1}{\sqrt{2}}\left[(1+16\Omega^2)^{1/2} + 1\right]^{1/2}\right\} \\ \lambda_i &= \tfrac{1}{2\sqrt{2}}\left[(1+16\Omega^2)^{1/2} - 1\right] \end{aligned} \tag{6.36)a,b}$$

Equations (6.25) and (6.26) with Denison and Baum's result for R_b, define the two families of curves drawn in Figure 6.7 for $\alpha = 0$, the only condition for which data are available. Acceptable results must have $A > 0$ (by definition of A) and must also lie to the left of the line for intrinsic stability.[13] Evidently Denison and Baum's result may represent the dynamics of A-35 (A=14, B=0.8) but not those of A-13. Possible reasons for the difference have not yet been explained. The two propellants had the same oxidizer particle size distribution and differed by only 1% in the amounts by mass. A-13 had 24% by mass of PBAN binder; A-35 contained 25% of an estane type of polyurethane binder. One might guess that the difference in dynamical behavior suggested by Figure 6.8 is related to the different binders, but details are lacking.

[13]The term "intrinsic stability" refers to unlimited growth of a disturbance in the burning rate which is dependent only on the dynamics of the propellant and which occurs without an external disturbance.

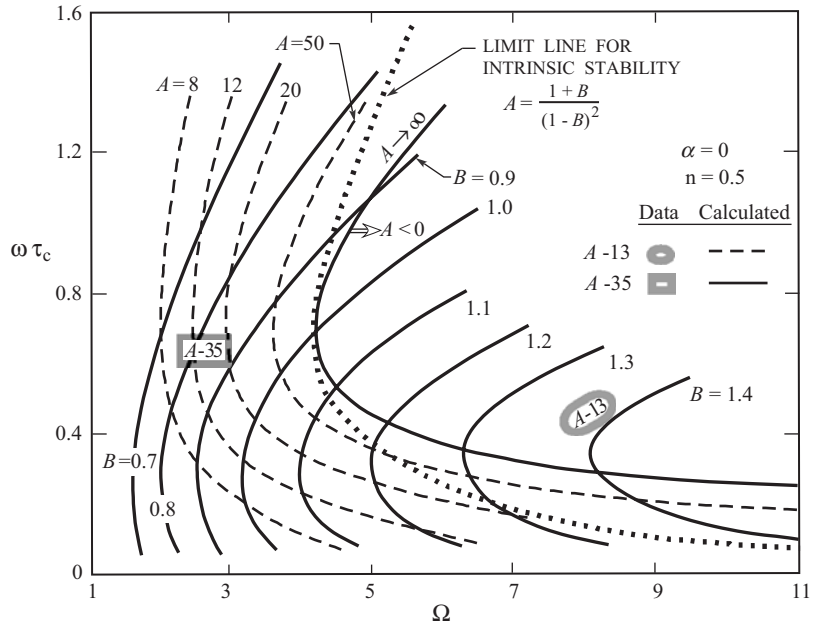

FIGURE 6.8. The L^*-chart for determining the parameters A and B. Data for the propellants A-13 and A-35 lie in the indicated regions. (Beckstead and Culick 1971).

6.3. A Formal Solution to the Problem of Linear Stability

By 'solution' we mean here formulas for calculating the amplitudes $\eta_n(t)$ of modes retained in the expansion for the pressure field, $p'(\mathbf{r},t) = \bar{p}\Sigma\eta_n(t)\psi_n(\mathbf{r})$. The amplitudes satisfy the oscillator wave equations (4.36) with N replaced by n:

$$\frac{d^2\eta_n}{dt^2} + \omega_n^2\eta_n = F_n + F_n^c \qquad (n = 1, 2, \dots) \tag{6.37}$$

where F_n^c stands for the generalized 'force' associated with the exercise of control; and F_n is the spatial average of that part (sometimes called the "projection" on the basis function ψ_n) of the internal processes affecting the motion of the nth oscillator, given by (4.30):[14]

$$F_n = -\frac{\bar{a}^2}{\bar{p}E_n^2}\left\{\int h\psi_n dV + \oint\!\!\!\oint f\psi_n dS\right\} \qquad (n = 1, 2, \dots) \tag{6.38}$$

and

$$E_n^2 = \int \psi_n^2 dV \tag{6.39}$$

Here we will suppress F_n^c because we are concerned only with the internal behavior of the system.[15] In general, the F_n contain contributions associated with the motions of oscillators other than the nth—i.e., the modes are coupled. For analysis of linear stability we are justified in ignoring that coupling, for reasons given by Culick (1997). Each F_n is a linear function of the amplitude and velocity of the oscillator, having

[14]In this chapter and subsequently we will often indicate integration over volume by single integral signs, as here, to avoid unnecessary use of $\iiint$.

[15]The functions $\mathcal{F}$ and $\mathcal{P}$ implicitly contain all effects of control; the generality of subsequent calculations is therefore not reduced by removing F_n^c.

the form

$$F_n = F_n^{\eta}\eta_n + F_n^{\dot{\eta}}\frac{d\eta_n}{dt} \qquad (n = 1, 2, \dots) \tag{6.40}$$

where the F_n^{η} and $F_n^{\dot{\eta}}$ are constants, depending only on the mode.

With these assumptions, the oscillator equations (6.37) are the uncoupled set

$$\frac{d^2\eta_n}{dt^2} - F_n^{\dot{\eta}}\frac{d\eta_n}{dt} + \left(\omega_n^2 - F_n^{\eta}\right)\eta_n = 0 \qquad (n = 1, 2, \dots) \tag{6.41}$$

Because the equations are uncoupled, the normal modes ψ_n for the corresponding classical acoustic problem are also the normal modes for the linear problem of combustor dynamics. The general problem of determining linear stability has therefore come down to the problem of determining the stability of the normal modes. In the usual fashion we assume sinusoidal time dependence with complex frequency Ω ($\Omega \equiv \bar{a}k$ below):

$$\eta_n(t) = \hat{\eta}_n e^{-i\Omega t} \qquad (n = 1, 2, \dots) \tag{6.42}$$

Equation (6.41) gives the quadratic equation for Ω_n:

$$\Omega^2 + iF_n^{\dot{\eta}}\Omega - \left(\omega_n^2 - F_n^{\eta}\right) = 0 \tag{6.43}$$

having solution

$$\Omega = -i\frac{1}{2}F_n^{\dot{\eta}} + \omega_n\sqrt{1 - \frac{1}{\omega_n^2}\left[F_n^{\eta} + \frac{1}{4}\left(F_n^{\dot{\eta}}\right)^2\right]} \tag{6.44}$$

where we take the (+) sign on the radical to give a positive real frequency. Hence the amplitudes are

$$\eta_n(t) = e^{\frac{1}{2}F_n^{\dot{\eta}}t}e^{-i\omega_n\sqrt{1-\zeta^2}t} \tag{6.45}$$

with the definition

$$\zeta_n = \frac{1}{\omega_n}\sqrt{F_n^{\eta} + \frac{1}{4}\left(F_n^{\dot{\eta}}\right)^2} \tag{6.46}$$

The nth mode is stable of

$$F_n^{\dot{\eta}} < 0 \tag{6.47}$$

That is, the coefficient of $\dot{\eta}_n$ in the expression for F_n must be negative for the nth mode to be stable. That formal condition means that the nth mode has positive damping.

According to the methods of Fourier analysis, an arbitrary disturbance at some initial time (say $t = 0$) in the chamber can be synthesized of the normal modes. The time-evolution of the disturbance is therefore determined by the $\eta_n(t)$. In particular, an arbitrary disturbance in a combustor is stable if (and only if) all of the normal modes are stable and we arrive at the general result for the linear stability of a combustor:

(i) Write the linearized function for the force acting on the nth oscillator (spatially averaged acoustic mode) in the form

$$F_n = F_n^{\eta}\eta_n + F_n^{\dot{\eta}}\frac{d\eta_n}{dt}$$

(ii) Then any initial disturbance in a combustor is stable if and only if all the $F_n^{\dot{\eta}}$ are negative:

$$\text{Linear Stability} \iff F_n^{\dot{\eta}} < 0 \quad (\text{all } n)$$

The preceding calculation, and its conclusion, illustrate further a point first made in Chapter 3: We have found a means of computing the linear stability of a combustor without knowing the actual linear motions themselves. The complex frequency (6.44) is in fact the frequency for the actual linear modes including the influences of all the processes accounted for. But calculation of the F_n^η and $F_n^{\dot\eta}$ with the formula (6.38) requires knowledge only of the **unperturbed** normal modes—their frequencies ω_n and shapes $\psi_n(\mathbf{r})$. The formal statement of this property is that the eigenvalues (Ω_n) to any order in the relevant expansion parameter (here $\bar{M}_r := \mu$ defined in Chapter 3) can be computed knowing the eigenfunctions (ψ_n) only to one less order. The eigenvalues Ω_n are here given to first order in the Mach number of the average flow but only the unperturbed classical eigenfunctions ψ_n are required. This is the basic characteristic of the expansion procedures with spatial averaging that makes the method devised here so useful in practice, as we have emphasized in Chapter 4; examples of this important result are widespread in the field of combustion instabilities generally, but may be found especially in the literature for solid rockets.

6.4. An Alternative Calculation of Linear Stability

An equivalent calculation of the result for linear stability makes direct use of the formula for the wavenumber. Write

$$\eta_n = \hat{\eta}_n e^{-i\bar{a}kt} \quad ; \qquad F_n = \hat{F}_n e^{-i\bar{a}kt}$$

and substitute in (6.37) with F_n^c ignored to find $(\bar{a}k)^2 = (\bar{a}k_n)^2 - \hat{F}_n/\hat{\eta}_n$, or

$$(\bar{a}k)^2 = (\bar{a}k_n)^2 - \frac{1}{\hat{\eta}_n}\left(\hat{F}_n^{(r)} + i\hat{F}_n^{(i)}\right) \tag{6.48}$$

where $(\quad)^{(r)}$ and $(\quad)^{(i)}$ identify real and imaginary parts. With[16] $\bar{a}k = \omega + i\alpha$, this formula is

$$\omega^2 + i(2\alpha\omega) - \alpha^2 = \omega_n^2 - \frac{1}{\hat{\eta}_n}\left(\hat{F}_n^{(r)} + i\hat{F}_n^{(i)}\right)$$

Because α and $\hat{F}_n$ are first order in the expansion parameter and terms of higher order must be dropped[17], we ignore α^2 with respect to ω^2. Then the real and imaginary parts of the last equation give

$$\begin{aligned} \omega^2 &= \omega_n^2 - \frac{1}{\hat{\eta}_n}\hat{F}_n^{(r)} \\ \alpha &= -\frac{1}{2\omega_n}\hat{F}_n^{(i)} \end{aligned} \tag{6.49)a,b}$$

where ω has been set equal to ω_n in the right-hand sides to ensure that higher order terms are not retained. Now take the square root of the first equation and again drop higher order terms to find

$$\begin{aligned} \omega &= \omega_n - \frac{1}{2\omega_n}\frac{\hat{F}_n^{(r)}}{\hat{\eta}_n} \\ \alpha &= -\frac{1}{2\omega_n}\frac{\hat{F}_n^{(i)}}{\hat{\eta}_n} \end{aligned} \tag{6.50)a,b}$$

The system is unstable if $\hat{F}_n^{(i)}$ is negative, so α is positive. This condition is essentially a generalized form of Rayleigh's Criterion discussed further in Section 6.6.

After higher order terms are dropped from (6.44), the real and imaginary parts of $\Omega \equiv \bar{a}k = \omega + i\alpha$ are

$$\begin{aligned} \omega &= \omega_n - \frac{1}{2\omega_n}F_n^\eta \\ \alpha &= -\frac{1}{2}F_n^{\dot\eta} \end{aligned} \tag{6.51)a,b}$$

[16] Thus $\alpha > 0$ for instability: $e^{-i\bar{a}kt} \equiv e^{-i(\omega+i\alpha)t} = e^{-i\omega t}e^{\alpha t}$ which grows without limit in time when $\alpha > 0$.
[17] Recall remarks in Chapters 3 and 4.

Comparison of (6.50)a,b and (6.51)a,b gives the connections between the two representations of the forcing function:

$$F_n^{\eta} = \frac{\hat{F}_n^{(r)}}{\hat{\eta}_n}$$
$$F_n^{\dot{\eta}} = \frac{1}{\omega_n}\frac{\hat{F}_n^{(i)}}{\hat{\eta}_n} \qquad (6.52)\text{a,b}$$

Generally F_n will contain several processes, each of which will depend linearly on η_n and $\frac{d\eta_n}{dt}$, and appears additively in F_n. Hence, formulas corresponding to (6.52)a,b apply to each of the individual processes. They are often useful, if only for checking correctness, in detailed calculations.

6.5. Linear Stability with a Heat Source and Motion of the Boundary

As a first approximation to problems of combustion instabilities it is useful to ignore all processes involving interactions between the unsteady and steady fields, and focus attention on the two generic causes of instabilities: time-dependent energy addition and motions of the boundary. With suitable interpretation the second may represent the influence of unsteady combustion of a solid propellant. Then in dimensional variables the linearized pressure and momentum equations (3.46)d and (3.46)b, and the boundary condition (3.57)b on the pressure fluctuations are

$$\frac{\partial p'}{\partial t} + \gamma\bar{p}\nabla\cdot\mathbf{u}' = \frac{R}{C_v}\dot{Q}' \qquad (6.53)$$

$$\bar{\rho}\frac{\partial \mathbf{u}'}{\partial t} + \nabla p' = 0 \qquad (6.54)$$

$$\hat{\mathbf{n}}\cdot\nabla p' = -\bar{\rho}\frac{\partial \mathbf{u}'}{\partial t}\cdot\hat{\mathbf{n}} \qquad (6.55)$$

Now form the wave equation as in Section 3.4, so the problem is governed by the two equations

$$\nabla^2 p' - \frac{1}{\bar{a}^2}\frac{\partial^2 p'}{\partial t^2} = h$$
$$\hat{\mathbf{n}}\cdot\nabla p' = -f \qquad (6.56)\text{a,b}$$

where

$$h = -\frac{1}{\bar{a}^2}\frac{R}{C_v}\frac{\partial \dot{Q}'}{\partial t}$$
$$f = \bar{\rho}\frac{\partial \mathbf{u}'}{\partial t}\cdot\hat{\mathbf{n}} \qquad (6.57)\text{a,b}$$

The expansion procedure and application of spatial averaging leads to the explicit oscillator equations (4.36):

$$\frac{d^2\eta_n}{dt^2} + \omega_n^2\eta_n = -\frac{\bar{a}^2}{\bar{p}E_n^2}\left\{\int\left[-\frac{1}{\bar{a}^2}\frac{R}{C_v}\frac{\partial\dot{Q}'}{\partial t}\right]\psi_n dV + \oint\left[\bar{\rho}\frac{\partial\mathbf{u}'}{\partial t}\cdot\hat{\mathbf{n}}\right]\psi_n dS\right\} \qquad (6.58)$$

As a simple example, consider the one-dimensional problem of waves excited in a tube fitted with a piston, Figure 6.9, and with distributed heat addition provided, say, by an electrically heated coil. Only longitudinal modes are considered, and

$$\psi_n = \cos(k_n x) \quad , \qquad k_n = n\frac{\pi}{L} \quad , \qquad E_n^2 = \frac{1}{2}S_c L \qquad (6.59)$$

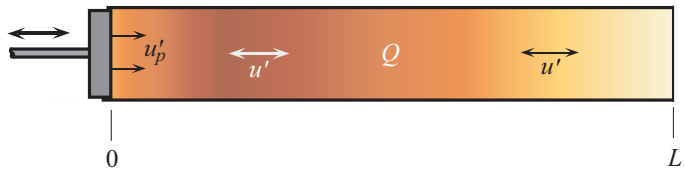

FIGURE 6.9. A tube with distributed heat addition and an oscillating piston to drive waves.

where $S_c = \pi R_c^2$ is the cross-section area of the tube. We ignore any average motion in the tube, and suppose that the average thermodynamic properties are maintained constant and uniform by suitable steady heat losses through the walls of the tube. The heat addition and motion of the piston are sinusoidal, having phases ϕ_Q and ϕ_u with respect to pressure oscillations:

$$\begin{aligned} \dot{Q}' &= \left|\hat{\dot{Q}}(x)\right| e^{-i(\bar{a}kt+\phi_Q)} \\ \mathbf{u}'_p \cdot \hat{\mathbf{n}} &= |\hat{u}_p|\, e^{-i(\bar{a}kt+\phi_u)} \end{aligned} \tag{6.60)a,b}$$

Hence for use in h and f:

$$\begin{aligned} \frac{\partial \dot{Q}'}{\partial t} &= -i\bar{a}k \left|\hat{\dot{Q}}(x)\right| e^{-i(\bar{a}kt+\phi_Q)} \\ \frac{\partial}{\partial t}\left(\mathbf{u}'_p \cdot \hat{\mathbf{n}}\right) &= -i\bar{a}k\, |\hat{u}_p|\, e^{-i(\bar{a}kt+\phi_u)} \end{aligned} \tag{6.61)a,b}$$

With $\eta_n = \hat{\eta}_n e^{-i\bar{a}kt}$, substitution in the oscillator equations (6.58) leads to

$$\begin{aligned} \left[-(\bar{a}k)^2 + \omega_n^2\right]\hat{\eta}_n = -\frac{\bar{a}^2}{\bar{p}E_n^2}\Bigg\{ &-\frac{1}{\bar{a}^2}\frac{R}{C_v}(-i\bar{a}k)\int \cos(k_n x)\left|\hat{\dot{Q}}(x)\right| e^{-i\phi_Q}\, dV \\ &-i\bar{\rho}\bar{a}k \oiint \cos(k_n x)|\hat{u}_p| e^{-i\phi_u}\, dS \Bigg\} \end{aligned}$$

After some rearrangement, and setting $\bar{a}k = \omega + i\alpha$, we find

$$\begin{aligned} (\omega+i\alpha)^2 = \omega_n^2 + i(\omega+i\alpha)\frac{\bar{a}^2}{\bar{p}(\frac{1}{2}S_c L)}\Bigg\{ &\frac{1}{\bar{a}^2}\frac{R}{C_v}S_c\int_0^L \cos(k_n x)\frac{\left|\hat{\dot{Q}}(x)\right|}{\hat{\eta}_n} e^{-i\phi_Q}\, dx \\ &+ \bar{\rho}S_c\frac{|\hat{u}_p|}{\hat{\eta}_n}e^{-i\phi_u}\Bigg\} \end{aligned}$$

Because $|\hat{\dot{Q}}|$ and $|\hat{u}_p|$ are small perturbations we can write this equation to first order in small quantities:

$$\omega^2 + i(2\alpha\omega) = \omega_n^2 + i\omega_n\frac{2}{\bar{p}L}\left\{\frac{R}{C_v}\int_0^L \cos(k_n x)\frac{\left|\hat{\dot{Q}}(x)\right|}{\hat{\eta}_n}e^{-i\phi_Q}\, dx + \bar{\rho}\bar{a}^2\frac{|\hat{u}_p|}{\hat{\eta}_n}e^{-i\phi_u}\, dx\right\}$$

Take the real and imaginary parts to find

$$\begin{aligned} \omega^2 &= \omega_n^2 + \frac{2\omega_n}{\bar{p}L}\left\{\frac{R}{C_v}\int_0^L \cos(k_n x)\frac{\left|\hat{\dot{Q}}(x)\right|}{\hat{\eta}_n}\sin\phi_Q\, dx + \bar{\rho}\bar{a}^2\frac{|\hat{u}_p|}{\hat{\eta}_n}\sin\phi_u\right\} \\ \alpha &= \frac{1}{\bar{p}L}\left\{\frac{R}{C_v}\int_0^L \cos(k_n x)\frac{\left|\hat{\dot{Q}}(x)\right|}{\hat{\eta}_n}\cos\phi_Q\, dx + \bar{\rho}\bar{a}^2\frac{|\hat{u}_p|}{\hat{\eta}_n}\cos\phi_u\right\} \end{aligned} \tag{6.62)a,b}$$

Internal feedback, and hence a condition for instability, exists if either or both of $|\hat{\dot{Q}}|$ and $|\hat{u}_p|$ depend on the fluctuating pressure (or velocity). For example, set

$$\begin{aligned} |\hat{\dot{Q}}| &= q_0 \hat{\eta}_n \psi_n = q_0 \hat{\eta}_n \cos k_n x \\ |\hat{u}_p| &= u_0 \hat{\eta}_n \end{aligned} \tag{6.63)a,b}$$

and (6.62)a becomes

$$\omega^2 = \omega_n^2 + 2\omega_n \left(A q_0 \sin \phi_q + B u_0 \sin \phi_u \right)$$

where

$$A = \frac{1}{2\bar{p}} \frac{R}{C_v} \quad ; \qquad B = \frac{\gamma}{L} \tag{6.64}$$

To first order in small quantities we find the results for the frequency and decay or growth constant:

$$\begin{aligned} \omega &= \omega_n + A q_0 \sin \phi_Q + B u_0 \sin \phi_u \\ \alpha &= A q_0 \cos \phi_Q + B u_0 \cos \phi_u \end{aligned} \tag{6.65)a,b}$$

Remarks:

(i) The nth mode is unstable if $A q_0 \cos \phi_Q + B u_0 \cos \phi_u > 0$.

(ii) If $0 \leq \phi_u \leq \frac{\pi}{2}$ then a necessary condition for instability is $0 \leq \phi_Q \leq \frac{\pi}{2}$.

(iii) Instability of the nth mode is encouraged if $|\hat{\dot{Q}}(x)| \cos k_n x$ is larger, i.e., if the heat addition is greater where the mode shape of the pressure takes its largest values, an example of Rayleigh's Criterion.

It is important also to notice that due to the spatial averaging, one cannot distinguish among the ultimate effects of volumetric and surface processes. There is an equivalence of the influences of the various processes, their importance in respect to position within the chamber being dominated by their location relative to the mode shapes. That characteristic has far-reaching consequences in applications to combustion chambers.

6.6. Rayleigh's Criterion and Linear Stability

As part of his research on the excitation of acoustic waves by heat addition[18] in chambers, Lord Rayleigh (1878, 1945) formulated the following explanation for the production of tones in a Rijke tube:

> **"If heat be periodically communicated to, and abstracted from, a mass of air vibrating (for example) in a cylinder bounded by a piston, the effect produced will depend upon the phase of the vibration at which the transfer of heat takes place. If heat be given to the air at the moment of greatest condensation, or be taken from it at the moment of greatest rarefaction, the vibration is encouraged. On the other hand, if heat be given at the moment of greatest rarefaction, or abstracted at the moment of greatest condensation, the vibration is discouraged."**

That paragraph has become probably the most widely cited 'explanation' for the presence of combustion instabilities generally. For easy reference, the explanation has long been referred to as "Rayleigh's Criterion."

It is important to realize that Rayleigh addressed only the conditions under which unsteady heat addition 'encourages' oscillations, i.e., is a destabilizing influence. Other processes, stabilizing or destabilizing, are

[18] The literature in the 19th century included many works on 'singing flames' which also formed part of the background for Rayleigh's Criterion. It was only in the late 20th century that the close basic connections between the behavior of 'singing flames' and the Rijke tube were understood.

neither excluded nor included, and there is certainly no implication that satisfaction of the criterion is either a necessary or a sufficient condition for instability to exist. Several published examples exist of quantitative realizations of the criterion (Putnam and Dennis 1953, Putnam 1971; Chu 1956a; Chu 1956b; Zinn 1986; Culick 1987, 1992). The purpose of this section is to establish a generalized form of Rayleigh's Criterion by using the analysis based on spatial averaging, and to show the equivalence of Rayleigh's Criterion and the principle of linear stability.

The main idea is that a positive change of the time-averaged energy of a modal oscillator in a cycle of oscillation is exactly equivalent to the principle of linear instability, that the growth constant should be positive for a motion to be unstable. To establish the connection we use the oscillator equations,

$$\frac{d^2\eta_n}{dt^2} + \omega_n^2\eta_n = F_n \tag{6.66}$$

The instantaneous energy[19] of the nth oscillator is

$$\varepsilon_n = \frac{1}{2}\left(\dot{\eta}_n^2 + \omega_n^2\eta_n^2\right) \tag{6.67}$$

and the change of energy in one cycle is the integral over one period of the rate at which work is done by the force F_n:

$$\Delta\varepsilon_n = \int_t^{t+\tau_n} F_n(t')\dot{\eta}_n(t')dt' \tag{6.68}$$

Under the integral, F_n and $\dot{\eta}_n$ must be real quantities; here we use the real parts of both functions,

$$\begin{aligned} \eta_n &= \hat{\eta}_n e^{-i\bar{a}kt} = |\hat{\eta}_n|e^{-i\bar{a}kt} \\ F_n &= \hat{F}_n e^{-i\bar{a}kt} = |\hat{F}_n|e^{-i(\bar{a}kt+\phi_F)} = |\hat{F}_n|\left(\cos\phi_F + i\sin\phi_F\right)e^{-i\bar{a}kt} \end{aligned} \tag{6.69)a,b}$$

We measure all phases with respect to the pressure, so $\hat{\eta}_n$ is real and, being the maximum amplitude, is positive. Substitution in the oscillator equations gives

$$k^2 = \frac{1}{\bar{a}^2}\left(\omega_n^2 - \frac{\hat{F}_n}{\hat{\eta}_n}\right)$$

of which the real and imaginary parts are to first order in small quantities:

$$\begin{aligned} \omega^2 &= \omega_n^2 - Re\left(\frac{\hat{F}_n}{\hat{\eta}_n}\right) = \omega_n^2 - \left|\frac{\hat{F}_n}{\hat{\eta}_n}\right|\cos\phi_F \\ \alpha_n &= \frac{-1}{2\omega_n}Im\left(\frac{\hat{F}_n}{\hat{\eta}_n}\right) = \frac{-1}{2\omega_n}\left|\frac{\hat{F}_n}{\hat{\eta}_n}\right|\sin\phi_F \end{aligned} \tag{6.70)a,b}$$

The oscillator's motion is stable if α_n is *negative* (see Footnote 9), i.e. if the imaginary part of $\hat{F}_n$ is *positive*.

Also for use in (6.68) we have

$$\dot{\eta}_n = -i\bar{a}k|\hat{\eta}_n|e^{-i\bar{a}kt} = \bar{a}k|\hat{\eta}_n|e^{-i\left(\bar{a}kt+\frac{\pi}{2}\right)} \approx \omega_n|\hat{\eta}_n|e^{-i\left(\omega_n t+\frac{\pi}{2}\right)}$$

so

$$Re(\dot{\eta}_n) = \omega_n|\hat{\eta}_n|\cos\left(\omega_n t + \frac{\pi}{2}\right) = -\omega_n|\hat{\eta}_n|\sin\omega_n t \tag{6.71}$$

The real part of F_n is

$$Re(F_n) = |\hat{F}_n|\cos\left(\omega_n t + \phi_F\right) = |\hat{F}_n|\left\{\cos\omega_n t\cos\phi_F - \sin\omega_n t\sin\phi_F\right\} \tag{6.72}$$

[19] ε_n is not the energy of the nth acoustic mode, which is given by the integral of (5.72) over the volume of the chamber.

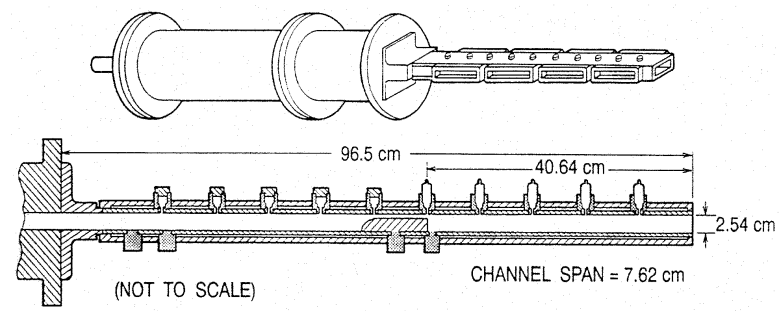

FIGURE 6.10. The Caltech dump combustor.

Hence the right-hand side of (6.68) is

$$\Delta\varepsilon_n = \int_t^{t+\tau_n} Re(F_n)Re(\eta_n)dt' = \omega|\hat{F}_n| \int_t^{t+\tau_n} \left\{ \sin^2 \omega_n t' \sin\phi_F - \frac{1}{2}\sin 2\omega_n t' \cos\phi_F \right\} dt'$$
$$= \omega|\hat{F}_n||\hat{\eta}_n|\frac{\tau_n}{2}\sin\phi_F$$

Substitution of (6.33)b leads to the formula

$$\Delta\varepsilon_n = 2\pi\alpha_n\omega_n|\hat{\eta}_n|^2 \tag{6.73}$$

which establishes the desired connection between Rayleigh's Criterion and linear stability.

Remarks:

(i) Positive α_n (the system is linearly unstable) implies that the average energy of the oscillator increases, and vice-versa.

(ii) Rayleigh's original criterion is equivalent to the principle of linear instability **if** only heat exchange is accounted for and is **neither** a necessary **nor** a sufficient condition for existence of a combustion instability.

(iii) The extended form (6.73) of Rayleigh's Criterion is exactly equivalent to the principle of linear instability, all linear processes being accounted for.

Putnam (1971) has made the most extensive use of Rayleigh's Criterion in practical situations. His book and papers give many examples of applying the Criterion as an aid to making changes of design to avoid oscillations generated by heat release, particularly in power generation and heating systems.

In the past fifteen years many groups have been making direct observations on laboratory systems to check the validity of the Criterion's implications. The key step is based on the assumption that radiation by certain intermediate species in hydrocarbon reactions (CH and OH are the most common identifiers) can be interpreted as a measure of the rate of chemical reactions taking place and hence of the rate at which energy is released. Simultaneous measurements are made of the spatial distribution of radiation in a system, and of the pressure oscillations. The results then allow at least a qualitative assessment of the extent to which the oscillations are being driven by the energy released in the combustion field, or whether other mechanisms may be active and important. It is an important method with many useful applications. However, there are serious matters of interpretation, e.g., due to poorly known rates of collisional de-activation of radiating species. Measurements of time-dependent energy release is an active research topic.

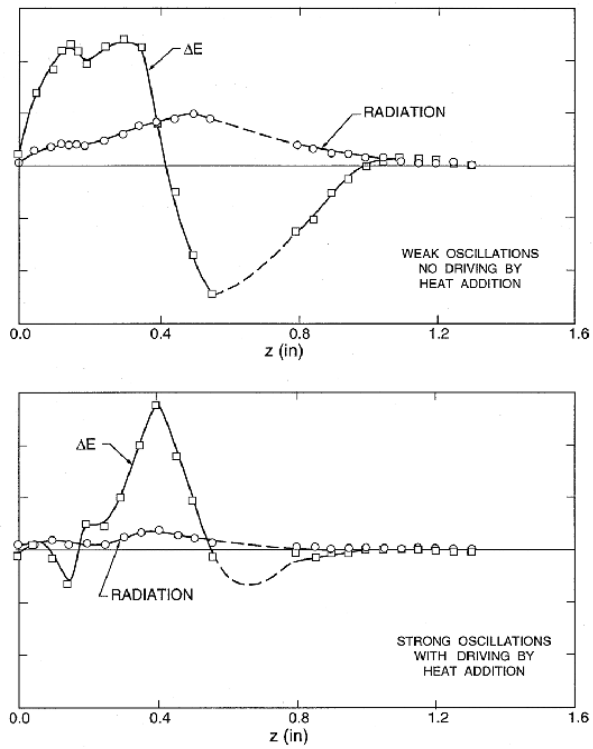

FIGURE 6.11. Experimental confirmation of Rayleigh's Criterion. Data obtained from chemiluminescence of OH (Sterling and Zukoski, 1991).

It seems that the first report of simultaneous measurements of pressure and radiation allowing confirmation of Rayleigh's Criterion appeared in a Ph.D. thesis (Sterling, 1987; Sterling and Zukoski, 1991). Figure 6.10 is a sketch of the dump combustor used as the test device, and Figure 6.11 shows the main result. The integral of ΔE over the volume of the chamber (here the integral over the length is equivalent) is a measure of the severity of oscillations. For the case shown in the lower portion of the figure, the integral of ΔE over the length is clearly positive, consistent with the observed presence of oscillations.

6.7. Some Results for Linear Stability in Three Dimensions

The term 'stability of motions' has several meanings for flows in combustion chambers, including:

(i) the stability of laminar steady flow when viscous and inertial properties of the medium dominate, leading to formation of large vortices or to turbulence, a field of distributed vorticity if the steady flow is unstable;

(ii) the stability of shear layers, commonly producing large scale vortex motions when a shear layer is unstable;

(iii) the stability of laminar flame fronts, responsible for one source of turbulent combustion when fronts are unstable;

(iv) the stability of small disturbances which, when the compressibility and inertia of the medium dominate the motions, can develop into acoustic waves.

In terms of the modes of motion mentioned in Section 3.1 and discussed further in Section 3.3, the phenomena (i)–(iii) are classified as waves of vorticity and the fourth comprises acoustic waves which, depending on the physical situation, may possess or generate vorticity as well. The perturbations must in some sense be small, as we have stressed with examples we examined in Chapter 2 and already in the present chapter. Even these 'small' perturbations produce realistic and useful results. According to remarks we made in connection with the derivation of the formalism in Chapter 3, the results derived there are general; further progress depends on modelling and more explicit calculations.

We discuss in the following section results for motions that are 'one-dimensional', an approximation that holds a special position in fluid mechanics generally for two reasons: It is often a surprisingly accurate approximation; and solution to a one-dimensional problem is enormously simpler than its three–dimensional counterpart. This has been a particularly productive approach to analyzing combustion instabilities. While it might seem logical to cover the simpler analysis first, we believe that some of the special aspects of the subject are more readily understood by working out the three-dimensional results first. As 'special aspects' we have in mind especially the contributions of 'flow-turning' and 'pumping' associated with flow at or through lateral surfaces of a combustion chamber. Those phenomena will be treated in a more rigorous fashion using the proper three-dimensional formalism in Sections 6.9 and 6.12 which accommodate vorticity, the true physical origin of both flow-turning and pumping. In his work, Flandro (1995 and later works) has been careful to emphasize this connection.

6.7.1. Linear Stability of Three-Dimensional Motions. The formulas (6.14)a,b are general, restricted only by the approximations used in formulating the analytical framework. Hence the problem of obtaining results specific to any given problem apparently comes down to finding explicit forms for F_n^{η} and $F_n^{\dot{\eta}}$, by evaluating the integrals defining F_n, equation (6.38). Section 3.3 and Annex A contain details forming the functions h and f given to second order, defined by (3.62)a,b. Here we need only the linear parts, i.e. terms of order ε and of order $\mu\varepsilon$ in the expansions.

While the use of dimensionless variables is virtually a practical necessary for systematic development of the formal expansions in Chapters 3 and 4, there are certain advantages here in working with primitive dimensional variables. According to the results of Section 6.3, we know everything about linear stability once we know the driving force F_n in the system of oscillator equations. To make the procedure as clear as possible, we repeat some of the results and display some details where it seems helpful. The nonlinear wave equation and its boundary condition are (D.3)a,b:

$$\begin{aligned} \nabla^2 p' - \frac{1}{\bar{a}^2}\frac{\partial^2 p'}{\partial t^2} &= h \\ \hat{\mathbf{n}}\cdot\nabla p' &= -f \end{aligned} \tag{6.74)a,b}$$

The linear parts of (D.4)a,b are

$$\begin{aligned} h &= -\bar{\rho}\nabla\cdot\{[\mathbf{u}]\}_1 + \frac{1}{\bar{a}^2}\frac{\partial}{\partial t}\{[p]\}_1 + \nabla\cdot\bar{\boldsymbol{\mathcal{F}}}' - \frac{1}{\bar{a}^2}\frac{\partial \mathcal{P}'}{\partial t} \\ f &= \bar{\rho}\frac{\partial \mathbf{u}'}{\partial t}\cdot\hat{\mathbf{n}} + \bar{\rho}\hat{\mathbf{n}}\cdot\{[\mathbf{u}]\}_1 - \boldsymbol{\mathcal{F}}'\cdot\hat{\mathbf{n}} \end{aligned} \tag{6.75)a,b}$$

where

$$\begin{aligned} \{[\mathbf{u}]\}_1 &= \bar{\rho}\,(\bar{\mathbf{u}}\cdot\nabla\mathbf{u}' + \mathbf{u}'\cdot\nabla\bar{\mathbf{u}}) \\ \{[p]\}_1 &= \bar{\mathbf{u}}\cdot\nabla p' + \gamma p'\nabla\cdot\bar{\mathbf{u}} \end{aligned} \tag{6.76)a,b}$$

Expansion of the pressure fluctuation in normal modes is the representation we use for the zeroth order approximation to the pressure field,

$$p'(\mathbf{r},t) \quad = \quad \bar{p}\sum_{m=0}^{M}\eta_m(t)\psi_m(\mathbf{r}) \tag{6.77}$$

$$\mathbf{u}'(\mathbf{r},t) \quad = \quad \sum_{m=1}^{M} \frac{\dot{\eta}_m(t)}{\gamma k_m^2} \nabla \psi_m(\mathbf{r}) \tag{6.78}$$

After spatial averaging has been carried out, the system of oscillator equations is (4.36),

$$\frac{d^2\eta_n}{dt^2} + \omega_n^2 \eta_n = F_n \tag{6.79}$$

with the definition (4.32)

$$F_n = -\frac{\bar{a}^2}{\bar{p}E_n^2}\left\{\int h\psi_n dV + \oiint f\psi_n dS\right\} \tag{6.80}$$

We write the linear contributions to F_n

$$F_n = -\frac{\bar{a}^2}{\bar{p}E_n^2}\left\{\bar{\rho}I_1 + \frac{1}{\bar{a}^2}I_2 + \oiint \bar{\rho}\frac{\partial \mathbf{u}'}{\partial t}\cdot\hat{\mathbf{n}}\psi_n dS - \int \boldsymbol{\mathcal{F}}'\cdot\nabla\psi_n dV - \frac{1}{\bar{a}^2}\int \frac{\partial \mathcal{P}'}{\partial t}\psi_n dV\right\} \tag{6.81}$$

and from Annex D, equations (D.10)a,b:

$$\begin{aligned} I_1 &= \int (\bar{\mathbf{u}}\cdot\nabla\mathbf{u}' + \mathbf{u}'\cdot\nabla\bar{\mathbf{u}})\cdot\nabla\psi_n dV \\ I_2 &= \frac{\partial}{\partial t}\int (\gamma p'\nabla\cdot\bar{\mathbf{u}} + \bar{\mathbf{u}}\cdot\nabla p')\psi_n dV \end{aligned} \tag{6.82)a,b}$$

With use of two vector identities, I_1 can be re-written

$$I_1 = \int \nabla(\bar{\mathbf{u}}\cdot\mathbf{u}')\cdot\nabla\psi_n dV - \int (\mathbf{u}'\times\nabla\times\bar{\mathbf{u}})\cdot\nabla\psi_n dV - \int (\bar{\mathbf{u}}\times\nabla\times\mathbf{u}')\cdot\nabla\psi_n dV$$

The first integral can be put in the more convenient form

$$\int \nabla(\bar{\mathbf{u}}\cdot\mathbf{u}')\cdot\nabla\psi_n dV = \oiint (\bar{\mathbf{u}}\cdot\mathbf{u}')\nabla\psi_n\cdot\hat{\mathbf{n}}dS - \int (\bar{\mathbf{u}}\cdot\mathbf{u}')\nabla^2\psi_n dV = k_n^2\int (\bar{\mathbf{u}}\cdot\mathbf{u}')\psi_n dV$$

because on the boundary surface $\nabla\psi_n$ is everywhere parallel to the surface, so $\nabla\psi_n\cdot\hat{\mathbf{n}} = 0$. Hence I_1 is more simply

$$I_1 = k_n^2\int (\bar{\mathbf{u}}\cdot\mathbf{u}')\psi_n dV - \int (\mathbf{u}'\times\nabla\times\bar{\mathbf{u}})\cdot\nabla\psi_n dV - \int (\bar{\mathbf{u}}\times\nabla\times\mathbf{u}')\cdot\nabla\psi_n dV \tag{6.83}$$

and the 'force' acting on the nth oscillator is

$$\begin{aligned} F_n = -\frac{\bar{a}^2}{\bar{p}E_n^2}\Bigg\{&\bar{\rho}k_n^2\int (\bar{\mathbf{u}}\cdot\mathbf{u}')\psi_n dV - \bar{\rho}\int (\mathbf{u}'\times\nabla\times\bar{\mathbf{u}} + \bar{\mathbf{u}}\times\nabla\times\mathbf{u}')\cdot\nabla\psi_n dV \\ &+\frac{1}{\bar{a}^2}\frac{\partial}{\partial t}\int (\gamma p'\nabla\cdot\bar{\mathbf{u}} + \bar{\mathbf{u}}\cdot\nabla p')\psi_n dV + \bar{\rho}\oiint \frac{\partial \mathbf{u}'}{\partial t}\cdot\hat{\mathbf{n}}\psi_n dS \\ &- \int \boldsymbol{\mathcal{F}}'\cdot\nabla\psi_n dV - \frac{1}{\bar{a}^2}\int \frac{\partial \mathcal{P}'}{\partial t}\psi_n dV\Bigg\} \end{aligned} \tag{6.84}$$

This form can be simplified further since within the linear approximation, we take $\mathbf{u}'$ and p' equal to their unperturbed acoustic values in the volume integrals in F_n[20]; for harmonic motions the uth terms of (6.77) and (6.78) are

$$\begin{aligned} p' &= \hat{p}e^{-i\bar{a}k_n t} = \bar{p}\hat{\eta}_n\psi_n e^{-i\bar{a}k_n t} \\ \mathbf{u}' &= \hat{\mathbf{u}}e^{-i\bar{a}k_n t} = -i\frac{\bar{a}}{\gamma k_n}\hat{\eta}_n\nabla\psi_n e^{-i\bar{a}k_n t} \end{aligned} \tag{6.85)a,b}$$

[20]In the surface integral, $\partial\mathbf{u}'/\partial t\cdot\hat{\mathbf{n}}$ is a non-zero perturbation because $\mathbf{u}'$ is not given by the classical acoustic value at the surface. For example, this term could represent the influence of motions of a loudspeaker set in a wall. Thus we correctly set $\mathbf{u}' = \hat{\mathbf{u}}e^{-i\bar{a}k_n t}$ and $\hat{\mathbf{u}}$ is left to be specified according to the desired boundary condition.

Then $\boldsymbol{\mathcal{F}}' = \hat{\boldsymbol{\mathcal{F}}} e^{-i\bar{a}kt}$, $\mathcal{P}' = \hat{\mathcal{P}} e^{-i\bar{a}kt}$, $F_n = \hat{F}_n e^{-i\bar{a}kt}$ and 6.84 becomes

$$\hat{F}_n = \hat{\eta}_n \frac{\bar{a}^2}{\bar{p}E_n^2}(-i\bar{\rho}\bar{a}k_n)\left\{\frac{1}{\gamma}\int(\bar{\mathbf{u}}\cdot\nabla\psi_n)\psi_n dV - \frac{1}{\gamma k_n^2}\int(\nabla\psi_n\times\nabla\times\bar{\mathbf{u}} + \bar{\mathbf{u}}\times\nabla\times\nabla\psi_n)\cdot\nabla\psi_n dV \right.$$
$$\left. + \frac{\gamma\bar{p}}{\bar{\rho}\bar{a}^2}\int(\psi_n\nabla\cdot\bar{\mathbf{u}} + \frac{1}{\gamma}\bar{\mathbf{u}}\cdot\nabla\psi_n)\psi_n dV + \oint\!\!\!\oint \frac{\hat{\mathbf{u}}}{\hat{\eta}_n}\cdot\hat{\mathbf{n}}\psi_n dS\right\}$$
$$+\frac{\bar{a}^2}{\bar{p}E_n^2}\left\{\int\hat{\boldsymbol{\mathcal{F}}}\cdot\nabla\psi_n dV - i\frac{k_n}{\bar{a}}\int\hat{\mathcal{P}}\psi_n dV\right\}$$

The integrand of the second integral vanishes because the first term in the parentheses is perpendicular to $\nabla\psi_n$ and in the second, $\nabla\times\nabla\psi_n = 0$. From the definition of the speed of sound, $\gamma\bar{p}/\bar{\rho}\bar{a}^2 = 1$ and the amplitude of the force is

$$\hat{F}_n = \hat{\eta}_n \frac{\bar{a}^2}{\bar{p}E_n^2}(i\bar{\rho}\bar{a}k_n)\left\{\frac{2}{\gamma}\int(\bar{\mathbf{u}}\cdot\nabla\psi_n)\psi_n dV + \int\psi_n^2\nabla\cdot\bar{\mathbf{u}}dV + \oint\!\!\!\oint\frac{\hat{\mathbf{u}}}{\hat{\eta}_n}\cdot\hat{\mathbf{n}}\psi_n dS\right\}$$
$$+\hat{\eta}_n\frac{\bar{a}^2}{\bar{p}E_n^2}\int\left[\frac{\hat{\boldsymbol{\mathcal{F}}}}{\hat{\eta}_n}\cdot\nabla\psi_n - i\frac{k_n}{\bar{a}}\frac{\hat{\mathcal{P}}}{\hat{\eta}_n}\psi_n\right]dV \tag{6.86}$$

Use the identity

$$(\bar{\mathbf{u}}\cdot\nabla\psi_n)\psi_n = \frac{1}{2}\left[\nabla\cdot(\bar{\mathbf{u}}\psi_n^2) - \psi_n^2\nabla\cdot\bar{\mathbf{u}}\right]$$

and combine terms to write $\hat{F}_n$ in the form

$$\hat{F}_n = \hat{\eta}_n \frac{\bar{a}^2}{\bar{p}E_n^2}(i\bar{\rho}\bar{a}k_n)\left\{\oint\!\!\!\oint\left[\frac{\hat{\mathbf{u}}}{\hat{\eta}_n}\cdot\hat{\mathbf{n}} + \frac{1}{\gamma}\bar{\mathbf{u}}\cdot\hat{\mathbf{n}}\psi_n\right]\psi_n dS + \frac{\gamma-1}{\gamma}\int\psi_n^2\nabla\cdot\bar{\mathbf{u}}dV\right\}$$
$$+\hat{\eta}_n\frac{\bar{a}^2}{\bar{p}E_n^2}\int\left[\frac{\hat{\boldsymbol{\mathcal{F}}}}{\hat{\eta}_n}\cdot\nabla\psi_n - i\frac{k_n}{\bar{a}}\frac{\hat{\mathcal{P}}}{\hat{\eta}_n}\psi_n\right]dV \tag{6.87}$$

Four remarks are important:

(i) The mean flow field may be rotational ($\nabla\times\bar{\mathbf{u}} \neq 0$) and time-averaged sources of mass are accommodated ($\nabla\cdot\bar{\mathbf{u}} \neq 0$).

(ii) With the iterative procedure discussed in Chapters 3 and 4, the substitutions of classical acoustic mode shapes are required in the right-hand side, except in the surface integral where the correct boundary condition on the velocity must be used:

$$p' = p'_a = \bar{p}\eta_n(t)\psi_n(\mathbf{r})\ ; \quad \mathbf{u}' = \mathbf{u}'_a = \frac{1}{\gamma k_n^2}\frac{d\eta_n}{dt}\nabla\psi_n \tag{6.88}$$

(iii) The calculations in Section 4.6 have shown that to first order in the average Mach number, the unsteady field may also be rotational. However, the greatest influences of rotationality have not been included here. Those are represented by two terms associated with behavior at a burning surface, discussed in Sections 6.9 and 6.12. There are also some important effects associated with vorticity, contained in the terms $I_{\Omega\Omega}$ and $I_{a\Omega}$. They have been dropped from (6.87), but they will be discussed later in Sections 6.12 and 7.4.

(iv) The processes of 'pumping' and 'flow-turning' are implied by these results, but are obtained only after considerable further calculations discussed in Sections 6.9 and 6.12. The integrals containing $\hat{\mathcal{F}}$ and $\hat{\mathcal{P}}$ are central in this respect, containing pieces related to production of vorticity. See the last remark in the introduction to this section. It's true that there is a bit of 'after-the-fact' flavor here, but that is within the spirit of the construction of 6.79 and 6.87. These do not, and are not intended to, constitute a 'theory' based on first principles. To give $\boldsymbol{\mathcal{F}}'$ and $\mathcal{P}'$ specific forms for particular

processes, requires using special results calculated independently of the apparatus constructed here, namely those found by Flandro (1995)a. The required computations have not been done.

Now we follow the procedure explained in Section 4.1 to find the formula for the complex wavenumber. For linear harmonic motions (6.37) and (6.48) give

$$k^2 - k_n^2 = -\frac{1}{\bar{a}^2}\frac{\hat{F}_n}{\hat{\eta}_n} \tag{6.89}$$

Substitution of (6.87) in (6.89) gives

$$\begin{aligned} k^2 - k_n^2 = -i\frac{k_n}{\bar{a}E_n^2}\left\{\oiint\left[\frac{\gamma\hat{\mathbf{u}}}{\hat{\eta}_n}\cdot\hat{\mathbf{n}} + \bar{\mathbf{u}}\cdot\hat{\mathbf{n}}\psi_n\right]\psi_n dS + (\gamma-1)\int\psi_n^2\nabla\cdot\bar{\mathbf{u}}dV\right\} \\ -\frac{1}{\bar{p}E_n^2}\int\left[\frac{\hat{\boldsymbol{\mathfrak{F}}}}{\hat{\eta}_n}\cdot\nabla\psi_n - i\frac{k_n}{\bar{a}}\frac{\hat{\mathcal{P}}}{\hat{\eta}_n}\psi_n\right]dV \end{aligned} \tag{6.90}$$

This formula is actually quite general due to the functions $\hat{\boldsymbol{\mathfrak{F}}}$ and $\hat{\mathcal{P}}$, which have not been assigned specific forms, for reasons examined in Section 6.7; at least two important processes, 'flow-turning' and 'pumping' are not shown explicitly.

Let the right-hand side be denoted by iK so (6.90) is

$$k^2 - k_n^2 = iK = iK^{(r)} + K^{(i)}$$

Because $k = (\omega + i\alpha)/\bar{a}$ and k_n is real, this equation can be expanded to give

$$\left(\frac{\omega}{\bar{a}}\right)^2 - \left(\frac{\alpha}{\bar{a}}\right)^2 + i\left(2\frac{\omega\alpha}{\bar{a}^2}\right) - \left(\frac{\omega_n}{\bar{a}}\right)^2 = iK^{(r)} - K^{(i)} \tag{6.91}$$

All parts of the right-hand side of (6.90) written in dimensionless form are of first order in the Mach number of the mean flow. Hence the last equation shows that α^2 is of second order and can be ignored. Similarly, the real part is of the same order, so ω differs from ω_n by terms of first order and

$$\left(\frac{\omega}{\bar{a}}\right)^2 - \left(\frac{\omega_n}{\bar{a}}\right)^2 = \left(\frac{\omega}{\bar{a}} - \frac{\omega_n}{\bar{a}}\right)\left(\frac{\omega}{\bar{a}} + \frac{\omega_n}{\bar{a}}\right) \approx \left(\frac{\omega}{\bar{a}} - \frac{\omega_n}{\bar{a}}\right)\left(2\frac{\omega_n}{\bar{a}}\right) + 0(\bar{M}_r^2) \tag{6.92}$$

Thus, for use in (6.90), $k^2 - k_n^2 \approx (\omega - \omega_n)(2\omega_n/\bar{a}^2) + i(2\omega_n\alpha/\bar{a}^2)$ so $\omega - \omega_n = \frac{\bar{a}^2}{2\omega_n}K^{(r)}$ and $\alpha = \frac{\bar{a}^2}{2\omega_n}K^{(i)}$. With these approximations, and $K^{(r)}$, $K^{(i)}$ replaced by their explicit forms, (6.91) leads to the formulas for $\omega - \omega_n$ and α:

$$\omega - \omega_n = \frac{1}{2}\frac{\gamma}{E_n^2}\oiint\frac{\hat{\mathbf{u}}^{(i)}}{\hat{\eta}_n}\cdot\hat{\mathbf{n}}\psi_n dS - \frac{\bar{a}^2}{2\omega_n\bar{p}E_n^2}\int\left[\frac{\hat{\boldsymbol{\mathfrak{F}}}^{(r)}}{\hat{\eta}_n}\cdot\nabla\psi_n + \frac{k_n}{\bar{a}}\frac{\hat{\mathcal{P}}^{(i)}}{\hat{\eta}_n}\psi_n\right]dV \tag{6.93}$$

$$\begin{aligned} \alpha = -\frac{1}{2E_n^2}\left\{\oiint\left[\gamma\frac{\hat{\mathbf{u}}^{(\mathbf{r})}}{\hat{\eta}_{\mathbf{n}}}\cdot\hat{\mathbf{n}}\psi_n + (\bar{\mathbf{u}}\cdot\hat{\mathbf{n}})\psi_n^2\right]dS + (\gamma-1)\int\psi_n^2\nabla\cdot\bar{\mathbf{u}}dV\right\} + \\ -\frac{\bar{a}^2}{2\omega_n\bar{p}E_n^2}\int\left[\frac{\hat{\boldsymbol{\mathfrak{F}}}^{(i)}}{\hat{\eta}_n}\cdot\nabla\psi_n + \frac{k_n}{\bar{a}}\frac{\hat{\mathcal{P}}^{(r)}}{\hat{\eta}_n}\psi_n\right]dV \end{aligned} \tag{6.94}$$

With slight rearrangement, the formulas (6.90), (6.93) and (6.94) have been given as (86)–(88) by Culick and Yang (1992)[21]

[21] Here, with $p' = \hat{p}e^{-i\bar{a}kt}$ and $\bar{a}k = \omega + i\alpha$, $e^{-i\bar{a}kt} = e^{\alpha t}e^{-i\omega t}$, stability requires $\alpha < 0$, i.e. α must be negative.

Both $\omega - \omega_n$ and α are sums of contributions from the various processes accounted for. Most importantly, the formula for the growth constant has the form

$$\begin{aligned}\alpha = (\alpha)_{\text{combustion}} &+ (\alpha)_{\text{meanflow/acoustics}} + (\alpha)_{\text{nozzle}} \\ &+ (\alpha)_{\text{particles}} + (\alpha)_{\text{injectionsystem}} \\ &+ (\alpha)_{\text{inertsurfaces}} + \cdots\end{aligned} \tag{6.95}$$

By suitable interpretation of the first two integrals in (6.93), the first three pieces of α are given explicitly; the last three are generated by the terms involving $\hat{\mathfrak{F}}^{(i)}$ and $\hat{\mathcal{P}}^{(r)}$ and hence cannot be written explicitly at this point.

For most combustion systems, the six contributions shown explictly seem to cover practically all dynamical behavior, with the exception of two surface contributions mentioned in note (iv) above. Those are fundamentally important in solid rockets; see Section 6.9. Interactions of the oscillations with turbulence may also be significant but that subject remains essentially undeveloped; no results have been reported for the effects of turbulence on instabilities in full-scale systems. Descriptions of some major contributions to (6.95) are given in Section 6.6.

That the growth constant representing the difference between gains and losses of acoustic energy has the form (6.95) for a linear system has long been known (McClure *et al.* 1960). At least implicitly, (6.95) has been a part of all considerations of combustion instabilities. However, extensive data giving good quantitative results for the transient growth of oscillations have been obtained only for solid propellant rockets and related laboratory devices. Despite the widespread attention to the problem in liquid rockets (see, for example, Crocco and Cheng 1956, Crocco 1965 and Harrje and Reardon 1972), including theoretical predictions, and observations of stability boundaries, little experimental data exists for the values of α itself under conditions of true linear instability. The same can be said of other liquid and gas-fueled systems: Emphasis in most treatments has been on the stability boundary where $\alpha = 0$.

When α is negative (i.e.,small disturbances decay) its value may be regarded as a measure of the stability margin of the system. During development of the liquid rockets for the Apollo vehicle, an experimental method for assessing the stability margin was worked out, based on measurement of the decay of disturbances following injection of a small explosive charge (Harrje and Reardon 1972, Chapters 9 and 10). There seem to be no reports of efforts to determine the values of the various contributions to the decay constants determined in those tests. The same may be said of the very extensive experimental work carried out in Russia over many years (Dranovsky 2006).

There may be other reasons for those conclusions but the main one seems to be due to an intrinsic difference in the nature of the systems. A liquid or gas-fueled system can be tested repeatedly, so as a practical matter, improvement of the dynamical behavior can be pursued on a trial-and-error basis. Development of the F-1 engine (Oefelein and Yang 1993) is perhaps the outstanding example. The processes responsible for the instabilities are so complicated that theory and experiments directed to understanding the mechanisms in detail would have been expensive, time-consuming and perhaps even impossible to complete successfully with the tools available forty years ago.

In contrast, no solid rocket can be retested without repeating the expensive process of cleaning and preparing the motor case and nozzle; manufacturing propellant; loading the motor; and allowing the material to cure. Moreover, there is likely no control of the firing. Hence, practically from the beginnings of solid rocketry, attention has been paid to time-dependent behavior during tests. When linear stability theory became available, it was natural to develop sufficiently good instrumentation and methods of data processing to obtain accurate values for α and its constituent parts. In recent years, great efforts have been expended on measurement and interpretation of the growth constant for many solid rockets and under many experimental conditions.

The growth constant has a useful quantitative interpretation. With the definition

$$p'(\mathbf{r},t) = \hat{p}(\mathbf{r})e^{-i\bar{a}kt} = \hat{p}e^{-i(\omega+i\alpha)t} = \hat{p}e^{-i\omega t}e^{\alpha t} \ ,$$

we find the ratio of values of two peaks of the oscillation at a fixed location, occurring at times t_1 and $t_2 = t_1 + mT = t_1 + m2\pi/\omega$.

$$\frac{|p_2'|_{\text{peak}}}{|p_1'|_{\text{peak}}} = \left| \frac{e^{-i\omega\left(t_1 + m\frac{2\pi}{\omega}\right)}e^{\alpha t_2}}{e^{-i\omega t_1}e^{\alpha t_1}} \right| = e^{m2\pi\alpha/\omega} \tag{6.96}$$

because $e^{-im2\pi} = \cos m2\pi + i\sin m2\pi = \pm 1$. Hence the peak value is e times larger when $m2\pi\alpha/\omega = 1$, or

$$\frac{\omega}{\alpha} = 2\pi m \text{ or } \frac{f}{\alpha} = m \tag{6.97}$$

Hence, f/α is the number of cycles required for the peak value of the pressure oscillation to increase by e (or decrease by $1/e$ if $\alpha < 0$). This interpretation suggests the potential practical value of measuring transient growths and decay. Normally, many tens or perhaps hundreds of cycles are required for e-folding of the peak values. That is the best and most convincing evidence for the essential assumption on which the analysis is based, that perturbations of the acoustic field are 'small', implying α and $\omega - \omega_n$, equations (6.93) and (6.94) are both small compared with ω.

6.7.2. The Admittance and Response Functions for a Burning Surface. The term $\hat{\mathbf{u}} \cdot \hat{\mathbf{n}}$ in the surface integral, equation (6.90), arises from the part $\bar{\rho}\partial\mathbf{u}/\partial t \cdot \hat{\mathbf{n}}$ of f, equation (6.38). Although $\hat{\mathbf{u}} \cdot \hat{\mathbf{n}} = 0$ is required for the basis functions used here, it is allowed to be non-zero in f to account for motion of the surface in the actual problem; in other words, it is a perturbation. In general, the boundary surface is not rigid. At burning surfaces, the unsteady combustion process produces fluctuations of burning rate, and hence velocity, of the order of the average Mach number. A model of the processes involved and calculation of the fluctuations have been discussed in Section 2.2. The response function R_p defined for the fluctuation of mass flux, by the relation (2.4), is given in its simplest form as equation (2.52).

It is a convention in classical acoustics, that has become standard practice in the subject of this book, to replace fluctuations of the velocity at the boundary by admittance functions. The idea is that if a small pressure fluctuation is imposed on a boundary, the surface will move, at a velocity proportional, in first approximation, to the pressure fluctuation. In solid rockets, there are chiefly three classes of boundaries: inert impermeable surfaces; burning surfaces; and areas through which flow may pass, mainly the exhaust nozzle. Most other systems contain only the first and third types.

No exposed surface in a solid rocket chamber is truly inert, but erosion of insulation material is slow compared with combustion rates. Thus, we may consider the material to be inert as a good first approximation. In that case, there is negligible motion of the surface, and the acoustic field is influenced primarily by viscous effects confined to an acoustic boundary layer, treated in the following section.

Burning surfaces and regions of flow through the boundary may be treated together. From the definition of mass flux, $m_b = -\rho_s \mathbf{u} \cdot \hat{\mathbf{n}}$, and with the perfect-gas law, we have

$$-\hat{\mathbf{u}} \cdot \hat{\mathbf{n}} = \frac{\hat{m}_b}{\bar{\rho}_s} - \bar{\mathbf{u}} \cdot \hat{\mathbf{n}}\frac{\Delta\hat{T}_s}{\bar{T}_s} + \frac{\hat{p}}{\gamma\bar{p}}\bar{\mathbf{u}} \cdot \hat{\mathbf{n}} \tag{6.98}$$

where subscript s denotes the value at the surface. The minus sign appears on $\hat{\mathbf{u}} \cdot \hat{\mathbf{n}}$ because $\hat{\mathbf{n}}$ is positive outward but $\hat{\mathbf{u}}$ and m_b are positive inward (i.e., into the chamber). The quantity $\Delta\hat{T}_s$ represents the difference between the actual temperature change $\hat{T}_s$ and the isentropic temperature fluctuation associated with the

pressure disturbance:

$$\Delta\hat{T}_s = \hat{T}_s - \frac{\gamma-1}{\gamma}\frac{\hat{p}}{\bar{p}}\bar{T}_s \tag{6.99}$$

With $\gamma\bar{p} = \bar{\rho}\,\bar{a}^2$, and $\hat{p}/\bar{p} = \hat{\eta}_n\psi_n$, (6.98) can be solved for the combination appearing in the first integral of (6.90):

$$\frac{\gamma}{\hat{\eta}_n}(\hat{\mathbf{u}}\cdot\hat{\mathbf{n}})\psi_n + (\bar{\mathbf{u}}\cdot\hat{\mathbf{n}})\psi_n^2 \equiv -\gamma\left(\frac{\hat{m}_b}{\bar{\rho}_s} - \bar{\mathbf{u}}\cdot\hat{\mathbf{n}}\frac{\Delta\hat{T}_s}{\bar{T}_s}\right)\frac{\psi_n}{\hat{\eta}_n} \tag{6.100}$$

Analysis of the unsteady response of a burning surface produces most directly results for fluctuations of the mass flux $\hat{m}_b$, whereas measurements provide directly the combination on the left-hand side of (6.100). Hence, two functions have been introduced in the literature for solid rockets, the response function R_b and the admittance function A_b, defined by the relations

$$\begin{aligned}\frac{\hat{m}_b}{\bar{m}_b} &= R_b\frac{\hat{p}}{\gamma\bar{p}}\\ -\frac{\hat{\mathbf{u}}\cdot\hat{\mathbf{n}}}{\bar{a}} &= A_b\frac{\hat{p}}{\gamma\bar{p}}\end{aligned} \tag{6.101)a,b}$$

With these definitions, the combination (6.100) gives

$$\frac{1}{\bar{a}}\left(\gamma\frac{\hat{\mathbf{u}}\cdot\hat{\mathbf{n}}}{\hat{\eta}_n\psi_n} + \bar{\mathbf{u}}\cdot\hat{\mathbf{n}}\right) \equiv -(A_b + \bar{M}_b) \equiv -\bar{M}_b\left(R_b + \gamma\frac{\Delta\hat{T}_s/\bar{T}_s}{\hat{\eta}_n\psi_n}\right) \tag{6.102}$$

where the subscript b has been introduced to indicate conditions at the burning surface.

Because the processes at burning surfaces are ultimately the source of the energy for instabilities in solid rockets, the problem of coupling to acoustical motions has received much attention for many years. It is not possible to compute accurate values of the response function for a given propellant. Experimental methods carry considerable uncertainties but have advanced to the point of being effective for comparing propellants, and for assessing trends of behavior accompanying compositional changes. (Section 2.2)

Denison and Baum (1961) first discovered an approximation to the response function now commonly used for correlating data and in computations of stability of solid rockets, Culick (1968)b reviewed the analyses of the response function available in the late 60s. As we have shown in Section 2.2, because of common assumptions of the physical behavior, almost all results have the same form as Denison and Baum's formula,

$$R_b = \frac{nAB}{\lambda + \frac{A}{\lambda} - (1+A) + AB} \tag{6.103}$$

if combustion processes at the surface are insensitive to pressure.

More recently, there have been continuing attempts to improve the representation (6.103), based on test results and incorporating ideas relating to the basic behavior of modern propellants. See, for example, Section 2.2; the final reports of the MURI programs (Culick 2002; Krier and Hofenrichter 2002); and papers by the investigators involved. The representation (6.103) remains the basic result used as a first approximation in studies of the internal dynamics of solid propellant rockets. Deviations from this form (see Chapter 2) are extremely important and continue to be a subject of research in this area.

6.7.3. The First Measurements of the Stability Boundary for a Solid Rocket. Probably the first systematic experimental investigation of the stability boundary for a solid rocket was carried out by Brownlee as his dissertation (Brownlee 1959). A useful summary of some of the results was published by Brownlee and Marble (1960). Brownlee's work fitted into a larger program on unstable burning in solid

rockets carried out at the Jet Propulsion Laboratory (JPL) during the 1950s and 1960s. A companion paper by Landsbaum, Kuby and Spaid (1960) appeared in the same volume with Brownlee and Marble's report. Further aspects of the tests are discussed there, but the topics are not germane to the present discussion.

The portion of the results relevant here were interpreted by Culick (1966) using a form of the theory worked out in this book. Figure 6.12 is a sketch of the cylindrical motors used and a typical pressure trace suggesting how the onset of a linear instability was defined with the data. The boundary was defined to be reached when the mean pressure rose above its predicted value in steady combustion. Stability boundaries for the motors tested are shown in Figure 6.13. Data from 250 firings were used.

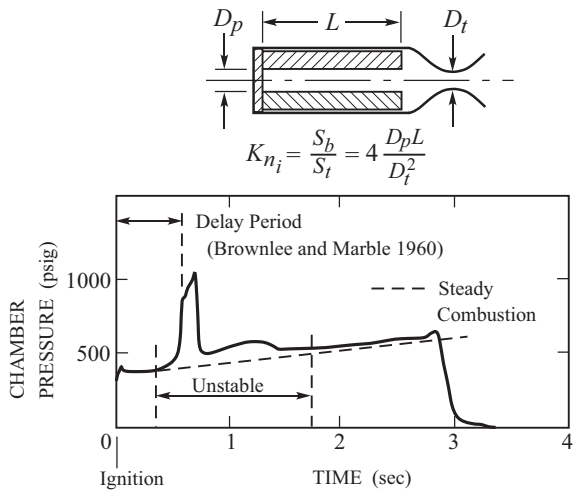

FIGURE 6.12. Geometrical parameters defined by Brownlee and a typical time history of the mean chamber pressure (Brownlee and Marble 1960).

In all tests the instability was dominated by the first tangential $(lmn) := (010)$ mode. More recently, roughly in the last 20–30 years, longitudinal modes have been more commonly unstable. The important difference is that the velocity fluctuation parallel to the axis of the motor is very small when a tangential mode is excited (zero in the classical limit). However, in both cases the fluctuating motion is largely parallel to the surface. The scouring effect—a kind of unsteady erosive burning—is likely the cause of the large increase of the mean pressure appearing in Figure 6.12. This is the mechanism commonly referred to as "velocity coupling." Stability boundaries are shown in Figure 6.13. Two features are especially striking: The boundaries are nearly straight with positive slope; and the boundaries have slope increasing with the length of the motor.

The reasoning by Culick (1966) led to the conclusion that the stability boundary was determined by the balance of energy loss through the nozzle and energy gain from combustion. After the Mach number at the burning surface has been eliminated in favor of $K_n :=$ area of burning surface/area of the nozzle throat, the power balance leads to

$$K_n = 0.0935\frac{\Gamma\bar{a}}{\sqrt{\gamma}}\frac{L}{D_p}\left(A_b^{(r)} + m_1^2\right) \tag{6.104}$$

where $m_1 = 1.84$. At the time (1966) this analysis was carried out, the admittance for the propellant was not known. Therefore the tack was taken to fit the data reasonably well by choosing $A_b^{(r)}$, especially its dependence on the chamber diameter D_p, that is, frequency. Figure 6.14 is a plot of the values of $A_b^{(r)}$ inferred to provide an exact fit for $L = 31''$, requiring $K_n = 2.13L\,D_p$. The data are for an early composite

propellant tested in a T-burner (Angelus 1960). Then the stability boundaries for other values of L are calculated, with the results shown in Figure 6.13.

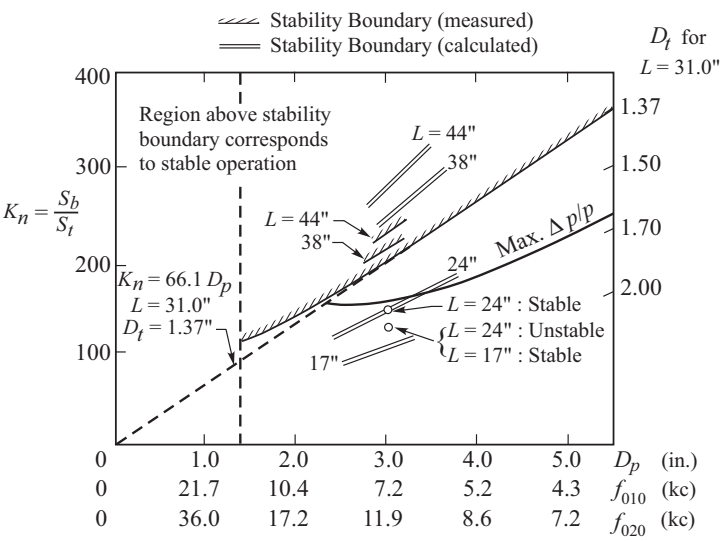

FIGURE 6.13. Stability boundaries for the 010 mode: experimental (measured) (Brownlee and Marble 1960); theoretical (calculated) (Culick 1966).

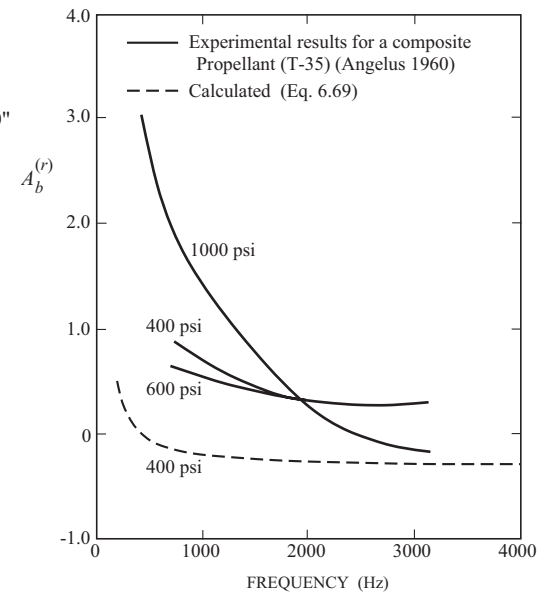

FIGURE 6.14. Dependence of the admittance function on frequency inferred from Brownlee's measurements (Culick 1966).

While these results are useful and seem clearly to contain much truth, they are certainly not free of questions. An important one in particular is raised by the use of the admittance function as the boundary condition for the 010 mode. Because this mode has no velocity component in the direction normal to the burning surface, it is by no means clear that one can even use A_b as it is defined in terms of the normal velocity component. The same difficulty arises for longitudinal modes with burning surfaces not perpendicular to the direction of propagation. This matter has been addressed in development of the theory of longitudinal modes treated within the one-dimensional approximation, discussed in the following section.

A second question concerns the possible influences of 'flow-turning' and other rotational contributions, a matter raised and presently being studied by Flandro and Perry (2006). On the other hand, it is not obvious that the situation here is analogous to that of a longitudinal wave. The difference is that for a longitudinal wave, the unsteady velocity is coplanar (locally) with the mean velocity, whereas for a transverse mode the unsteady and steady velocities are perpendicular. The analysis necessary to settle this question has not been worked out. Flow-turning is discussed in Section 6.12.

6.8. Stability of Oscillations in a Bulk Mode

Most oscillations occurring in combustion chambers are related to wave modes of motion. They can often be interpreted and analyzed as perturbed forms of individual or mixed classical acoustic modes. For many years, oscillations having very low frequencies were regarded as somehow different, but in the context of acoustics generally, that view misses the mark. In fact the oscillations at frequencies below that of the lowest acoustic mode are perturbed forms of the classical acoustic mode having frequency equal to zero, as

explained in Section 6.3. The purpose of this discussion is to show how the result for the bulk mode of a chamber—the L*-mode in a solid propellant rocket—is extracted quite easily from the results discussed already for wave modes. That this result should be true is fairly clear from the calculations in Section 6.3 because the distribution of burning surface was not required. This point was first made by Culick (1968) in a note generalizing Oberg's 1968 computation.

For the mode in a rocket chamber corresponding to the Nth classical acoustic mode, the wavenumber and mode shape for sinusoidal oscillations are given by equations (4.19) and (4.20), with $\kappa = 1$,

$$k^2 = k_N^2 + \frac{1}{E_N^2}\left\{\iiint_V \psi_N(\mathbf{r}_0)\hat{h}(\mathbf{r}_0)dV_0 + \oiint_S \psi_N(\mathbf{r}_{0s})\hat{f}(\mathbf{r}_{0s})dS_0\right\} \tag{6.105}$$

$$\hat{p}(\mathbf{r}) = \psi_N(\mathbf{r}) + \sum_{n=0}^{\infty}{}' \frac{\psi_n(\mathbf{r})}{E_n^2(k^2-k_n^2)}\left\{\iiint_V \psi_n(\mathbf{r}_0)\hat{h}(\mathbf{r}_0)dV_0 + \oiint_S \psi_n(\mathbf{r}_{0s})\hat{f}(\mathbf{r}_{0s})dS_0\right\} \tag{6.106}$$

The mode ψ_N has the classical shape for the bulk mode, namely $\psi_N = 1$, to which the corresponding value of k_N is $k_N = 0$. Thus $E_N^2 = \iiint \psi_N^2 dV = V$ and the two equations are

$$k^2 = \iiint \hat{h}(\mathbf{r}_0)dV_0 + \oiint \hat{f}(\mathbf{r}_{0s})dS_0 \tag{6.107}$$

$$\hat{p}(\mathbf{r}) = 1 + \sum_{n=0}^{\infty}{}' \frac{\psi_n(\mathbf{r})}{E_n^2(k^2-k_n^2)}\iiint \psi_n(\mathbf{r}_0)\hat{h}(\mathbf{r}_0)dV_0 + \oiint \psi_n(\mathbf{r}_{0s})\hat{f}(\mathbf{r}_{0s})dS_0 \tag{6.108}$$

Equation (6.108) shows that the pressure field differs from a constant value by an amount of order mean flow Mach number. With the formulas (6.75)a,b written for $\hat{h}$ and $\hat{f}$, there is a common factor k in all terms of (6.107), which can be written

$$k = \frac{i}{V}\oiint \bar{\mathbf{m}}_0 \cdot \hat{\mathbf{n}}\, dS_0 + \oiint A\, dS_0 \tag{6.109}$$

The first term represents the sum of acoustic energy convection through the boundary, and a contribution of work done on the oscillations due to interaction with the mean flow. Fluctuations at a non-rigid boundary, for which $A \neq 0$, cause work done on or by the surface.

With the definitions of A_b for a burning surface and A_n for a nozzle, the real and imaginary parts of (6.109) are

$$\begin{aligned}\frac{\omega}{\bar{a}} &= \frac{1}{V}\left[S_b A_b^{(i)} - S_n A_n^{(i)}\right]\\ \frac{\alpha}{\bar{a}} &= \frac{1}{V}\left[S_b(A_b^{(r)} + \bar{M}_b) - S_n(M_n + A_n^{(r)})\right]\end{aligned} \tag{6.110)a,b}$$

These equations assume the forms given in Section 6.3 after introducing the definitions of the response function, $R_b = (m'/\bar{m})/(p'/\bar{p})$, and setting the density fluctuation equal to its isentropic value in the relation

$$A_b = \frac{\gamma\bar{p}}{\bar{a}}\frac{u'}{p'} = \gamma\bar{M}_b\left[\frac{m'/\bar{m}}{p'/\bar{p}} - \frac{\rho'/\bar{\rho}}{p'/\bar{p}}\right] = \gamma\bar{M}_b\left[R_b - \frac{1}{\gamma}\right] \tag{6.111}$$

Then with the characteristic time $\tau_c = V/\gamma\bar{M}_b S_b\bar{a} = c^*\bar{V}/\bar{a}^2 S_t = c^* L^*/\bar{a}^2$,

$$\begin{aligned}\omega\tau_c &= R_b^{(i)} - \frac{1}{\gamma\bar{M}_b}\left(\frac{S_n}{S_b}\right)A_n^{(i)}\\ \alpha\tau_c &= R_b^{(r)} - \frac{1}{\gamma\bar{M}_b}\left(\frac{S_n}{S_b}\right)\left(\bar{M}_n + A_n^{(r)}\right)\end{aligned} \tag{6.112)a,b}$$

which are equivalent to (6.25) and (6.26).

6.9. Linear Stability in the One-Dimensional Approximation

Results corresponding to (6.90), (6.93) and (6.94) can be derived for the case when the one-dimensional approximation is used. The formulas found for the one-dimensional (1-D) case are in the first instance apparently much simpler to use than those found for three-dimensional (3-D) problems. Details of the grain configuration, for example, do not appear. Only the cross section of the port and its variation along the length of the motor must be known. Applications have apparently confirmed that the formula for the growth or decay constant seems to be sufficiently accurate for many purposes, but we will see that positive result is partly illusory.

The foundations of the calculations have been discussed by Culick (1970, 1973, 2001) and Culick and Yang (1992). This formulation is the basis of the Standard Stability Program (SSP) first written by Lovine *et al.* (1976) and in improved form by Nickerson *et al.* (1983). The corrected and improved version including extension to three-dimensional problems is currently under development (French 2004).

When longitudinal or axial acoustic modes are excited in a slender (i.e., L/D not small) solid rocket contain a uniform grain burning only at the lateral boundary, an important basic question arises: How are the waves driven? The difficulty in understanding the mechanism due to combustion processes confined to the boundary arises because the flow from the boundary enters normally to the surface but the mean and unsteady motions in the bulk of the volume are parallel to the surface. Evidently there must be a transition zone, an unsteady layer normally thin, because experimentally, the frequencies of the longitudinal modes are estimated quite closely by the classical formulas for organ pipe oscillations. As an attempt to address part of the question with a relatively simple analysis, Culick (1970, 1973) worked out the consequences of a strictly one-dimensional approximation to the problem; some omissions in that work are corrected here.

In the one-dimensional approximation, the equations to be solved are written for properties averaged over a cross section, with only the axial component of flow accounted for. The inflow of mass, momentum and energy from the combustion zone then appear as sources in the equations of motion. In particular, the inward momentum is assumed to have no axial component at the surface, but must acquire the axial component of the bulk flow at each section of the combustor. It is implied in the analysis that the adjustment occurs instantaneously so no account needs to be taken of any process of memory in the axial direction.

Much discussion, and correction of the original results, has been precipitated exactly because the formulation to treat 'one-dimensional' problems is, after all, an approximation. One must be aware that the question always is present: Does the one-dimensional approximation contain imperfect forms of *all* processes present in the *complete* three-dimensional formulation? The query is difficult to answer, partly because in the process of applying the one-dimensional approximation, some viscous effects may also be implied although the coefficient of viscosity does not appear (see, for example, Shapiro 1952). Only comparison of exact and approximate results may give an answer, and even then questions may remain. In this section we cover the procedure and results cited above; in Sections 6.9.1 and 6.9.2 we summarize the current results containing recent corrections.

The procedure for deducing the formula for the wavenumber is the same as that followed in Section 6.7 for three-dimensional problems. Annex B is a summary of the equations derived for the one-dimensional approximation, including source terms denoted by $(\quad)_s$ which are associated with flow through the lateral boundary. With only linear terms retained, the wave equation, its boundary condition, and the functions h_1 and f_1 are

$$\frac{1}{S_c}\frac{\partial}{\partial x}\left(S_c\frac{\partial p'}{\partial x}\right) - \frac{1}{a^2}\frac{\partial^2 p'}{\partial t^2} = h_1 \tag{6.113}$$

$$\frac{\partial p'}{\partial x} = -f_1 \qquad (x = 0, L) \tag{6.114}$$

where

$$h_1 = -\bar{\rho}\frac{1}{S_c}\frac{\partial}{\partial x}\left(S_c\frac{\partial}{\partial x}\bar{u}u'\right) + \frac{\bar{u}}{\bar{a}^2}\frac{\partial^2 p'}{\partial t\partial x} + \frac{\gamma}{\bar{a}^2}\frac{\partial p'}{\partial t}\frac{1}{S_c}\frac{d}{dx}(S_c\bar{u}) + \frac{1}{S_c}\frac{\partial}{\partial x}S_c(\mathcal{F}_1' + \mathcal{F}_{1s}') - \frac{1}{\bar{a}^2}\frac{\partial(\mathcal{P}_1' + \mathcal{P}_{1s}')}{\partial t} \tag{6.115}$$

$$f_1 = \bar{\rho}\frac{\partial u'}{\partial t} + \bar{\rho}\frac{\partial}{\partial x}(\bar{u}u') - (\mathcal{F}_1' + \mathcal{F}_{1s}') \tag{6.116}$$

Equations (6.113)–(6.116) correspond to (6.74)a,b and (6.75)a,b. **To simplify the formulae, and to emphasize several important points that do not depend on gas/particle interactions, we will assume that the flow contains no particulate matter**. Then $\mathcal{W}_1'$, $\mathcal{F}_1'$ and $\mathcal{P}_1'$ are found as the fluctuations of (B.8), (B.9) and (B.11) without the contributions from particles:

$$\mathcal{F}_1' = \frac{\partial \tau_v'}{\partial x} + m_e' + m_D' - \sigma_e' \approx 0 \tag{6.117}$$

$$\mathcal{P}_1' = \frac{R}{C_v}Q_1' + RT\mathcal{W}_1' \approx \frac{R}{C_v}Q_1' \tag{6.118}$$

$$\mathcal{W}_1' = \mathcal{W}_e' \approx 0 \tag{6.119}$$

Recall that $(\ )_e$ identifies external sources and m_D' is the fluctuation of mass associated with diffusional processes; see Annex A for the definition of m_D. With viscous terms ignored, only $\mathcal{P}_1'$ is non-zero. Finally, the surface terms $\mathcal{F}_{1s}'$ and $\mathcal{P}_{1s}'$ in h_1 and f_1 are found from the definitions (B.20) and B.22) to be

$$\mathcal{F}_{1s}' = \frac{1}{S_c}\left\{(\bar{u}_s - \bar{u})\int m_{sg}'dq + (u_s' - u')\int \bar{m}_{sg}dq\right\} \tag{6.120}$$

$$\mathcal{P}_{1s}' = \frac{R}{C_v}\frac{1}{S_c}\left\{(\bar{h}_{0s} - \bar{e}_0 + C_v\bar{T})\int m_{sg}'dq + (h_{0s}' - e_0' + C_vT')\int \bar{m}_{sg}dq\right\} \tag{6.121}$$

Expansion of the zero-order representations of the pressure and velocity fields have the forms corresponding to (6.77),

$$p'(x,t) = \bar{p}\sum_{\ell=1}^{M_1}\eta_\ell(t)\psi_\ell(x) \tag{6.122}$$

$$u'(x,t) = \sum_{\ell=1}^{M_1}\frac{\dot{\eta}_\ell}{\gamma k_\ell^2}\frac{d\psi_\ell}{dx} \tag{6.123}$$

where the ψ_ℓ are normal modes satisfying the homogeneous equations

$$\frac{1}{S_c}\frac{d}{dx}\left(S_c\frac{d\psi_\ell}{dx}\right) + k_\ell^2\psi_\ell = 0 \tag{6.124}$$

$$\frac{d\psi_\ell}{dx} = 0 \qquad (x = 0, L) \tag{6.125}$$

After substitution of (6.122) in (6.113) and spatially averaging the result, we find the system of oscillator equations and the 'forcing functions' F_ℓ:

$$\frac{d^2\eta_\ell}{dt^2} + \omega_\ell^2\eta_\ell = F_\ell \tag{6.126}$$

$$F_\ell = -\frac{\bar{a}^2}{\bar{p}E_\ell^2}\left\{\int_0^L h_1\psi_\ell S_c dx + [f_1\psi_\ell S_c]_0^L\right\} \tag{6.127}$$

and $E_\ell^2 = \int_0^L \psi_\ell^2 S_c dx$. Equations (6.126) and (6.127) correspond to (6.79) and (6.80).

For harmonic motions, $h_1 = \hat{h}_1 e^{-i\bar{a}kt}$, etc., substitution of (6.127) in (6.126) leads to the formula for the square of the wavenumber,

$$k^2 = k_\ell^2 + \frac{1}{\bar{p}E_\ell^2}\left\{\int_0^L \frac{\hat{h}_1}{\hat{\eta}_\ell}\psi_\ell S_c dx + \left[\frac{\hat{f}_1}{\hat{\eta}_\ell}\psi_\ell S_c\right]_0^L\right\} \tag{6.128}$$

where (6.115) and (6.116) are now

$$\hat{h}_1 = -\bar{\rho}\frac{1}{S_c}\frac{d}{dx}\left(S_c\frac{d}{dx}\bar{u}\hat{u}\right) - ik\frac{\bar{u}}{\bar{a}}\frac{d\hat{p}}{dx} - i\gamma\frac{k}{\bar{a}}\hat{p}\frac{1}{S_c}\frac{d}{dx}(S_c\bar{u}) + \frac{1}{S_c}\frac{d}{dx}S_c(\hat{\mathcal{F}}_1 + \hat{\mathcal{F}}_{1s}) + i\frac{k}{\bar{a}}(\hat{\mathcal{P}}_1 + \hat{\mathcal{P}}_{1s}) \tag{6.129}$$

$$\hat{f}_1 = -i\bar{\rho}\bar{a}k\hat{u} + \bar{\rho}\frac{d}{dx}(\bar{u}\hat{u}) - (\hat{\mathcal{F}}_1 + \hat{\mathcal{F}}_{1s}) \tag{6.130}$$

are the one-dimensional forms of equations (6.75)a,b.

The first three terms of $\hat{h}_1$ and the first two terms of $\hat{f}_1$, correspond exactly to their three-dimensional counterparts in (6.75)a,b; $\mathcal{F}_1' + \mathcal{F}_{1s}'$ and $\mathcal{P}_1' + \mathcal{P}_{1s}'$ correspond to $\boldsymbol{\mathcal{F}}'$ and $\mathcal{P}'$. Thus the special topics which we discuss shortly have to do mainly with $\mathcal{F}_{1s}'$ and $\mathcal{P}_{1s}'$ and parts of $\boldsymbol{\mathcal{F}}'$ and $\mathcal{P}'$. First we carry through the manipulations equivalent to those beginning with (6.77), but now for one-dimensional problems. Substitution of (6.129) and (6.130) into (6.128) gives

$$\begin{aligned} k^2 - k_\ell^2 = \frac{1}{\hat{\eta}_\ell\bar{p}E_\ell^2}&\left\{-\bar{\rho}\int_0^L \frac{1}{S_c}\frac{d}{dx}\left(S_c\frac{d}{dx}\bar{u}\hat{u}\right)\psi_\ell S_c dx - ik\int_0^L \frac{\bar{u}}{\bar{a}}\frac{d\hat{p}}{dx}\psi_\ell S_c dx - i\gamma\frac{k}{\bar{a}}\int_0^L \hat{p}\frac{1}{S_c}\frac{d}{dx}(S_c\bar{u})\psi_\ell S_c dx\right\} \\ &+\frac{1}{\hat{\eta}_\ell\bar{p}E_\ell^2}\left\{\int_0^L \frac{1}{S_c}\frac{d}{dx}S_c(\hat{\mathcal{F}}_1 + \hat{\mathcal{F}}_{1s})\psi_\ell S_c dx + i\frac{k}{\bar{a}}\int_0^L (\hat{\mathcal{P}}_1 + \hat{\mathcal{P}}_{1s})\psi_\ell S_c dx\right\} \\ &+\frac{1}{\hat{\eta}_\ell\bar{p}E_\ell^2}\left\{-i\bar{\rho}\bar{a}k\left[\hat{u}\psi_\ell S_c\right]_0^L + \bar{\rho}\left[\frac{d}{dx}(\bar{u}\hat{u})\psi_\ell S_c\right]_0^L - \left[(\hat{\mathcal{F}}_1 + \hat{\mathcal{F}}_{1s})\psi_\ell S_c\right]_0^L\right\} \end{aligned} \tag{6.131}$$

The zeroth order forms of $\hat{p}$ and $\hat{u}$ are given by the one-dimensional acoustic formulas,

$$\begin{aligned} (p')_{\substack{\text{zeroth}\\\text{order}}} &= p_\ell'(x,t) = \hat{p}_\ell(x)e^{-i\bar{a}k_\ell t} = \bar{p}\hat{\eta}_\ell\psi_\ell(x)e^{-i\bar{a}k_\ell t} \\ (u')_{\substack{\text{zeroth}\\\text{order}}} &= u_\ell'(x,t) = \hat{u}_\ell(x)e^{-i\bar{a}k_\ell t} = -i\frac{\bar{a}}{\gamma k_\ell}\hat{\eta}_\ell\frac{d\psi_\ell}{dx}e^{-i\bar{a}k_\ell t} \end{aligned} \tag{6.132)a,b}$$

Consistent with the general ordering procedure, these formulas are to be used anywhere $\hat{p}$ and $\hat{u}$ are multiplied by $\bar{u}(x)$ or its derivative(s). Thus, only the first term in the last set of brackets in (6.131) contains the perturbed form of $\hat{u}$ (not $\hat{u}_\ell$).

Integration by parts and use of equation (6.124) leads to the result

$$\begin{aligned} -\bar{\rho}\int_0^L \frac{1}{S_c}\frac{d}{dx}\left(S_c\frac{d}{dx}\bar{u}\hat{u}\right)\psi_\ell S_c dx &= -\bar{\rho}\left[\psi_\ell S_c\frac{d}{dx}(\bar{u}\hat{u})\right]_0^L + \bar{\rho}\left[\bar{u}\hat{u}S_c\frac{d\psi_\ell}{dx}\right]_0^L + \bar{\rho}k_\ell^2\int_0^L \bar{u}\hat{u}\psi_\ell S_c dx \\ &= -\bar{\rho}\left[\psi_\ell S_c\frac{d}{dx}(\bar{u}\hat{u})\right]_0^L + \bar{\rho}\left[\bar{u}\hat{u}S_c\frac{d\psi_\ell}{dx}\right]_0^L - i\frac{\hat{\eta}_\ell}{\gamma}\bar{\rho}\bar{a}k_\ell\int_0^L \bar{u}\psi_\ell\frac{d\psi_\ell}{dx}S_c dx \end{aligned} \tag{6.133}$$

The second and third terms in the first curly brackets of (6.131) are

$$-ik\int_0^L \frac{\bar{u}}{\bar{a}}\frac{d\hat{p}}{dx}\psi_\ell S_c dx = -i\bar{p}\hat{\eta}_\ell \frac{k_\ell}{\bar{a}}\int_\ell^L \bar{u}\psi_\ell \frac{d\psi_\ell}{dx}S_c dx \tag{6.134}$$

$$-i\gamma\frac{k}{\bar{a}}\int_0^L \hat{p}\frac{1}{S_c}\frac{d}{dx}(S_c\bar{u})\psi_\ell dx = -i\gamma\bar{p}\hat{\eta}_\ell\frac{k_\ell}{\bar{a}}\int_0^L \psi_\ell^2\left[\frac{1}{S_c}\frac{d(S_c\bar{u})}{dx}\right]S_c dx \tag{6.135}$$

and the terms in (6.131) containing $(\hat{\mathcal{F}}_1 + \hat{\mathcal{F}}_{1s})$ combine in an obvious fashion. With (6.133)–(6.135), the formula (6.131) can be written

$$\begin{aligned} k^2 - k_\ell^2 = -i\frac{k_\ell}{\bar{a}E_\ell^2}&\left\{2\int_0^L \bar{u}\psi_\ell\frac{d\psi_\ell}{dx}S_c dx + \gamma\int_0^L \psi_\ell^2\left[\frac{1}{S_c}\frac{d(S_c\bar{u})}{dx}\right]S_c dx\right\} \\ &-\frac{1}{\bar{p}E_\ell^2}\left\{\int_0^L\left[\left(\frac{\hat{\mathcal{F}}_1+\hat{\mathcal{F}}_{1s}}{\hat{\eta}_\ell}\right)\frac{d\psi_\ell}{dx} - i\frac{k_\ell}{\bar{a}}\left(\frac{\hat{\mathcal{P}}_1+\hat{\mathcal{P}}_{1s}}{\hat{\eta}_\ell}\right)\psi_\ell\right]S_c dx\right\} \\ &-i\frac{k_\ell}{\bar{a}}\frac{\gamma}{E_\ell^2}\left[\frac{\hat{u}}{\hat{\eta}_\ell}\psi_\ell S_c\right]_0^L \end{aligned} \tag{6.136}$$

Now we rewrite the terms in the first bracket set to show that (6.136) is exactly the one-dimensional form of (6.90). Integration of the first term by parts gives two terms, one of which is proportional to the last term in brackets and the other is a boundary term:

$$\begin{aligned} 2\int_0^L \bar{u}\psi_\ell\frac{d\psi_\ell}{dx}S_c dx &= \int_0^L \frac{d}{dx}(S_c\bar{u}\psi_\ell^2)dx - \int_0^L \psi_\ell^2\left[\frac{1}{S_c}\frac{d}{dx}(S_c\bar{u})\right]S_c dx \\ &= \left[S_c\bar{u}\psi_\ell^2\right]_0^L - \int_0^L \psi_\ell^2\left[\frac{1}{S_c}\frac{d}{dx}(S_c\bar{u})\right]S_c dx \end{aligned} \tag{6.137}$$

Substitution of (6.137) in (6.136) and some rearrangement gives

$$\begin{aligned} k^2 = k_\ell^2 - i\frac{k_\ell}{\bar{a}E_\ell^2}&\left\{\left[\left(\gamma\frac{\hat{u}}{\hat{\eta}_\ell} + \bar{u}\psi_\ell\right)\psi_\ell S_c\right]_0^L + (\gamma-1)\int_0^L \psi_\ell^2\left[\frac{1}{S_c}\frac{d}{dx}(S_c\bar{u})\right]S_c dx\right\} \\ &-\frac{1}{\bar{p}E_\ell^2}\int_0^L\left[\left(\frac{\hat{\mathcal{F}}_1+\hat{\mathcal{F}}_{1s}}{\hat{\eta}_\ell}\right)\frac{d\psi_\ell}{dx} - i\frac{k_\ell}{\bar{a}}\left(\frac{\hat{\mathcal{P}}_1+\hat{\mathcal{P}}_{1s}}{\hat{\eta}_\ell}\right)\psi_\ell\right]S_c dx \end{aligned} \tag{6.138}$$

which is (6.90) written from one-dimensional problems. However, the terms containing $\hat{\mathcal{F}}_{1s}$ and $\hat{\mathcal{P}}_{1s}$ are additional here because of the explicit accounting for flow through the lateral boundary.

6.9.1. The One-Dimensional Approximation to 'Flow-Turning'. The correspondence between the terms in (6.138) and (6.90) is clear. What is especially important are the effects represented by the sources at the lateral boundaries, $\hat{\mathcal{F}}_{1s}$ and $\hat{\mathcal{P}}_{1s}$, found from the formulas (6.120) and (6.121). It is important for interpretation of this result to remember (Annex B) that $\mathcal{F}_{1s}$ represents the source of momentum, and $\mathcal{P}_{1s}$ the pressure source, both associated with the mass source at the boundary. Moreover, the average values

of the sources may be zero (Annex C) or non-zero, as for a burning surface. We treat first the contribution to stability by unsteady momentum addition of flow at the boundary,

$$\int_0^L \frac{\hat{\mathfrak{F}}_{1s}}{\hat{\eta}_\ell}\frac{d\psi_\ell}{dx}S_c dx = \int_0^L \frac{1}{S_c}\left[(\bar{u}_s - \bar{u})\int \frac{\hat{m}_{sg}}{\hat{\eta}_\ell}dq + \left(\frac{\hat{u}_s - \hat{u}}{\hat{\eta}_\ell}\right)\int \bar{m}_{sg}dq\right]\frac{d\psi_\ell}{dx}S_c dx \tag{6.139}$$

Figure 6.15 shows interpretations of the various quantities appearing in (6.139).

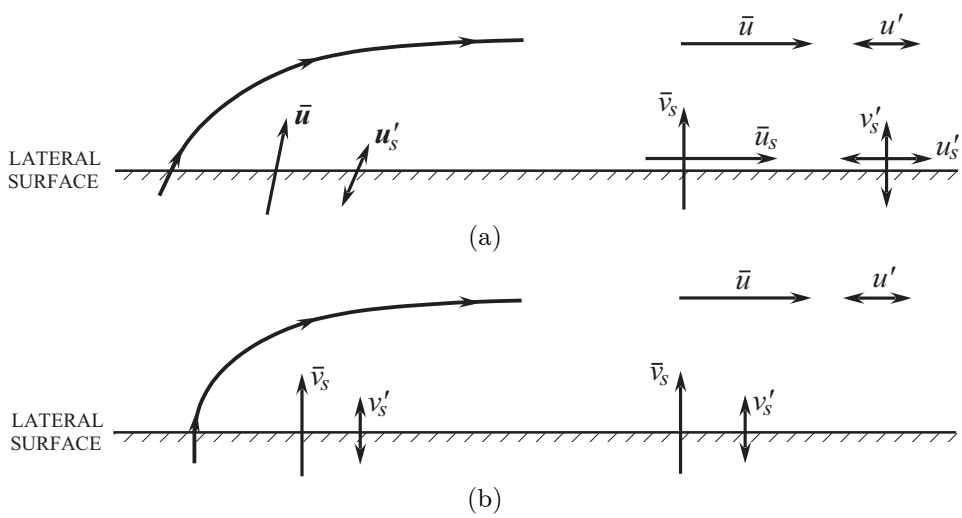

FIGURE 6.15. Velocity vectors for flow through a permeable boundary. (a) non-zero mean flow parallel to the boundary; (b) only normal flow at the boundary.

Observation, for example by use of films, and physical arguments, suggest that the average flow from the surface of a burning solid propellant is always normal to the surface. The situation sketched in Figure 6.15(a) apparantly does not exist. Hence we assume $\bar{u}_s = \hat{u}_s = 0$ as shown in Figure 6.15(b); (6.139) is therefore

$$\int_0^L \frac{\hat{\mathfrak{F}}_{1s}}{\hat{\eta}_\ell}\frac{d\psi_\ell}{dx}S_c dx = -\int_0^L \frac{1}{S_c}\left[\bar{u}\int \frac{\hat{m}_{sg}}{\hat{\eta}_\ell}dq + \frac{\hat{u}}{\hat{\eta}_\ell}\int \bar{m}_{sg}dq\right]\frac{d\psi_\ell}{dx}S_c dx \tag{6.140}$$

Substitute (6.89)b for $\hat{u}$ and the second term is

$$-\int_0^L \frac{1}{S_c}\frac{\hat{u}}{\hat{\eta}_\ell}\int \bar{m}_{sg}dq\frac{d\psi_\ell}{dx}S_c dx = i\frac{\bar{a}}{\gamma k_\ell}\int_0^L \left(\frac{d\psi_\ell}{dx}\right)^2 \int \bar{m}_{sg}dqdx \tag{6.141}$$

We estimate the first term in (6.140) by assuming $\hat{m}_{sg}$ to be independent of position on the surface; with $q(x)$ the total perimeter of the chamber at position x,

$$-\int_0^L \frac{1}{S_c}\bar{u}\int \frac{\hat{m}_{sg}}{\hat{\eta}_\ell}dq\frac{d\psi_\ell}{dx}S_c dx = -\frac{\hat{m}_{sg}}{\hat{\eta}_\ell}\int_0^L \bar{u}q\frac{d\psi_\ell}{dx}dx = -\left(\frac{1}{\hat{\eta}_\ell}\frac{\hat{m}_{sg}}{\bar{m}}\right)\bar{m}\int_0^L \bar{u}q\frac{d\psi_\ell}{dx}dx$$

The ratio in parentheses is the response function, of order unity (Chapter 2 equations (2.66) and (2.67), for example). Thus the term depends on the square of the mean velocity and must be ignored. Hence for use

in (6.138), combination of (6.140) and (6.141) gives

$$\frac{1}{\bar{p}E_\ell^2}\int_0^L \frac{\hat{\mathcal{F}}_{1s}}{\hat{\eta}_\ell}\frac{d\psi_\ell}{dx}S_c dx = i\frac{k_\ell}{\bar{\rho}\bar{a}E_\ell^2}\int_0^L \frac{1}{k_\ell^2}\left(\frac{d\psi_\ell}{dx}\right)^2 \int \bar{m}_{sg}dqdx \tag{6.142}$$

This result is the one-dimensional approximation to 'flow-turning'. It appeared first in equation (3.9) in Culick (1973), and has since been the motivation for considerable discussion in the literature and in various technical meetings. Always to be kept in mind is perhaps the most interesting aspect of the matter, the contrast with the results of three-dimensional analyses. An especially important property is the accuracy with which behavior that is necessarily three- (or two-) dimensional is approximated by the results of one-dimensional predictions.[22]

What has come to be accepted as the 'flow-turning' process has the following elementary interpretation for a burning solid propellant exposed to oscillations. We imagine that the solid/gas interface is fixed and that solid material advances to the interface with constant speed. As soon as the solid is transformed to gas, it begins to acquire both steady and oscillatory motion, partly due to viscous forces exerted by gas released earlier, but principally due to the oscillatory pressure. Thus the incoming fluid acquires sufficient unsteady motion to join the flow field existing at some distance from the interface. Figure 6.16 is a simplified interpretation of this process in two dimensions. From the interpretation just given, it is evident that, because work is done on the incoming fluid both to impart the oscillatory motions and to turn the flow as sketched in Figure 6.16, the process of 'flow-turning' constitutes a loss. For harmonic motions, oscillations parallel to the surface, the loss is given by (6.142) within the one-dimensional approximation. Twenty years after the approximation was deduced, Flandro (1995) showed rigorously with analysis of a two-dimensional flow that the result (6.142) is exact.

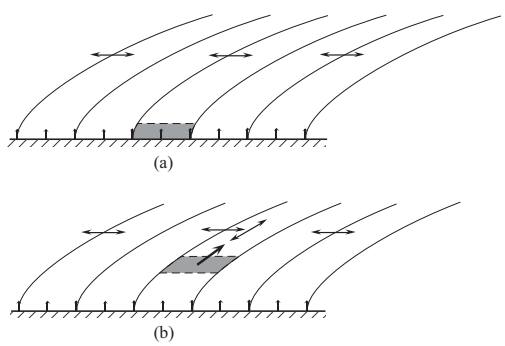

FIGURE 6.16. The origin of 'flow-turning': An element of fluid shown (a) at entry normal to a burning or porous surface, and (b) in an intermediate state of the process of acquiring the local axial velocity having mean and acoustic components.

If 'flow-turning' is the only contribution to momentum transfer at the lateral surface and there is no momentum addition within the volume ($\mathcal{F}_1 = 0$), the formula (6.138) becomes

$$\begin{aligned} k^2 = k_\ell^2 - i\frac{k_\ell}{\bar{a}E_\ell^2}&\left\{\left[\left(\gamma\frac{\hat{u}}{\hat{\eta}_\ell} + \bar{u}\psi_\ell\right)\psi_\ell S_c\right]_0^L + (\gamma-1)\int_0^L \psi_\ell^2\left[\frac{1}{S_c}\frac{d}{dx}(S_c\bar{u})\right]S_c dx\right\} \\ &-i\frac{k_\ell}{\bar{\rho}\bar{a}E_\ell^2}\int_0^L\left[\frac{1}{k_\ell^2}\left(\frac{d\psi_\ell}{dx}\right)^2\right]\int \bar{m}_{sg}dqdx + i\frac{k_\ell}{\bar{a}}\frac{1}{\bar{p}E_\ell^2}\int_0^L\left(\frac{\hat{\mathcal{P}}_1 + \hat{\mathcal{P}}_{1s}}{\hat{\eta}_\ell}\right)\psi_\ell S_c dx \end{aligned} \tag{6.143}$$

[22]We refer to behavior which, in principle at least, is covered by terms involving $\hat{\mathcal{F}}$ and $\hat{\mathcal{P}}$ in (6.90), and correspondingly may arise from $\hat{\mathcal{F}}_1$, $\hat{\mathcal{P}}_1$, $\hat{\mathcal{F}}_{1s}$ and $\hat{\mathcal{P}}_{1s}$ in (6.138).

6.9.2. The One-Dimensional Approximation to 'Pumping'. There is a second equally important contribution to the unsteady energy transfer accompanying flow through a lateral boundary. This process was mistakenly not included, with 'flow-turning', in the general analysis discussed by Culick (1973), although a restricted form was discussed at the end of the same paper (see Annex C). The basic process has acquired the name 'pumping', referring to the influence of the flow immediately adjacent to the boundary on the flow past the boundary. It arises because the flow *parallel* to the surface has a time-varying component which varies with position along the boundary. The discussion here concerns largely the one-dimensional counterpart of the two- or three-dimensional process first found and explained by Flandro (1995)a.

Due to conservation of mass, as demonstrated in Section 5.9.3, motion is then induced in the direction *normal* to the boundary. It is that portion of the fluid motion that is called 'pumping'. For the case of harmonic motions past an impermeable boundary, the fluid velocity accompanying the pumping action is given by equation (5.146). We investigate now the pumping action for the case when flow with average velocity $\bar{v}_b$ passes through the boundary. We assume that there is no fluctuating component of v at the surface: $v_b' = 0$.

Unlike the case for fully three-dimensional calculations, the first integral in (6.143), which has as part of its integrand the one-dimensional form of $\nabla \cdot \bar{u}$, is generally non-zero. The conservation of mass is expressed for one-dimensional flow by equation (B.2) written for steady purely gaseous flow,

$$\bar{u}\frac{d\bar{\rho}}{dx} = -\bar{\rho}\frac{1}{S_c}\frac{d}{dx}(S_c\bar{u}) + \frac{1}{S_c}\int \bar{m}_b dq$$

We take $\bar{\rho}$ to be strictly constant and the continuity equation for steady flow is

$$\frac{1}{S_c}\frac{d}{dx}(S_c\bar{u}) = \frac{1}{\bar{\rho}S_c}\int \bar{m}_b dq \tag{6.144}$$

Let $\bar{m}_b = \bar{m}_{sg}$ for the case here and substitute in (6.143) to give

$$\begin{aligned} k^2 = k_\ell^2 &- i\frac{k_\ell}{\bar{a}E_\ell^2}\left\{\left[\left(\gamma\frac{\hat{u}}{\hat{\eta}_\ell} + \bar{u}\psi_\ell\right)\psi_\ell S_c\right]_0^L + (\gamma-1)\int_0^L \psi_\ell^2 \int \frac{\bar{m}_{sg}}{\bar{\rho}}dqdx\right\} \\ &- i\frac{k_\ell}{\bar{a}E_\ell^2}\int_0^L\left[\frac{1}{k_\ell^2}\left(\frac{d\psi_\ell}{dx}\right)^2\right]\int\frac{\bar{m}_{sg}}{\bar{\rho}}dqdx + i\frac{k_\ell}{\bar{a}}\frac{1}{\bar{p}E_\ell^2}\int_0^L\left(\frac{\hat{\mathcal{P}}_1 + \hat{\mathcal{P}}_{1s}}{\hat{\eta}_\ell}\right)\psi_\ell S_c dx \end{aligned} \tag{6.145}$$

The definition (6.121) for $\mathcal{P}_1'$ gives the contribution from fluctuations of heat release within the flow,

$$\hat{\mathcal{P}}_1 = \frac{R}{C_v}\hat{Q}_1 = (\gamma-1)\hat{Q}_1 \tag{6.146}$$

From (6.121) we find the term representing the effect of flow through the lateral boundary,

$$\hat{\mathcal{P}}_{1s} = \frac{R}{C_v}\frac{1}{S_c}\left\{(\bar{h}_{0s} - \bar{e}_0 + C_v\bar{T})\int \hat{m}_{sg}dq + (\hat{h}_{0s} - \hat{e}_0 + C_v\hat{T})\int \bar{m}_{sg}dq\right\} \tag{6.147}$$

After substitution of the appropriate definitions,

$$h_{0s} - e_0 + C_vT := (C_pT_s + \frac{u_s^2}{2}) - (C_vT + \frac{u^2}{2}) + C_vT = C_p\Delta T_s + C_pT + \frac{1}{2}(u_s^2 - u^2)$$

where $\Delta T_s = T_s - T$. Because the kinetic energy is normally negligible in combustion chambers,

$$\frac{R}{C_v}(h_{0s} - e_0 + C_vT) \approx \frac{C_p}{C_v}RT + \frac{C_p}{C_v}R\Delta T = a^2 + \gamma R\Delta T \tag{6.148}$$

Hence (6.147) becomes

$$\hat{\mathcal{P}}_{1s} = \frac{1}{S_c}(\bar{a}^2 + \gamma R\Delta\bar{T}_s)\int \hat{m}_{sg}dq + \frac{1}{S_c}(\gamma R\hat{T} + \gamma R\Delta\hat{T}_s)\int \bar{m}_{sg}dq \tag{6.149}$$

Substitution of (6.146) and (6.149) into (6.145) gives

$$
\begin{aligned}
k^2 = k_\ell^2 &- i\frac{k_\ell}{\bar{a}E_\ell^2}\left\{\left[\left(\gamma\frac{\hat{u}}{\hat{\eta}_\ell}+\bar{u}\psi_\ell\right)\psi_\ell S_c\right]_0^L + (\gamma-1)\int_0^L \psi_\ell^2 \int \frac{\bar{m}_{sg}}{\bar{\rho}}dqdx\right\} \\
&- i\frac{k_\ell}{\bar{a}E_\ell^2}\int_0^L\left[\frac{1}{k_\ell^2}\left(\frac{d\psi_\ell}{dx}\right)^2\right]\int \bar{m}_{sg}dqdx + i\frac{k_\ell}{\bar{a}}\frac{1}{\bar{p}E_\ell^2}(\gamma-1)\int_0^L \frac{\hat{Q}_1}{\hat{\eta}_\ell}\psi_\ell S_c dx \qquad (6.150)\\
&+ i\frac{k_\ell}{\bar{a}}\frac{1}{\bar{p}E_\ell^2}\int_0^L \psi_\ell \int\left[(\bar{a}^2+\gamma R\Delta\bar{T}_s)\frac{\hat{m}_{sg}}{\hat{\eta}_\ell} + \left(\frac{\gamma R\hat{T}}{\hat{\eta}_\ell}+\gamma R\frac{\Delta\hat{T}_s}{\hat{\eta}_\ell}\right)\bar{m}_{sg}\right]dqdx
\end{aligned}
$$

Temporarily denote the last integral by P and rewrite the various terms in the following way:

$$
\begin{aligned}
\hat{\eta}_\ell P &= \int_0^L \psi_\ell \int\left[\left(\bar{a}^2+\gamma R\Delta\bar{T}_s\right)\hat{m}_{sg} + \gamma R(\hat{T}+\Delta\hat{T}_s)\bar{m}_{sg}\right]dqdx \\
&= \bar{\rho}\bar{a}^2\int_0^L \psi_\ell \int\left(\frac{\hat{m}_{sg}}{\bar{\rho}}+\frac{\Delta\hat{T}_s}{\bar{\rho}\bar{T}}\bar{m}_{sg}\right)dqdx + \gamma R\bar{T}\int_0^L \psi_\ell\frac{\hat{T}}{\bar{T}}\int \bar{m}_{sg}dqdx + \int_0^L \psi_\ell\int(\gamma R\Delta\bar{T}_s)\hat{m}_{sg}dqdx \\
&= \bar{\rho}\bar{a}^2\int_0^L \psi_\ell \int\left(\frac{\hat{m}_{sg}}{\bar{\rho}}+\frac{\Delta\hat{T}_s}{\bar{\rho}\bar{T}}\bar{m}_{sg}\right)dqdx + R\bar{T}(\gamma-1)\hat{\eta}_\ell\int_0^L \psi_\ell^2\int \bar{m}_{sg}dqdx + \int_0^L \psi_\ell\int(\gamma R\Delta\bar{T}_s)\hat{m}_{sg}dqdx
\end{aligned}
$$

The penultimate term can be written using the relation (6.144) for conservation of mass,

$$
\begin{aligned}
R\bar{T}(\gamma-1)\int_0^L \psi_\ell^2\int \bar{m}_{sg}dqdx &= R\bar{\rho}\bar{T}(\gamma-1)\int_0^L \psi_\ell^2\int\frac{\bar{m}_{sg}}{\bar{\rho}}dqdx \\
&= \bar{\rho}(\gamma-1)\int_0^L \psi_\ell^2\left[\frac{1}{S_c}\frac{d(S_c\bar{u})}{dx}\right]S_c dx
\end{aligned}
$$

Upon substitution of $\hat{\eta}_\ell P$ in (6.150), this term is cancelled by the second term in curly brackets; k^2 is now given by the sum of terms[23]

$$
\begin{aligned}
k^2 = k_\ell^2 &- i\frac{k_\ell}{\bar{a}E_\ell^2}\left[\left(\gamma\frac{\hat{u}}{\hat{\eta}_\ell}+\bar{u}\psi_\ell\right)\psi_\ell S_c\right]_0^L + i\frac{k_\ell}{\bar{a}}\frac{\gamma}{E_\ell^2}\int_0^L \psi_\ell\int\left(\frac{\hat{m}_{sg}}{\bar{\rho}}+\frac{\Delta\hat{T}_s}{\bar{\rho}\bar{T}}\bar{m}_{sg}\right)dqdx \\
&- i\frac{k_\ell}{\bar{a}E_\ell^2}\int_0^L\left[\frac{1}{k_\ell^2}\left(\frac{d\psi_\ell}{dx}\right)^2\right]\int \bar{m}_{sg}dqdx + i\frac{k_\ell}{\bar{a}}\frac{(\gamma-1)}{\bar{p}E_\ell^2}\int_0^L \frac{\hat{Q}_1}{\hat{\eta}_\ell}\psi_\ell S_c dx \qquad (6.151)\\
&+ i\frac{k_\ell}{\bar{a}}\frac{1}{\bar{p}E_\ell^2}\int_0^L \psi_\ell\int(\gamma R\Delta\bar{T}_s)\hat{m}_{sg}dqdx
\end{aligned}
$$

When interpreting this result, it is helpful to recall that with $\bar{a}k = \omega + i\alpha$, $e^{-i\bar{a}kt} = e^{-i(\omega+i\alpha)t} = e^{\alpha t - i\omega t}$, so $\alpha < 0$ for decay of waves, i.e., the imaginary part of the right-hand side of (6.151) must be negative for stability.

[23] Taking into account differences of definitions (mainly $e^{i\bar{a}kt}$ in earlier work is replaced by $e^{-i\bar{a}kt}$ here, and $p'_\ell = \hat{p}_\ell e^{i\bar{a}k_\ell t}$ is written $p'_\ell = \bar{p}\hat{\eta}_\ell\psi_\ell e^{-i\bar{a}k_\ell t}$) equation (6.151) agrees with equation (3.13) in Culick (1973) written for a flow without particles. The last term in (6.151) was mistakenly dropped from (3.13) in the earlier work.

For practical purposes it is necessary to have the real and imaginary parts of k, corresponding to the formulas (6.93) and (6.94) found for three-dimensional waves. Write (6.151) as

$$k^2 = k_\ell^2 + (A + iB)$$

Then with $\omega - \omega_\ell$ and α small,

$$\omega - \omega_\ell = \frac{\bar{a}^2}{2\omega_\ell} A$$
$$\alpha = \frac{\bar{a}^2}{2\omega_\ell} B$$

Then with $\bar{a}k_\ell/\omega_\ell = 1$, we find for the real and imaginary parts of (6.151),

$$\begin{aligned}\omega = \omega_\ell &- \frac{1}{2E_\ell^2}\left[\left(\gamma\frac{\hat{u}^{(i)}}{\hat{\eta}_\ell}\right)\psi_\ell S_c\right]_0^L - \frac{\gamma}{E_\ell^2}\int_0^L \psi_\ell \int\left(\frac{\hat{m}_{sg}^{(i)}}{\bar{\rho}} + \frac{\Delta\hat{T}_s^{(i)}}{\bar{\rho}\bar{T}}\bar{m}_{sg}\right)dqdx \\ &- \frac{(\gamma-1)}{2E_\ell^2}\int_0^L \frac{\hat{Q}_1^{(i)}}{\hat{\eta}_\ell}\psi_\ell S_c dx - \frac{1}{2E_\ell^2}\int_0^L \psi_\ell(\gamma R\Delta\bar{T}_s)\hat{m}_{sg}^{(i)}dqdx\end{aligned} \tag{6.152}$$

$$\begin{aligned}\alpha = &-\frac{1}{2E_\ell^2}\left[\left(\gamma\frac{\hat{u}^{(r)}}{\hat{\eta}_\ell} + \bar{u}\psi_\ell\right)\psi_\ell S_c\right]_0^L + \frac{\gamma}{2E_\ell^2}\int_0^L \psi_\ell \int\left(\overset{*}{\frac{\hat{m}_{sg}^{(r)}}{\bar{\rho}}} + \frac{\Delta\hat{T}_s^{(r)}}{\bar{\rho}\bar{T}}\bar{m}_{sg}\right)dqdx \\ &- \frac{\gamma}{2E_\ell^2}\int_0^L \left[\overset{**}{\frac{1}{k_\ell^2}\left(\frac{d\psi_\ell}{dx}\right)^2}\right]\int \bar{m}_{sg}dqdx + \frac{(\gamma-1)}{2E_\ell^2}\int_0^L \frac{\hat{Q}_1^{(r)}}{\hat{\eta}_\ell}\psi_\ell S_c dx \\ &+ \frac{1}{2E_\ell^2}\int_0^L \psi_\ell \int(\gamma R\Delta\bar{T}_s)\hat{m}_{sg}^{(r)}dqdx\end{aligned} \tag{6.153}$$

The terms containing $\Delta\hat{T}_s$ represent the effects of a frequency shift depending on $\Delta\hat{T}_s^{(i)}$, the part of $\Delta\hat{T}_s$ out-of-phase with the pressure oscillation; and attenuation depending on the in-phase part $\Delta\hat{T}_s^{(r)}$ associated with convection inward at the lateral boundary. Fluctuations of the mass flux inward affect the frequency shift and attenuation by carrying flow having an average temperature difference $\Delta\hat{T}_s$, represented by the last term of 6.152 and 6.153.

More significant are the terms identified by $*$ and $**$ which we will temporarily denote as the contributions $\tilde{\alpha}_{sp}$ and α_{FT} to α:

$$\tilde{\alpha}_{sp} = \frac{\gamma}{2E_\ell^2}\int_0^L \psi_\ell \int \frac{\hat{m}_{sg}^{(r)}}{\bar{\rho}}dqdx \tag{6.154}$$

$$\alpha_{FT} = -\frac{\gamma}{2E_\ell^2}\int_0^L \left[\frac{1}{k_\ell^2}\left(\frac{d\psi_\ell}{dx}\right)^2\right]\int \bar{m}_{sg}dqdx \tag{6.155}$$

The contribution α_{FT}, generally referred to as the 'flow-turning' damping, was discovered by Culick (1973) in his analysis of unsteady one-dimensional oscillations.

In his 1995a paper, Flandro found a second contribution which Culick had not identified[24] in his 1973 paper. This difference has directly—or indirectly—been part of the cause for much discussion, occasionally controversy. The difference (with hindsight!) is illusory: The 1973 result, equation (6.153) here, contains the important process called "pumping"[25] by Flandro.

In the 1973 work, the mass influx was implicitly taken to represent flow of combustion products from burning solid propellant. That was certainly what the author had in mind. But the quantity m_{sg} may of course represent flow normal to the lateral boundary due to any cause. For example, in Section 6 of Culick (1973) and here in Annex C, the fluctuation $m' = \bar{\rho}v'$ represents changes associated with the acoustic boundary layer. The time-averaged value $\overline{m'}$ is then zero. For the linear behavior we are dealing with, we may write m_{sg} as a superposition of various possible contributions. It is sufficient for our purpose to take m'_{sg} as the sum of the fluctuation m'_{sc} due to unsteady combustion; and the unsteadiness m'_{PU} produced by the flow:

$$m'_{sg} = m'_{sc} + m'_{PU} \tag{6.156}$$

Thus for harmonic variations in time, (6.154) becomes a sum,

$$\tilde{\alpha}_{sp} = \alpha_{sc} + \alpha_{PU} = \frac{\gamma}{2E_\ell^2}\int_0^L \psi_\ell \int \left(\frac{\hat{m}_{sc}^{(r)}}{\bar{\rho}} + \frac{\Delta\hat{T}_s^{(r)}}{\bar{\rho}\bar{T}}\bar{m}_{sg}\right) dqdx + \frac{\gamma}{2E_\ell^2}\int_0^L \psi_\ell \int \frac{\hat{m}_{PU}^{(r)}}{\bar{\rho}} dqdx \tag{6.157}$$

In the first form, $\hat{m}_{sc}^{(r)}$ may be replaced, for example, by its formula obtained after introducing the admittance or response function defined in Section 6.7.2. Together, the flow-turning contribution, (6.155), and the second term of (6.157), which is the one-dimensional form of the 'pumping' process, form the acoustic interaction at a surface,

$$\alpha_A = \alpha_{FT} + \alpha_{PU} = -\frac{\gamma}{2E_\ell^2}\int_0^L \left[\frac{1}{k_\ell^2}\left(\frac{d\psi_\ell}{dx}\right)^2\right] \int \bar{m}_{sg} dqdx + \frac{\gamma}{2E_\ell^2}\int_0^L \psi_\ell \int \frac{\hat{m}_{PU}^{(r)}}{\bar{\rho}} dqdx \tag{6.158}$$

This result is the one-dimensional counterpart of (49) in Flandro (1995)b, an identification we indicate here without decoding the various definitions of dimensionless quantities[26]:

$$\text{FLOW–TURNING} \qquad -\frac{\gamma}{2E_\ell^2}\int_0^L \left[\frac{1}{k_\ell^2}\left(\frac{d\psi_\ell}{dx}\right)^2\right] \int \bar{m}_{sg} dqdx \quad \longleftrightarrow \quad +\frac{1}{2E_m^2}\iint \frac{M_b}{k_m}\tilde{\mathbf{u}}^{(i)} \cdot \nabla p'_m dS_b \tag{6.159}$$

$$\text{PUMPING} \qquad \frac{\gamma}{2E_\ell^2}\int_0^L \psi_\ell \int \frac{\hat{m}_{PU}}{\bar{\rho}} dqdx \quad \longleftrightarrow \quad -\frac{1}{2E_m^2}\iint \hat{\mathbf{n}} \cdot \tilde{\mathbf{u}}^{(r)} p'_m dS_b \tag{6.160}$$

As an aid to recognizing that the correspondence noted is indeed true, four remarks are helpful:

(i) By Flandro's definition, p'_m does not contain any time dependence.
(ii) In the right-hand side of (6.159) specialized to one dimension, $\tilde{\mathbf{u}}^{(i)}$ and $\nabla p'_m$ both become proportional to $\frac{d\psi_\ell}{dx}$.
(iii) The mass flux $\bar{m}_{sg} = \bar{\rho}\bar{u}_{sg} = \bar{\rho}\bar{a}\frac{\bar{u}_{sg}}{\bar{a}} = \bar{\rho}\bar{a}\bar{M}_{sg}$, and $\bar{M}_{sg}$ is the same as M_b, the Mach number of the average flow departing the surface.
(iv) For the correspondence (6.160), we note that $p'_m \sim \psi_\ell$ and $\hat{\mathbf{n}} \cdot \tilde{\mathbf{u}}^{(r)} \sim \frac{\hat{m}_{PU}}{\bar{\rho}}$. To make equality hold in (6.160), closer attention must be paid to the details.

[24] An example was treated in Section 6 of Culick's 1973 paper, but the generality of the process was not recognized; see Annex C.

[25] It is referred to as "surface pumping" here, denoted $(\ )_{sp}$ to distinguish it from subscript $(\ )_p$ often used to identify contributions from particulate material.

[26] Note that $(\bar{\ })$ denotes the rotational part of velocity, which cannot be distinguished for one-dimensional flow.

Verifying the exact correspondence, which is only implied in (6.159) and (6.160), is not germane here. (See the following section.) The important point is that the one-dimensional approximation does in fact contain both 'flow-turning' and 'pumping'. The physical interpretation of flow-turning, always a mechanism of energy loss for flow inward, has already been described with reference to Figure 6.16. Annex C explains the pumping process which, the preceeding remarks show, must occur whether flow issues from the surface, or the surface is impermeable.

Much attention has been given these two processes because they can bring significant contributions to the rate of change of acoustic energy in a combustion chamber. Incorporating the form of the $*$ term in (6.153), written according to this discussion, we have

$$\begin{aligned}\alpha = &-\frac{1}{2E_\ell^2}\left[\left(\gamma\frac{\hat{u}^{(r)}}{\hat{\eta}_\ell}+\bar{u}\psi_\ell\right)\psi_\ell S_c\right]_0^L+\frac{\gamma}{2E_\ell^2}\int_0^L\psi_\ell\int\left(\frac{\hat{m}_{sc}^{(r)}}{\bar{\rho}}+\frac{\Delta\hat{T}_s^{(r)}}{\bar{\rho}\bar{T}}\bar{m}_{sg}\right)dqdx\\ &-\frac{\gamma}{2E_\ell^2}\int_0^L\left[\frac{1}{k_\ell^2}\left(\frac{d\psi_\ell}{dx}\right)^2\right]\int\bar{m}_{sg}dqdx+\frac{\gamma}{2E_\ell^2}\int_0^L\psi_\ell\int\frac{\hat{m}_{PU}^{(r)}}{\bar{\rho}}dqdx\\ &+\frac{\gamma-1}{2E_\ell^2}\int_0^L\frac{\hat{Q}_1^{(r)}}{\hat{\eta}_\ell}\psi_\ell S_c dx+\frac{1}{2E_\ell^2}\int_0^L\psi_\ell\int(\gamma R\Delta\bar{T}_s)\hat{m}_{sg}^{(r)}dqdx\end{aligned}\tag{6.161}$$

The terms in the first line contain the principal sources of driving due to combustion at the end of the chamber and on the lateral boundary; and attenuation due to the exhaust nozzle. Flow-turning and pumping are represented by the next two terms. The last line contains the effects of volumetric heat addition and the term representing the effect of unsteady mass addition when the temperature difference $\Delta\bar{T}_s = \bar{T}_s - \bar{T}$ is non-zero.

Flandro (1995)a has given an example showing clearly the effects of flow-turning and pumping in data taken by Harris (1994) for unstable oscillations in the laboratory motors sketched in Figure 6.17. Figure 6.18 shows the result reported by Flandro. The dashed line is the locus representing exact agreement between predicted and measured values of the growth rate. Flandro carried out calculations according to the Standard Stability Program, SSP (Nickerson *et al.* 1983) which did not contain the pumping term; and SSP with the pumping term added, giving points labeled "SSP with Vorticity." These results seem clearly to show that the pumping term is a positive ('driving') contribution improving the agreement between the experimental results and theoretical values. The latter were computed with $\hat{Q}_1^{(r)} = \Delta\bar{T}_s = 0$ and assumed values for the propellant response.

The test program conducted by Harris (1994) produced very useful data carefully reduced. Results for the decay rates shown in Figure 6.18 were obtained by measurements of the waves generated by pulses having amplitudes approximately 1% of the chamber pressure. In the reference cited, results are given for two grain diameters; three grain lengths; four grain configurations; three HTPB/AP propellants; and three chamber pressures. Figure 6.19 shows the decay of the fundamental mode in one test, the raw signal having been processed by a bandpass filter. In this case, the motor had a cylindrical grain, 2.55 inch diameter and 30.6 inches long. The data reported by Harris cover fairly broad conditions and can probably be used for wider checks of theoretical results than carried out to date.

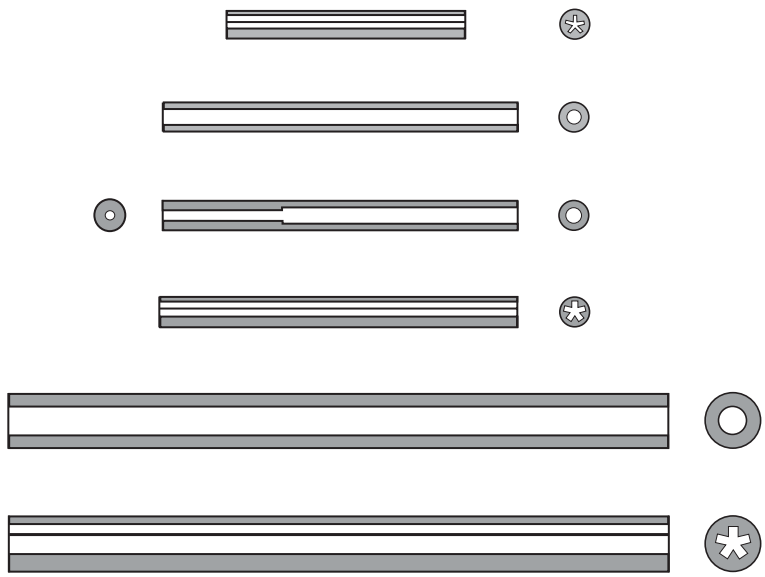

FIGURE 6.17. Grains used in laboratory motors for which data were taken for unstable oscillations (Harris 1994).

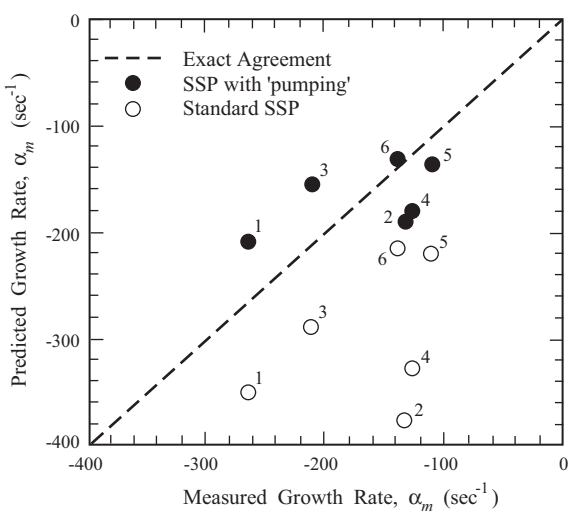

FIGURE 6.18. A comparison of data taken with the motors shown in Figure 6.17 with predictions according to (6.161) with $Q_1 = \Delta\bar{T}_s = \Delta\hat{T}_s^{(r)} = 0$. Accounting for the 'pumping' process gives closer agreement between theory and experiment (Flandro 1995b).

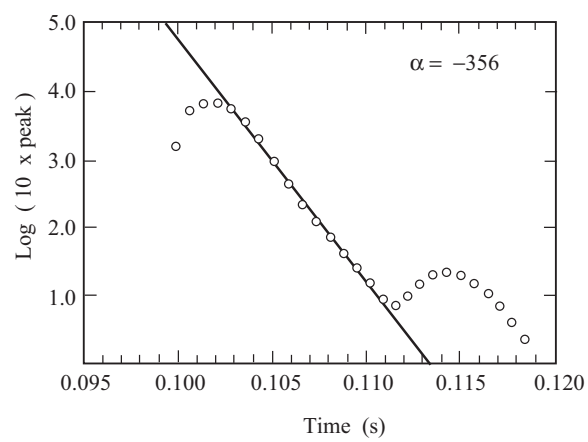

FIGURE 6.19. Calculation of the decay of the fundamental mode following a pulse (Harris 1994).

6.9.3. Stability of a Simple T-Burner. Since its invention, the T-burner has been widely used a device for measuring the dynamics of a burning solid propellant. For a number of reasons, largely associated with experimental difficulties, it has never fulfilled its great promise. Yet despite the appearance of several other promising methods (see Section 2.2.3), the T-burner remains generally the primary means considered for determining—at least qualitatively—the unsteady behavior of a new propellant. Another method may ultimately prove to be superior for a particular application, but first understanding the T-burner, how it works, and its practical deficiencies is usually the proper strategy to follow.

Two documents, "the T-Burner Manual," CPIA Publication 191 (1969) and "T-Burner Testing of Metallized Solid Propellants," Air Force Rocket Propulsion Laboratory Report AFRPL-TR-74-28, cover virtually all practices existing in the 1970s. Both volumes incorporated the experiences and contributions of all practitioners in the U.S. Two decades later, extended test programs involving groups in the U.S., France, Canada, and Australia collaborated in test programs based primarily on the "Pulsed T-burner," to refine the methods mainly for treating metallized propellants (Blomshield *et al.* 1991, 1992 and 1997).

In this section, we reproduce the simplest analysis of the T-burner, including comparison with early test data, to show some of the difficulties the method presents (Beckstead and Culick, 1971). Unresolved problems still remain. If we ignore the possibility that combustion produces particles in the flow, and we assume that combustion occurs only on the surfaces of discs having the diameter of the tube,[27] the square of the wavenumber of longitudinal oscillations is

$$k^2 = k_\ell^2 - 4i\frac{k_\ell}{L}(A_b + \overline{M}_b) + \alpha_\alpha\Big(\frac{k_\ell}{\bar{a}}\Big) \tag{6.162}$$

where α_α is the decay constant representing all losses in the system during a period of steady oscillations.

With $k^2 = (\omega - i\alpha)^2/\bar{a}^2 \approx (\omega/\bar{a})^2 - i(2\alpha\omega)/\bar{a}^2 \approx (\omega/\bar{a})^2 - i(2\alpha\omega_\ell/\bar{a}^2) \approx (\omega/\bar{a})^2 - i(2\alpha\ell\pi\bar{a}/L)$ and $k_\ell = \ell\pi/L$,

$$\Big(\frac{\omega}{\bar{a}}\Big) - i(2\alpha\ell\pi)\frac{1}{L\bar{a}} = \Big(\frac{\ell\pi}{L}\Big)^2 - i\frac{4\ell\pi}{L^2}(A_b + \overline{M}_{\bar{b}}) + \alpha_\alpha\Big(\frac{k_\ell}{\bar{a}}\Big)$$

The real and imaginary parts are

$$\Big(\frac{\omega L}{\bar{a}}\Big)^2 = (\ell\pi)^2 + 4(\ell\pi)A_b^{(i)} = (\ell\pi)^2 + 4\ell\pi\gamma\overline{M}R_b^{(i)} \tag{6.163}$$

$$\frac{\alpha L}{\bar{a}} = 2(A_b^{(r)} + \overline{M}_b) - \alpha_d\frac{L}{\bar{a}} = 2(\gamma\overline{M}_b R_b^{(r)}) - \alpha_d\frac{L}{\bar{a}} \tag{6.164}$$

The admittance function can be replaced by the response function with the definitions given in Section 6.7.2,

$$A_b = \gamma\frac{\bar{p}}{\bar{a}}\frac{\bar{u}}{p'}\Big(\frac{m'}{\overline{m}} - \frac{p'}{\bar{p}}\Big) = \gamma\overline{M}_b\Big(\frac{m'/\overline{m}}{p'/\bar{p}} - \frac{\rho'/\bar{\rho}}{p'/\bar{p}}\Big) = \gamma\overline{M}_b R_b - \overline{M}_b$$

in which the last equality rests on the approximation that the wave propagation is isentropic. Then (6.163) and (6.164) can be written

$$R_b^{(i)} = \frac{1}{4\gamma\ell\pi\overline{M}_b}\Big[\Big(\frac{\omega L}{\bar{a}}\Big)^2 - (\ell\pi)^2\Big] \tag{6.165}$$

$$R_b^{(r)} = \frac{1}{2\gamma\overline{M}_b}\frac{(\alpha + \alpha_d)L}{\bar{a}} \tag{6.166}$$

[27]Extension of the analysis to other grain configurations can be accomplished, but attention must be paid to the form of the average flowfield and to the effects of edges of the grains.

According to (6.165) and as observed experimentally, the frequency of oscillation is close to the classical longitudinal value, almost always the fundamental mode ($\ell = 1$), so

$$\left(\frac{\omega L}{\bar{a}}\right)^2 - (\ell\pi)^2 = \left(\frac{\omega L}{\bar{a}} + \ell\pi\right)\left(\frac{\omega L}{\bar{a}} - \ell\pi\right) \approx 2\ell\pi\left(\frac{\omega L}{\bar{a}} - \ell\pi\right)$$

and (6.165) becomes

$$R_b^{(i)} = \frac{1}{2\gamma\overline{M}_b}\left(\frac{\omega L}{\bar{a}} - \ell\pi\right) \tag{6.167}$$

Equations (6.166) and (6.167) correspond to (6.25) and (6.26) for an L^* burner. Hence if we assume the result found by Denison and Baum for the response function, we find the solutions (6.126) and (6.127) for the parameters A and B, but with

$$k_1 = \frac{1}{2\gamma\overline{M}_b}\left(\frac{\omega L}{\bar{a}} - \ell\pi\right); \qquad k_2 \frac{1}{2\gamma\overline{M}_b}\frac{(\alpha + \alpha_\alpha)L}{\bar{a}} \tag{6.168)a,b}$$

It has been common practice to interpret T-burner data using only equation (6.126), justified with the observation that the frequency of the oscillations has very closely the classical value, $\omega \approx \ell\pi\frac{\bar{a}}{L}$ so equation (6.127) can be ignored. Then, for example, if Denison and Baum's formula is used, correlations of experimental results are carried out with the two parameters A and B. In fact, one should use only one. Just as for data taken with an L^* burner, there are two parameters and two equations. If one equation is dropped then, in some sense, so should one parameter! Otherwise, the fit or no-fit to data cannot be interpreted as truth or falsity of Denison and Baum's result.

On the other hand, strictly one has the basis, equations (6.126) and (6.127), for a two-parameter family corresponding to equations (6.25) and (6.26), and Figure 6.8 for the L^*-burner. Assume that the T-burner oscillates in the lowest mode, the fundamental or first harmonic, and let $\zeta = (2\gamma\overline{M}_b)^{-1}$. Then equations (6.126) and (6.127) are

$$\begin{aligned} R_b^{(r)} &= \zeta(\alpha_d\tau_c + \alpha\tau_c) = \zeta\alpha_t\tau_c \\ R_b^{(i)} &= \zeta\left(\frac{\omega L}{\bar{a}} - \pi\right) = \zeta(\omega\tau_c - \pi) \end{aligned} \tag{6.169)a,b}$$

Beckstead and Culick chose to construct the two-parameter A, B family of curves in the $\alpha_t\tau_c, \Omega$ plane rather than the $\omega\tau_c^*, \Omega$ plane used for the L^* burner ($\tau_c^* = L^*c^*/RT$, $\tau_c = L/\bar{a}$). Figure 6.20 shows the result they found, with data taken for A-13 propellant. This interpretation of the dynamical behavior is clearly unsuccessful. The data for a given value of chamber pressure should lie on a vertical line; that is they should be independent of frequency.

The authors tried—unsuccessfully—to rationalize the result. It seems unlikely that the data is so wildly poor as the chart may suggest. The analysis is straightforward and transparent; the viewpoint taken seems to be correct, and unlikely to be deeply flawed in any event. Probably the source of the evident inaccuracy is the special form of the response function. While the Denison and Baum formula captures an important part of the behavior, the two-parameter formula is apparently an over-simplification. Several modifications are discussed briefly in Section 2.2. There seem to be no subsequent efforts to use data in the manner suggested by Beckstead and Culick. However, the approach taken in the present section, and in Section 6.2 with results produced by low frequency burners still appears to be worthwhile.

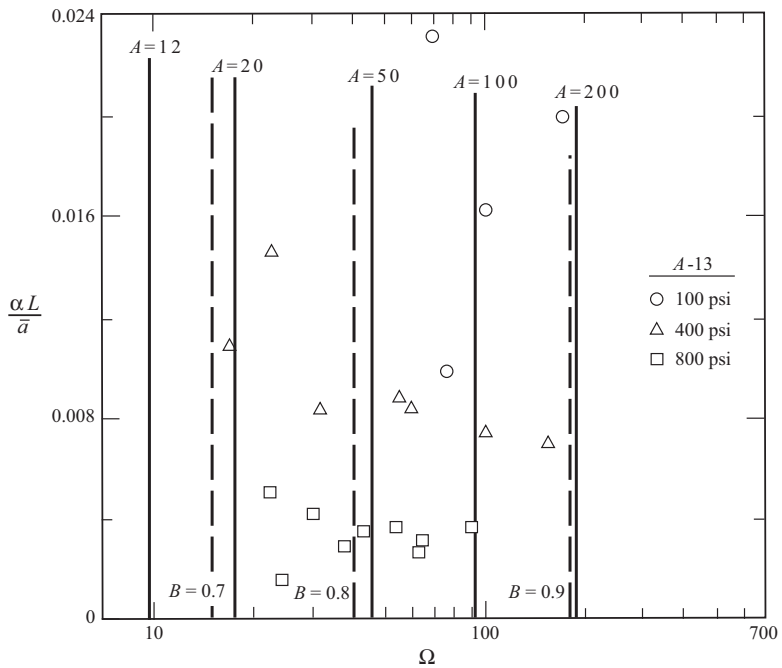

FIGURE 6.20. A T-burner chart for determining the parameters A and B; data are shown for the propellant A-13 (Beckstead and Culick 1971).

6.10. Combined Three-Dimensional and One-Dimensional Results

There remains a significant gap in the formal treatment of stability. In Section 6.7 we have deduced the formula (6.90) for the wavenumber and (6.94) for the growth or decay rate, of three-dimensional disturbances. Separately in Section 6.9 we have found the approximations (6.151) and (6.161) to the corresponding quantities for one-dimensional motions. For easy comparison, we repeat the results here, preceded by their origins. The reasoning begins with the precise correspondence between (6.90) and (6.138):

3-D Equation (6.90)

$$\begin{aligned} k^2 - k_n^2 = -i\frac{k_n}{\bar{a}E_n^2}\left\{\oiint\left[\gamma\frac{\hat{\mathbf{u}}}{\eta_n}\cdot\hat{\mathbf{n}} + \bar{\mathbf{u}}\cdot\hat{\mathbf{n}}\psi_n\right]\psi_n dS + (\gamma-1)\int\psi_n^2\nabla\cdot\bar{\mathbf{u}}dV\right\} \\ - \frac{1}{\bar{p}E_n^2}\int\left[\frac{\hat{\boldsymbol{\mathcal{F}}}}{\hat{\eta}_n}\cdot\nabla\psi_n + i\frac{k_n}{\bar{a}}\frac{\hat{\mathcal{P}}}{\hat{\eta}_n}\psi_n\right]dV \end{aligned} \tag{6.170}$$

1-D Equation (6.138)

$$\begin{aligned} k^2 - k_\ell^2 = -i\frac{k_\ell}{\bar{a}E_\ell^2}\left\{\left[\left(\gamma\frac{\hat{u}}{\eta_\ell} + \bar{u}\psi_\ell\right)\psi_\ell S_c\right]_0^L + (\gamma-1)\int_0^L\psi_\ell^2\left[\frac{1}{S_c}\frac{d}{dx}(S_c\bar{u})\right]S_c dx\right\} \\ - \frac{1}{\bar{p}E_\ell^2}\int_0^L\left[\left(\frac{\hat{\mathcal{F}}_1 + \hat{\mathcal{F}}_{1s}}{\eta_\ell}\right) + i\frac{k_\ell}{\bar{a}}\left(\frac{\hat{\mathcal{P}}_1 + \hat{\mathcal{P}}_{1s}}{\hat{\eta}_\ell}\right)\psi_\ell\right]S_c dx \end{aligned} \tag{6.171}$$

As the development in Section 6.9 showed, the term containing $\hat{\mathcal{F}}_{1s}$ leads to the formula for 'flow-turning', which is therefore a consequence of momentum transfer between the flow entering at the boundary and the flow in the chamber. Then (6.138) becomes (6.143); if we retain the possibility for momentum addition

within the volume, $\hat{\mathcal{F}}_1$ is non-zero, and (6.138) is

$$k^2 - k_\ell^2 = -i\frac{k_\ell}{\bar{a}E_\ell^2}\left\{\left[\left(\gamma\frac{\hat{u}}{\hat{\eta}_\ell} + \bar{u}\psi_\ell\right)\psi_\ell S_c\right]_0^L + (\gamma-1)\int_0^L \psi_\ell^2\left[\frac{1}{S_c}\frac{d}{dx}(S_c\bar{u})\right]S_c dx\right\}$$
$$-\frac{1}{\bar{p}E_\ell^2}\int\frac{\hat{\mathcal{F}}_1}{\hat{\eta}_\ell}\frac{d\psi_\ell}{dx}S_c dx - i\frac{k_\ell}{\bar{\rho}\bar{a}E_\ell^2}\int_0^L\left[\frac{1}{k_\ell^2}\left(\frac{d\psi_\ell}{dx}\right)^2\right]\int\bar{m}_{sg}dqdx + i\frac{k_\ell}{\bar{a}}\frac{1}{\bar{p}E_\ell^2}\int_0^L\left(\frac{\hat{\mathcal{P}}_1+\hat{\mathcal{P}}_{1s}}{\hat{\eta}_\ell}\right)\psi_\ell S_c dx \tag{6.172}$$

This is (6.145) with the addition of the integral containing $\hat{\mathcal{F}}_1$ and (6.144) used in the first integral.

The 'pumping' term in k^2 arises from $\hat{\mathcal{P}}_{1s}$ while $\hat{\mathcal{P}}_1$ produced the term containing heat release, equation (6.146). If we do not write $\hat{\mathcal{P}}_1$ as the heat release, and ignore the cancellation noted just before (6.151), equation (6.172) is

$$k^2 = k_\ell^2 - i\frac{k_\ell}{\bar{a}E_\ell^2}\overset{\text{3D}}{\left[\left(\gamma\frac{\hat{u}}{\hat{\eta}_\ell} + \bar{u}\psi_\ell\right)\psi_\ell S_c\right]_0^L} - \frac{ik_\ell}{\bar{a}E_\ell^2}(\gamma-1)\int_0^L\psi_\ell^2\overset{\text{3D}}{\left[\frac{1}{S_c}\frac{d}{dx}(S_c\bar{u})\right]}S_c dx$$
$$-\frac{1}{\bar{p}E_\ell^2}\overset{\text{3D}}{\int_0^L\frac{\hat{\mathcal{F}}_1}{\hat{\eta}_\ell}\frac{d\psi_\ell}{dx}S_c dx} + i\frac{k_\ell}{\bar{a}}\frac{1}{\bar{p}E_\ell^2}\overset{\text{3D}}{\int_0^L\frac{\hat{\mathcal{P}}_1}{\hat{\eta}_\ell}\psi_\ell S_c dx} - i\frac{k_\ell}{\bar{\rho}\bar{a}E_\ell^2}\int_0^L\overset{FT}{\left[\frac{1}{k_\ell^2}\left(\frac{d\psi_\ell}{dx}\right)^2\right]}\int\bar{m}_{sg}dqdx \tag{6.173}$$
$$+ i\frac{k_\ell}{\bar{a}}\frac{1}{\bar{p}E_\ell^2}\int_0^L\psi_\ell\int\left[\overset{sc+PU}{\left(\bar{a}^2}+\overset{\Delta T}{\gamma R\Delta\bar{T}_s}\right)\hat{m}_{sg} + \overset{is}{\gamma R\left(\hat{T}}+\overset{\Delta T}{\Delta\hat{T}_s}\right)\bar{m}_{sg}\right]dqdx$$

The symbols above the terms in this equation are only for identification according to the following discussion.

With the definition (6.144) for the mass addition in steady flow, the first integral corresponds to the integral $\int\psi_n^2\nabla\cdot\hat{\mathbf{u}}dV$ and there is precise correspondence between all of (6.170) and (6.173) without the last two integrals. Those two integrals represent, within the approximations used here, the entire difference between the three-dimensional formulation and the one-dimensional 'approximation.'

'Approximation' is set off by quotes because it is a little surprising that the one-dimensional 'approximation' possesses *more* information than the three-dimensional formulation. The term in (6.173) containing $\frac{1}{k_\ell^2}\left(\frac{d\psi_\ell}{dx}\right)^2$ is pure imaginary and gives the flow-turning contribution to α; hence define

$$k_{FT}^2 = -i\frac{k_\ell}{\bar{\rho}\bar{a}E_\ell^2}\int_0^L\left[\frac{1}{k_\ell^2}\left(\frac{d\psi_\ell}{dx}\right)^2\right]\int\bar{m}_{gs}dqdx \tag{6.174}$$

Write

$$\frac{1}{S_c}\frac{d}{dx}(S_c\bar{u}) = (\nabla\cdot\bar{\mathbf{u}})_1$$

as the one-dimensional divergence of $\bar{u}$; the first integral in (6.173) and the integral containing $\gamma R\hat{T}$ in the last line are[28]

$$k_{is}^2 = -i\frac{k_\ell}{\bar{a}E_\ell^2}(\gamma-1)\int_0^L\psi_\ell^2(\nabla\cdot\bar{\mathbf{u}})_1 S_c dx + i\frac{k_\ell}{\bar{a}}\frac{1}{\bar{p}E_\ell^2}\int_0^L\psi_\ell(\gamma R\hat{T})\bar{m}_{sg}dqdx \tag{6.175}$$

[28]The flow through the surface corresponding to the second term in (6.175) is accounted for in the boundary conditions in three-dimensions.

The calculation immediately preceding (6.151) showed that these two terms together vanish if we assume that $\hat{T}$ is a consequence of an isentropic motion. This is the one-dimensional counterpart of the statement that $\nabla \cdot \mathbf{u} = 0$ in three dimensions, eliminating the first volume integral in (6.170). There is no surface contribution corresponding to the second term of (6.175) in three dimensions. We therefore ignore these terms in the following discussion, $k_{is}^2 = 0$.

The terms dependent upon $\Delta\bar{T}_s$ and $\Delta\hat{T}_s$ will have values dependent on the thermodynamics of the flow through the surface. Flandro and Majdalani have not considered such processes. Write

$$k_{\Delta T}^2 = i\frac{k_\ell}{\bar{a}}\frac{1}{\bar{p}E_\ell^2}\int_0^L \psi_\ell \int \left[(\gamma R\Delta\bar{T}_s)\bar{m}_{sg} + (\gamma R\Delta\hat{T}_s)\bar{m}_{sg}\right] q dx \tag{6.176}$$

As we defined with (6.156) the sum of fluctuations m'_{sc} due unsteady combustion and m'_{PU} produced by unsteady flow, so $m'_{sg} = m'_{sc} + m'_{PU}$, we can write the remaining term in (6.173) as

$$k_{PU}^2 + k_{sc}^2 = i\frac{k_\ell}{\bar{a}}\frac{1}{\bar{p}E_\ell^2}\int_0^L \psi_\ell \int \bar{a}^2\hat{m}_{sg} dq dx = i\frac{k_\ell}{\bar{a}}\frac{1}{\bar{p}E_\ell^2}\int_0^L \psi_\ell \int \bar{a}^2\hat{m}_{PU} dq dx + i\frac{k_\ell}{\bar{a}}\frac{1}{\bar{p}E_\ell^2}\int_0^L \psi_\ell \int \bar{a}^2\hat{m}_{sc} dq dx \tag{6.177}$$

Finally, let $k_{3\mathrm{D}}^2$ denote those terms in (6.173) which have precise correspondences in the perturbed three-dimensional problem,

$$k_{3\mathrm{D}}^2 = -i\frac{k_\ell}{\bar{a}E_\ell^2}\left[\left(\gamma\frac{\bar{u}}{\hat{\eta}_\ell} + \bar{u}\psi_\ell\right)\psi_\ell S_c\right]_0^L - \frac{1}{\bar{p}E_\ell^2}\int_0^L \frac{\hat{\mathcal{F}}_1}{\hat{\eta}_\ell}\frac{d\psi_\ell}{dx}S_c dx + i\frac{k_\ell}{\bar{a}}\frac{1}{\bar{p}E_\ell^2}\int_0^L \frac{\hat{\mathcal{P}}_1}{\hat{\eta}_\ell}\psi_\ell S_c dx \tag{6.178}$$

Substituting (6.174), (6.176), (6.177) and (6.178) into (6.173) with the combination (6.175) dropped, gives

$$k^2 = k_\ell^2 + k_{3\mathrm{D}}^2 + k_{FT}^2 + k_{PU}^2 + k_{sc}^2 + k_{\Delta T}^2 \tag{6.179}$$

Equation (6.179) is the most general form obtained to date for the wave number of motions represented by the one-dimensional approximation. By suitable interpretation, according to comparison of (6.170) and (6.172), of the first two terms on the right-hand side, (6.179) also contains the purely three-dimensional formula for which the last four terms on the right-hand side are absent.

Then (6.179) evidently serves as the basis for constructing a formula for three-dimensional wavenumber including flow-turning, pumping, and the unsteady processes generating the wavenumbers k_{sc}^2 and $k_{\Delta T}^2$. The recipe implies replacing k_ℓ^2 by k_n^2; calculating $k_{3\mathrm{D}}^2$ with the right-hand side of (6.170); and retaining k_{FT}^2, k_{PU}^2, k_{sc}^2 and $k_{\Delta T}^2$ given by their definitions quoted above as surface integrals:

$$k^2 = k_n^2 + k_{3\mathrm{D}}^2 + k_{FT}^2 + k_{PU}^2 + k_{sc}^2 + k_{\Delta T}^2 \tag{6.180}$$

No results are available to confirm or deny the truth of this conjecture.

6.11. An Example of Linear Stability for a Solid Rocket

Results for a simple example, a longitudinal mode for a solid propellant rocket, are shown in Figures 6.21–6.23 (Culick and Yang 1992). It is a common problem encountered particularly in the development of tactical motors. The calculations were carried out with linear and nonlinear gasdynamics. The example was first covered by Culick and Yang (1992, pp. 769–774).

Linear contributions from the exhaust nozzle, small particles (inert Al_2O_3) coupling with the mean flow, and unsteady burning were included. The effects of 'flow-turning' and 'pumping' were not considered. At

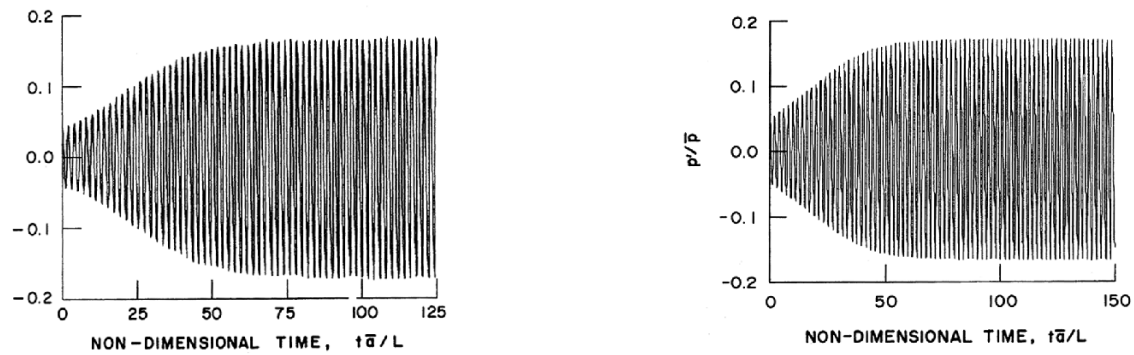

(a) approximate analysis

(b) numerical simulation

FIGURE 6.21. Growth of unstable motions according to (a) the approximate analysis; and (b) a numerical simulation of the same problem (Culick and Yang 1992).

the time, the authors did not realize that those contributions in fact sum to zero for this special case, a result that explains the quite good agreement between the approximate and numerical results. That the difference between the two calculations was not much greater was a puzzling conclusion at the time, but now constitutes a marvelous vindication of the one-dimensional approximation. Remarks concerning the effects of 'flow-turning' in calculations for a 'complete' problem, Culick and Yang (1992), must be ignored. See Section 6.12.

The effects of the exhaust nozzle are represented by the first bracketed terms in (6.161),

$$\begin{aligned}\alpha_{\text{nozzle}} \equiv \alpha_N &= -\frac{1}{2\omega_\ell E_\ell^2}\left(\frac{\bar{\rho}\bar{a}^2}{\gamma\bar{p}}\right)(\bar{a}k_\ell)\left[\left(\frac{\hat{u}^{(r)}}{\gamma\hat{\eta}_\ell}\psi_\ell + \bar{u}\psi_\ell^2\right)S_c\right]_{z=L} \\ &= -\frac{1}{2E_\ell^2}\left[\left(\gamma\frac{\hat{u}^{(r)}}{\hat{\eta}_\ell}\psi_\ell + \bar{u}\psi_\ell^2\right)S_c\right]_{z=L}\end{aligned} \tag{6.181}$$

in which $E_\ell^2 = \int_0^L \psi_\ell^2 S_c dz = S_c L/2$. At $z = L$, $\psi_\ell^2 = \cos^2(k_\ell L) = 1$ for $k_\ell = \ell\pi/L$ and with (6.181) written for $z = L$, so $-(A_b + \bar{M}_b) \to (A_N + \bar{M}_N)$,

$$\alpha_N = -\frac{\bar{a}}{L}\left(A_N^{(r)} + \bar{M}_N\right) \tag{6.182}$$

For the approximation (6.204) quoted later, valid if the nozzle is 'short',

$$A_N^{(r)} + \bar{M}_N = \bar{M}_N\left(\frac{\gamma-1}{2}+1\right) = \bar{M}_N\frac{\gamma+1}{2} \tag{6.183}$$

and

$$\alpha_N = -\frac{\gamma+1}{2}\frac{\bar{a}}{L}\bar{M}_N \tag{6.184}$$

Note that, according to the derivations of (6.94) and (6.181), the term $\bar{M}_N$ in (6.182) represents part of the net effects of the acoustics/mean flow interactions.

We will find in Section 6.14.3 that under quite broad realistic conditions in solid rockets, the presence of Al_2O_3 as liquid drops in motors, can be the source of substantial attenuation of oscillations. If all the

particles are spherical and have the same diameter, the attenuation constant is given by (6.152)a below, with X_1 and X_2 represented by the formulas (6.211)a,b:

$$\alpha_\ell = -\frac{1}{2}\frac{C_m}{1+C_m}\left[X_1 + (\gamma-1)\frac{C}{C_p}X_2\right] \tag{6.185}$$

where subscript $(\quad)_\ell$ stands for 'liquid.'

Least well-known are the contributions from unsteady combustion. For this example, the simplest result was used, the formula (6.103) for Denison and Baum's response function. We use the relation (6.102) and assume $\Delta\hat{T}_s = 0$. The corresponding formula for the contribution of surface combustion to the growth constant is

$$\alpha_e = \frac{\bar{v}_b}{r_c}R_p^{(r)} \tag{6.186}$$

Table 6.1 is a list of the property values required is the calculations of the instability. Calculations were done both with numerical solution to the one-dimensional equations (the method of Baum and Levine 1982) and using the results of the approximate analysis. Figures 6.21–6.23. Table 6.2 contains the linear growth constants and frequency shifts, $\omega - \omega_n = -\theta$, calculated with the results of the approximate analysis. Table 6.3 contains the total values of the growth constants and frequency shifts.

TABLE 6.1. Values of the Geometrical, Combustion and Physical Properties (used in the example discussed in Section 6.7.1).

Geometrical properties:	
length	$L = 0.5969\,\mathrm{m}$
radius of cylindrical port	$r_c = 0.0253\,\mathrm{m}$
throat radius	$r_t = 0.00936\,\mathrm{m}$
Combustion properties:	
mean pressure	$\bar{p} = 1.06 \times 10^7\,\mathrm{Pa}$
linear burning rate	$\bar{r}_b = 0.0078[\bar{p}/(3.0 \times 10^6)]^{0.3} = 0.01145\,\mathrm{m/s}$
parameters in the combustion response	$A = 6.0$ $B = 0.55$
chamber temperature	$\bar{T} = 3539\,\mathrm{K}$
mass particles/mass gas	$C_m = 0.36$
particle diameter	$\sigma = 2 \times 10^{-6}\,\mathrm{m}$
Physical properties:	
Prandtl number	$Pr = 0.8$
thermal diffusivity of propellant	$\kappa_p = 1.0 \times 10^{-7}\,\mathrm{m^2/s}$
specific heat of gas	$C_p = 2020\,\mathrm{J/kg\ K}$
specific heat of condensed material	$C = 0.68C_p$
viscosity	$\mu = 0.8834 \times 10^{-4}(T_c/3485)^{0.66} = 8.925 \times 10^{-5}\,\mathrm{kg/m\text{-}s}$
particle density	$\rho_s = 4.0\,\mathrm{g/cm^3} = 4 \times 10^3\,\mathrm{kg/m^3}$
propellant density	$\rho_p = 1,766\,\mathrm{kg/m^3}$
gas density	$\bar{\rho}_g = 7.97\,\mathrm{kg/m^3}$
γ (gas only)	$\gamma = 1.23$
$\bar{\gamma}$ (mixture)	$\bar{\gamma} = [\gamma(1 + C_m C/C_p)]/(1 + C_m\gamma C/C_p) = 1.18$
gas constant	$R = (\gamma - 1)C_p/\gamma = 377.72\,\mathrm{J/kg\ K}$
speed of sound in gas/particle mixture	$\bar{a} = \sqrt{(\bar{\gamma}RT_c)/(1 + C_m)} = 1075\,\mathrm{m/s}$
speed of combustion products at the burning surface	$\bar{v}_b = (\rho_p/\rho)\bar{r}_b = 1.86\,\mathrm{m/s}$
Mach number at the burning surface	$\bar{M}_b = 0.00173$

TABLE 6.2. Linear Growth Constants and Frequency Shifts.

Mode	α_c	θ_c	α_N	θ_N	α_P	θ_P
1	288.1	32.2	−160.1	0	−46.6	2.6
2	28.5	80.5	−160.1	0	−184.8	20.5
3	16.7	48.5	−160.1	0	−417.7	69.1
4	13.6	36.0	−160.1	0	−727.4	160.5
5	12.0	29.3	−160.1	0	−1107.5	305.5

TABLE 6.3. Total Values of the Linear Growth Constants and Frequency Shifts.

Mode	α_n	θ_n
1	81.4	34.8
2	−316.4	100.9
3	−561.1	117.6
4	−873.9	196.6
5	−1255.6	334.8

TABLE 6.4. Frequencies and Amplitudes of Acoustic Pressures.

	Frequency, Hz					Amplitude, $\lvert p'/\bar{p}\rvert$				
Mode	1	2	3	4	5	1	2	3	4	5
Numerical	926	1824	2698	3595	4491	0.151	0.042	0.0234	0.0203	—
Approximate	895	1785	2683	3571	4449	0.151	0.0478	0.0280	0.0153	0.0188

For direct comparison of the numerical and approximate results, Table 6.4 contains the values of the frequencies and amplitudes computed for the first two modes. A few cycles of the limiting waveforms are plotted in Figure 6.21 showing results for both the approximate and numerical computations: Figure 6.22 is the spectrum for the numerical results.

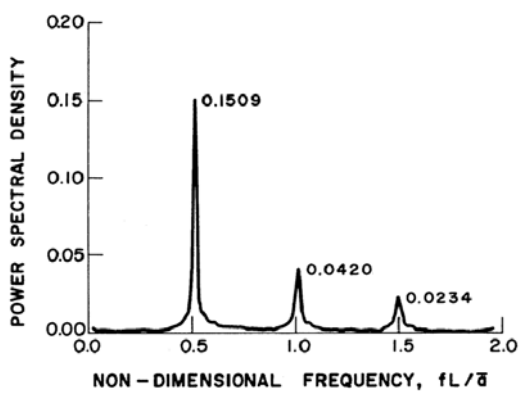

FIGURE 6.22. Spectrum for the calculated waveform shown in Figure 6.21(b) (Culick and Yang 1992).

The approximate analysis produces quite accurate values of the frequencies (within 3%) and the approximate total waveform is reasonably close to the "exact" result except for some rippling due to the absence of higher frequencies. Even so, the amplitudes of the individual modes found with the approximate analysis agree well with those computed with the numerical analysis except for the highest ($n = 5$) mode. The reason for the high value (even larger than that for $n = 4$) is that there is no transfer of energy to higher modes. Because the rate of energy dissipation from the highest mode considered, represented by its attenuation constant, must be such that the total energy loss equals the total rate of energy gain, the amplitude of the highest mode must be such as to satisfy this condition. Even with only two modes accounted for, the frequencies and total waveform are quite well predicted. The frequencies are the same as for the case of five

modes; Figure 6.23 shows the waveforms. However, according to Table 6.4, the approximate amplitudes of the individual modes differ considerably from the exact values. The phases of the two modes in the approximate solution apparently assume values that compensate for the consequences of the inaccurate amplitudes. Figure 6.15a,b

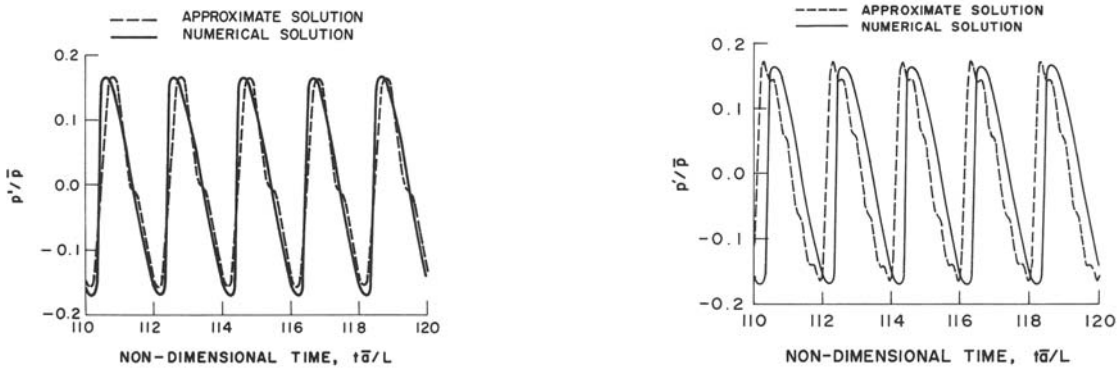

FIGURE 6.23. Effect of truncation in the waveforms (Culick and Yang 1992).

6.12. Vorticity and Stability in Solid Propellant Rockets

Vorticity appears in combustion chambers chiefly on three forms: random motions associated with turbulence; large 'coherent' vortices growing out of unstable shear layers; and waves of vorticity generated by interactions between the acoustic field and a flow entering the chamber through the lateral boundary. In Section 7.6 we regard all random motions together as noise and show how the net pressure may affect the acoustic pressure field. Here we are concerned only with distributed vorticity, either as waves carried by the mean flow or as large vortices.

Probably the first observations of possible consequences of vorticity[29] in a combustor are those reported by Boys and Schofield (1942). Some features of recorded pressure histories and of grain erosion caused them to speculate the presence of " ... some abnormal flow on oscillation ... as if the gas were swirling with a high velocity." (Quoted by Flandro 1967). Since that time, many examples of scoured lateral boundaries have been reported, both in liquid rockets and in solid rockets, all for laboratory tests or static firings of full-scale motors. Green (1958) reported visual observations of swirling flows in a solid rocket.

By conservation of angular momentum, exhaust of a swirling or vortex flow from a combustor must be accompanied by a roll torque (of the opposite sign) exerted about the axis of symmetry. Substantial roll torques were first observed in flight tests of the Sergeant motor (Flandro 1964). An extreme example occurred in the first flight test of the Scout space probe which failed when the control system was unable to compensate large roll motions (Mayhue 1962).

Swithenbank and Sotter (1963; 1964a,b) were first to attempt a theoretical explanation of the generation of roll torques by adapting an analysis of finite amplitude transverse waves by Maslen and Moore (1956). Partly due to errors in the latter paper, and partly due to some misinterpretations, the results by Swithenbank and Sotter are incomplete. The main idea is that acoustic streaming generated by the transverse waves carries angular momentum causing the roll torque.

[29]We refer to the effects of streamwise vorticity or vortices. The discussion in Section 6.12.1 and subsequently is concerned primarily with azimuthal vorticity generated by processes associated with nonuniform flow inward at the lateral boundary. The two kinds of vortices are illustrated in Figure 6.24.

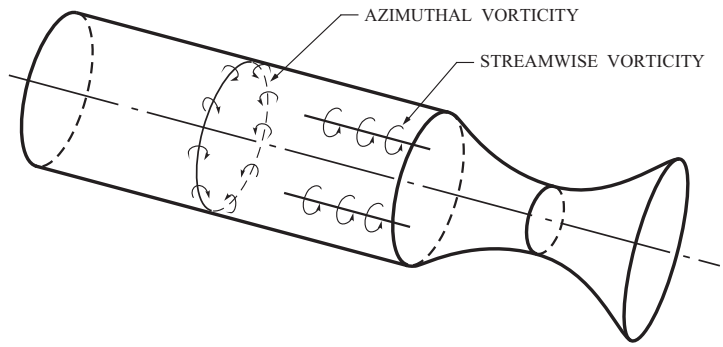

FIGURE 6.24. Stylized rendition of azimuthal and streamwise vortices in a solid propellant rocket chamber.

In a fine piece of work, Flandro (1967) corrected the deficiencies of Swithenbank and Sotter's work and produced what is essentially the correct explanation for the generation of roll torques in solid propellant rockets. That work probably makes unnecessary any further theory of the phenomenon. The details of Flandro's work need not be covered here. Its importance in the present context is that the analysis is the first application of the scheme developed here in Chapters 4 and 5, in which vorticity is explicitly accommodated in a calculation of the acoustic field. The most significant technical point in the analysis is proper satisfaction of the no-slip boundary condition at the boundary. When a tangential or transverse acoustic mode is present, which necessarily has a velocity component parallel to the surface, a second contribution to the velocity is required to cancel the acoustical motion. That second component arises with generation of vorticity convected into the chamber. Eventually, the vorticity combined with a travelling transverse wave mode produces the angular moment in the flow. The reaction to the loss of that angular momentum appears as a roll torque. Further discussion of the possible flow fields and the connection with acoustic streaming are discussed briefly in Chapter 7.

It's a beautiful model of the problem and successfully explains the observed behavior. Technically, the essential result was making explicit the basic connection between acoustics and vorticity, the vehicle for the connection being the mean flow, and the consequence being generation of angular momentum experienced as a roll torque. The analytical procedure served as a precursor to Flandro's later analysis of waves of vorticity generated in response to the presence of longitudinal acoustic instabilities in solid propellant rockets. (Flandro 1995). That work has several times been misinterpreted and consequently has been unjustifiably and incorrectly criticized.

6.12.1. Generation of Large Vortices; Parietal Vortex Shedding. Oscillations found in large solid rocket motors, developed as boosters for launching spacecraft, have presented problems somewhat different from those discussed in most of this book. The primary examples are the Space Shuttle booster (Mason, Folkman and Behring 1979; Mathes 1980; Blomshield and Mathes 1993); the Titan solid rocket (Alden 1980; Brown *et al.* 1981); and the Ariane 5 MPS P230 (Scippa *et al.* 1994). All these motors have had relatively low-level pressure, and thrust, oscillations at frequencies suggesting that the first longitudinal mode is unstable. Yet estimates based on the ideas developed in Chapters 3 and 4, or similar arguments, led to the conclusion in each case that the longitudinal mode should be unquestionably stable. For example, such a conclusion was reached by Kumar and Culick (1977) before the first test firing of the SRM in the late 1970s. When the motor was fired, vibrations at approximately 15 Hz were detected at levels high enough to cause concern, both in respect to oscillatory accelerations of some structural components and motions of the pilots' cabin. The existing stability analysis could not explain the observation because, as it turned out, a contribution was missing. That missing contribution was due to vortex shedding from inhibitor material exposed at the joints of the segmented motor.

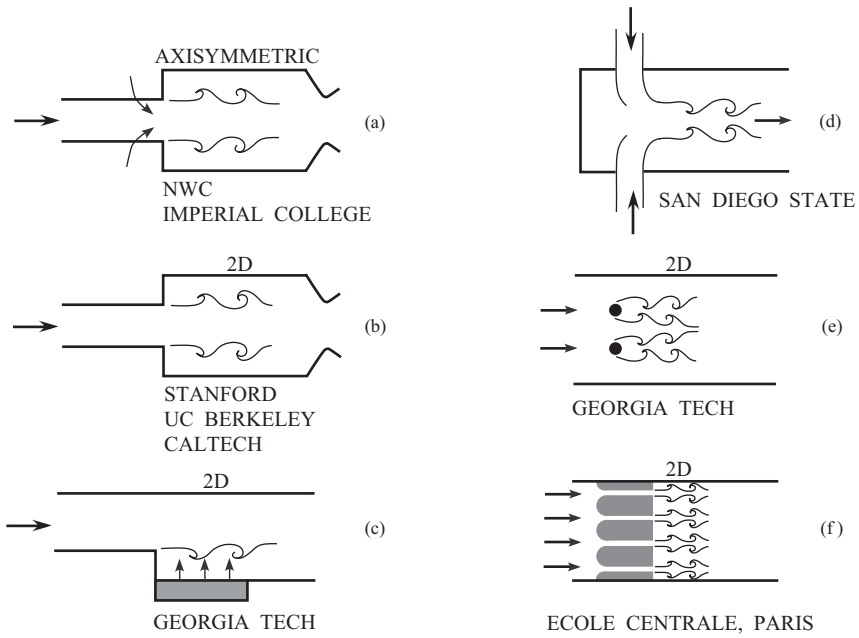

FIGURE 6.25. Some configurations used in observations of vortex shedding and instabilities (adapted from Schadow 2001).

The earlier suggestion by Flandro and Jacobs (1975) that vortex shedding could couple to acoustic modes of the motor was recalled. That prompted the simple laboratory tests by Culick and Magiawala (1979) followed later by the extended work of Nomoto and Culick (1982), and Aaron and Culick (1985). The last contains a simple approximation to the excitation of acoustic waves by the impingement of vortices on an obstruction. Meanwhile the idea was pursued vigorously in the Titan program, with convincing results published by Dunlap and Brown (1981) and Brown *et al.* (1981). At about the same time, Byrne (1981, 1983) suggested vortex shedding in dump combustor configurations as the mechanism for oscillations found in ramjets (Culick 1980; Culick and Rogers 1980). Thus by 1981, vortex shedding had been established as a fundamental mechanism of instabilities in combustion systems.

Subsequently, vortex shedding was found to be even more widespread than previously considered. It was well-established experimentally, especially by the work of Schadow and his colleagues at the Naval Weapons Center, China Lake, to be a potentially significant mechanism for oscillations in laboratory dump combustors; a good summary of the matter was given by Schadow and Gutmark (1992). In his lecture, part of the Short Course "Active Control of Engine Dynamics" held at the von Karman Institute (VKI), Schadow (2001) gave a useful tutorial emphasizing vortex shedding in damp combustors. Figure 6.25 summarizes the main configurations that have been studied; and locations of principal experimental efforts. The Short Course given at the Glenn Research Center (Culick 2001) also includes as Section 9 a summary of the subject, with references. Section 8.6 contains a discussion of vortex shedding and its modification as a means of passive control.

A quite different form of vortex shedding as a driving mechanism for oscillations in a combustor was discovered in series of fine experimental and theoretical works by French investigators motivated by the Ariane 5 problem. Put most succinctly, they found that unlike all previous demonstrations, and (therefore) contrary to general expectations, neither obstacles nor edges are required to generate large vortices in a stream. Lupoglazoff and Vuillot (1996) named the phenomenon "parietal vortex shedding" because the vortices formed in the region close to a wall through which fluid was injected. They discovered the phenomenon experimentally while carrying out a lengthy series of tests devoted broadly to clarifying the coupling between

vortex shedding and acoustic modes. The investigations began in the early 1990s, driven by serious practical considerations. The payload of the Ariane 5 might be reduced (it eventually was) by the mass of devices added to the solid rocket boosters as protection against the oscillatory accelerations. For example, Prévost *et al.* (1996) cited a maximum amplitude of 0.28 bar (14.5 psi) at 20 Hz); the mean chamber pressure is around 50 bar. Oscillations of this magnitude have persisted in the motor and the Ariane 5 has consequently suffered a reduction of payload equal to several hundred pounds.[30] Hence the primary goal of the work was evidently elimination of the vortex shedding or the coupling between the vortices and the acoustic modes.

The problem of oscillations produced by the formation of large vortices was apparently encountered quite early in the development of the Ariane 5 (c. 1990 in subscale work and during the first full-scale tests beginning in 1993). It was the subject of serious concern in the early 1990s; the French work was summarized in the informative paper by Vuillot (1995) written just prior to the discovery of parietal vortex shedding, reported by Lupoglazoff and Vuillot (1996). A series of tests was carried out in 1/15 scale laboratory motors, named LP3A-E shown in Figure 6.26. The results are reported in several places, but the contribution of Vuillot and Casalis (2002) to the VKI Short Course "Internal Aerodynamics in Solid Rocket Propulsion" (2002) is the best summary.

There was no flow visualization of the hot firings in the LP3 test series. Careful interpretation of the data, and numerical simulation established conclusively that parietal vortex shedding had been shown. Direct confirmation was provided by Avalon *et al.* (2001) using PLIF with acetone. Figure 6.27 reproduces a picture they obtained with the ONERA VECLA[31] apparatus.

Casalis and coworkers have carried out analyses establishing conclusively the origin of parietal vortex shedding. (Vuillot and Casalis 2002 Part II, and references there to the original work.) As background, recall that vortex shedding from edges or obstacles is initiated by an instability of a shear layer. Parietal vortex shedding occurs because the flow itself is unstable. Figure 6.28 shows some results of numerical simulations for the three cases. The case has been established for the profile in a cylindrical cavity closed at one end having a uniform porous lateral boundary passing a uniform flow (Taylor 1956, Culick 1966b). The analysis shows, as observed, that the vortex shedding begins some distance from the closed end of the cylinder where the profile in question is unstable to small disturbances (Urgutas *et al.* 2000).

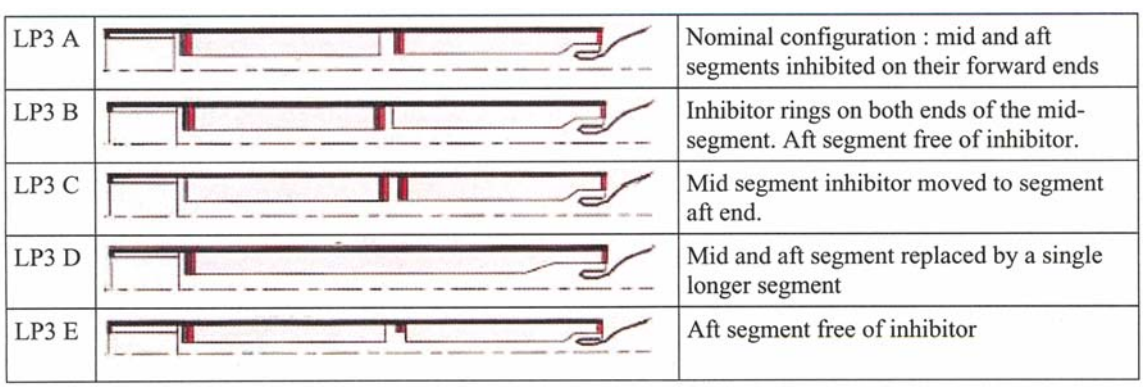

FIGURE 6.26. The five two-dimensional configurations of the LP3 test motors. Parietal vortex shedding was discovered in model D. (Vuillot *et al.* 1993; Prévost *et al.* 1996).

[30]The payload of the Space Shuttle also was reduced in the late 1980s, by an even larger amount due to design changes following the loss of the Challenger. In that case, parietal vortex shedding was not an issue.

[31]Veine d'Etude de la Couche Limité Acoustique. The test device operated with air injection through the porous sidewalls, to allow the flow visualization shown in Figure 6.27.

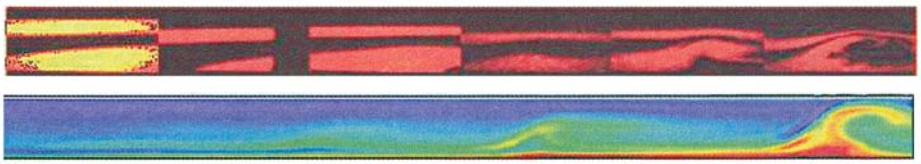

FIGURE 6.27. Upper image: flow visualization of parietal vortex shedding, using PLIF with acetone; Lower image: result of numerical calculations (Avalon *et al.* 2001).

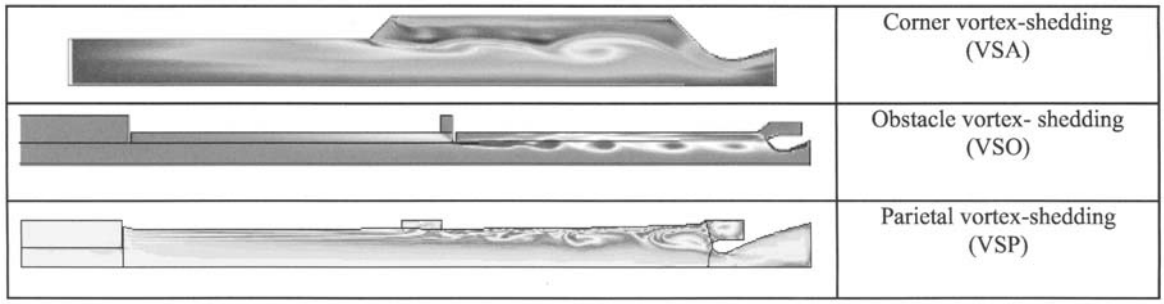

FIGURE 6.28. The three kinds of vortex shedding (Fabignon *et al.* 2003).

Prévost, Godon, and Innegrave (2005) have reported the most recent tests supporting the view that parietal vortex shedding may be a significant contribution to the problem of oscillations in the Ariane 5. Three series of sub-scale tests have been carried out, a total of seventy-six firings in configurations identified as LP6(1/15 scale), LP9(1/35 scale) and LP10(1/35 scale). In the series LP6, the propellant was changed to a non-metallized form during the series. In all tests having no restrictors at the ends of propellant segments, parietal vortex shedding occurred. Figure 6.29 is a drawing of the test device; Figure 6.30 shows typical results.

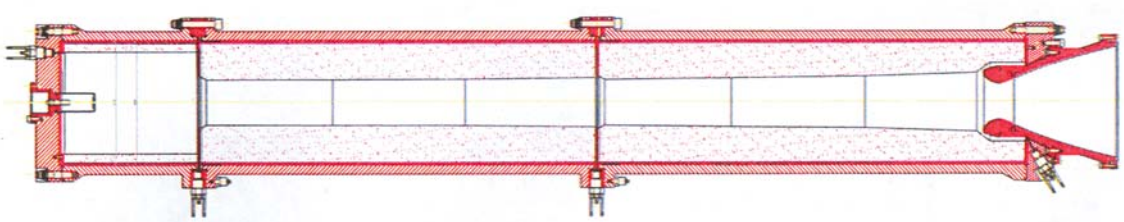

FIGURE 6.29. A sketch of the LP6 test device (Prévost *et al.* 2005).

Test series for the LP9 and LP10 configurations showed the presence of oscillations apparently due to parietal vortex shedding. Accompanying analysis by Chedevergne and Casalis (2005) supports that explanation. No direct confirmation by flow visualization was reported, but that may be an unnecessary step. An interesting comment was made in connection with Figure 17 of the paper by Chedevergne and Casalis, that "...all the instabilities begin at the burnout of the propellant around the submerged nozzle."

The significance of the parietal form of vortex shedding may be great indeed. If this really is the source of the acoustic waves (modes) excited in the Ariane 5 or other large boosters), then there are significant

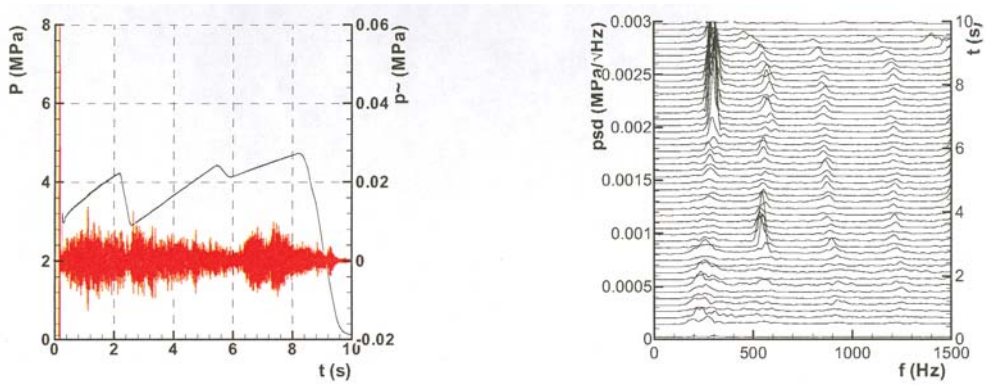

FIGURE 6.30. Experimental results for a test in the LP6 configuration showing parietal vortex shedding (Prévost *et al.* 2005).

implications for design of new motors to avoid the problem. However, despite the extensive and impressive accomplishments by the French research program for the Ariane 5, it seems that available evidence doesn't prove conclusively that familiar vortex shedding originating with an unstable shear layer formed at an edge is eliminated is a (the?) potential cause in the full-scale motor. Direct confirmation is difficult. However, it is not clear at this time that the more familiar formation of vortices at the joints of the segments of the grain can be dismissed as the primary cause, even in the Ariane 5.

6.13. Predictions of Stability Boundaries for Liquid Rockets

Stability boundaries were apparently first treated systematically for liquid rockets, in the early 1950's. In 1956 Crocco and Cheng completed their book treating one-dimensional motions, with the $n-\tau$ representation of the unsteady conversion of liquid to combustion products. That idea, introduced a few years earlier by von Karman and Summerfield (1950) achieved an enormous simplification of the actual processes. Combined with significant approximations to the spatial extent of the unsteady combustion, the model was the basis for much work in the theory of combustion instabilities in liquid rockets. Attempts to extend application of the $n-\tau$ model to solid propellant rockets (Cheng 1954a) and other liquid-fueled systems (e.g., Reardon 1983) seem to have had few useful consequences.

From the early 1950s through the 1980s in the U.S. the $n-\tau$ model dominated the views and practical considerations of unsteady combustion in liquid-fueled systems. First linear behavior and then, beginning in the early 1960s, nonlinear combustion instabilities were investigated. It is important to appreciate that, as discussions in Chapter 2 and in the next chapter show clearly, the geometries of combustion chambers treated in those works were all quite simple variations of a cylindrical chamber with a sonic exhaust nozzle. Thus the basic flow fields in all cases shared nearly the same characteristics, differences arising from the absence or presence of a shock wave and the spatial extent of the combustion processes. The general methods used are cumbersome to apply to distributed combustion. Consequently, most of the analyses were restricted to concentrated combustion. For example a common choice, perhaps a reasonable approximation to combustion of fast burning propellants, was combustion in a plane located at the head end of the chamber. One exception was examination of distributed combustion by Crocco and Cheng (1956; pp. 103ff). The practical difficulties with a formulation based on differential equations become apparent fairly soon.

Probably the apex of the Princeton work on linear stability was reached with Crocco's long paper given at the Tenth Combustion Symposium (1965). Crocco spent at least half of the paper on explicit modeling of

combustion processes and on nonlinear behavior, virtually signaling the conclusion of their research dealing with linear problems.

The way in which stability boundaries were treated with the $n - \tau$ representation has been explained in Section 2.4.2. It is important to realize that apart from estimates, no work seems to have been done to predict values of n and τ, so there really are no true predictions of stability boundaries using the $n - \tau$ model. The usual approach in applications has been based on the assumption that all other contributions to the formula for the growth constant are known. Then setting $\alpha = 0$ gives a relation between n and τ on the stability boundary. Or, if one more correctly uses both the real and imaginary parts of the eigenvalue for wave motions, then there are two relations. These have the forms (2.127)a,b which can, in principle be used to define a stability boundary and the variation of the frequency along the boundary.

However, no true predictions of stability boundaries are available without knowledge of n and τ. Consequently, for applications to a real system, and to obtain some understanding of the way in which its stability may depend on important parameters and operating conditions, experimental data are required. Examples are given in Section 2.4.2; extended discussions may be found in Harrje and Reardon (1972).

Theorists in Russia took a very different approach not married so tightly to a simple representation of the principle mechanism for instabilities in liquid rockets. Natanzon (1984, 1999) has written the best known treatise on instabilities in liquid rockets. The work covers several methods not well-known in the West and includes a summary of some experimental work on hysteresis. Since it is based entirely on differential equations, Natanzon's work has little overlap with the methods covered in this book.

6.14. Contributions to the Growth Constant for Linear Stability

It is one of the great benefits of the linear analysis that the influences of the processes causing or discouraging instabilities are displayed additively. Their relative importance is therefore easily assessed and the basis is given for determining where most effort should be expended to provide good predictions of stability in actual systems. Consequently much expense and effort in the field of combustion instabilities generally has been planned according to the formal organization of the subject suggested by the results (6.94) and (6.161) for the linear growth constant. In this section we will discuss several contributions which are important mainly in solid propellant rockets. The subjects of Section 6.14.1 and 6.14.2 arise in all types of propulsion systems.

6.14.1. Mean Flow/Acoustics Interactions. Of the many processes participating in combustion instabilities those that are purely fluid-mechanical are best known, mainly for two reasons: Their foundations are understood; and usually they can be investigated experimentally with laboratory tests at room temperature. It is a fortunate peculiarity of the fluid mechanics that the formal results are relatively simple to first order in the amplitude and in the mean flow speed. For internal flows, the first order interactions combine in such a way that the net result appears as convection through the boundary, the surface integral containing $(\bar{\mathbf{u}} \cdot \hat{\mathbf{n}})\psi_n$ in (6.87), (6.90) and (6.94).

Thus, to lowest order, the mean flow/acoustics interactions are simple both in form and interpretation. As the manipulations leading to (6.87) show, the surface integral in fact accounts for some contributions occurring in the volume. It is a fortunate accident that for a finite volume, their net contribution turns out to be represented as a surface effect only.

On the other hand, when viscous effects and especially flow separation occur, the situation becomes immeasurably more complicated. For example, all of the phenomena associated with shear layers and vortex

shedding enter the picture. We have discussed them elsewhere in this book. It is best to treat them in the physical contexts where they arise.

6.14.2. Attenuation by a Choked Exhaust Nozzle. Liquid and solid propellant rockets, ramjets and augmentors for gas turbines all exhaust through choked nozzles. In a gas turbine, the combustor supplies the turbine directly and the exit flow from the combustor has traditionally been well below sonic speeds. In modern gas turbines the exit Mach number is larger, approaching unity in some cases. Combustion instabilities have become troublesome in gas turbines in recent years, mainly a consequence of the need to operate at lower fuel/air ratios as part of the strategy to minimize the generation of nitrogen oxides. Otherwise, undesirable oscillations have been relatively infrequent in such systems.

On the basis of those observations—crude but nevertheless valid—one is tempted to offer the generalization that any combustion system possessing a choked exhaust is liable to exhibit combustion instabilities. Is there any reason why such a simple characterization might contain some truth? In fact there is, broadly, a reason: A system having a choked exhaust nozzle in general will have lower acoustic losses than it would if the exhaust flow were not choked. The main purpose of this section is to clarify how this result comes about; and to show how those losses are determined theoretically and experimentally. A useful consequence is that with the solution we discover how to obtain a good estimate for the length of chamber to use for approximate calculation of the frequency of an instability.

The essential idea is quite simple, as sketched in Figure 6.31. An acoustic wave is incident from the left on an axisymmetric sonic nozzle, Figure 6.31(a), or two-dimensional nozzle, Figure 6.31(b). The wave propagates in the direction parallel to the axis of the nozzle but in general has an unspecified distribution of variables in planes normal to the axis. For this analysis we assume the flow upstream of the entrance to the nozzle is uniform. Because we consider only linear behavior, it is consistent with the analysis of motions in the chamber to assume the first-order representation of the incident wave in the radial and azimuthal coordinates,[32]

$$\begin{aligned} &J_m(\kappa_{mn} r)\cos n\theta \quad \text{(standing waves)} \\ &J_m(\kappa_{mn} r)e^{\pm in\theta} \quad \text{(travelling or “spinning” waves)} \end{aligned} \tag{6.187}$$

For the two-dimensional case, the incident waves have amplitude independent of y defined in Figure 6.31(b) and dependence on $\cos(k_l\, x)$ upstream of the nozzle. A source of the steady incident waves is assumed to exist somewhere far to the left (upstream) of the nozzle and is ideal in the sense that it perfectly absorbs any waves travelling after reflection from the nozzle.

A large fraction of the incident waves passes through the nozzle and the remainder is reflected back to the chamber. That is the result of complicated interactions between the waves, the mean flow and the nozzle itself. The last introduces explicit dependence of the reflected waves on the shape of the nozzle. Most available calculations of the nozzle admittance function rest partly on the approximation that the nozzle is slender;[33] that restriction eliminates explicit dependence on the shape, where ‘shape’ means the variation of cross section with position.

Reflection of a portion of the incident waves therefore occurs because the average flow is non-uniform in the streamwise direction. Without the shape of the nozzle appearing in the problem, satisfying any conditions on a lateral boundary is unnecessary—indeed not possible. The form of a wave having structure

[32] We use dimensionless coordinates, r standing for r/R and z for z/L where R is the radius of the nozzle at its entrance and L is the length from the entrance to the throat. For the two-dimensional nozzle, R is replaced by $W/2$; see Figure 6.31.

[33] ‘Slender’ means that the slope of the nozzle boundary, the rate of change of the diameter of the cross section with position, along the axis is small. We will not try to make this statement more precise. See the cited references for somewhat closer estimates.

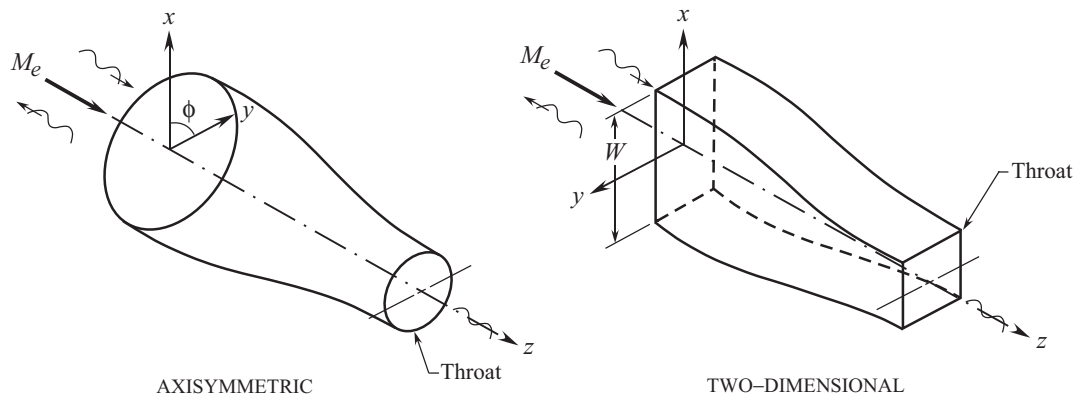

FIGURE 6.31. Idealized axisymmetric and two-dimensional nozzles for calculating admittance functions.

in transverse planes is set by its form at the entrance. As a result of these approximations we have described only qualitatively, determining the wave system produced in the nozzle by its action on the planar incident wave, comes down to finding the variation of one quantity in the flow through the nozzle. Usually that quantity has been chosen to be the density, or the pressure, of the wave system.

In his seminal work, Tsien (1952) assumed that the oscillations in the nozzle are isothermal, an approximation corrected by Crocco (1953). Crocco's analysis of purely longitudinal waves for which the velocity fluctuations are parallel to the axis of the nozzle in included as Appendix B of Crocco and Cheng (1956). That is probably the best place to become acquainted with analysis of the problem; we follow Crocco's analysis with little change. The linearized continuity and momentum equations for one-dimensional unsteady motions can be written

$$\frac{\partial}{\partial t}\left(\frac{\rho'}{\bar{\rho}}\right) + \bar{u}\frac{\partial}{\partial z}\left(\frac{\rho'}{\bar{\rho}} + \frac{u'}{\bar{u}}\right) = 0 \tag{6.188}$$

$$\frac{\partial}{\partial t}\left(\frac{u'}{\bar{u}}\right) + \left(\frac{\rho'}{\bar{\rho}} + 2\frac{u'}{\bar{u}}\right)\frac{d\bar{u}}{dz} + \bar{u}\frac{\partial}{\partial z}\left(\frac{u'}{\bar{u}}\right) = \frac{p'}{\bar{p}}\frac{d\bar{u}}{dz} + \frac{\bar{p}}{\bar{\rho}\,\bar{u}}\frac{\partial}{\partial z}\left(\frac{p'}{\bar{p}}\right) \tag{6.189}$$

We assume that the entropy of an element of fluid does not change in passage through the nozzle, so the linearized equation is

$$\left(\frac{\partial}{\partial t} + \bar{u}\frac{\partial}{\partial z}\right)\frac{s'}{C_v} = \left(\frac{\partial}{\partial t} + \bar{u}\frac{\partial}{\partial z}\right)\left(\frac{p'}{\bar{p}} - \gamma\frac{\rho'}{\bar{\rho}}\right) = 0 \tag{6.190}$$

Note that the averaged quantities $\bar{\rho}$, $\bar{p}$, $\bar{u}$ are all functions of position. They are assumed known from the shape of the nozzle.

The last equation is integrated to give

$$\frac{s'}{C_v} = \frac{p'}{\bar{p}} - \gamma\frac{\rho'}{\bar{\rho}} = F\left(t - \int_{z_e}^{z}\frac{dz'}{\bar{u}(z')}\right) \tag{6.191}$$

in which the function F is determined by the (presumed known) time dependence of the entropy at z_e, the entrance plane of the nozzle. To make the connection with Crocco's analysis easy to follow, we assume

harmonic time dependence[34] and introduce the definitions of $\varphi(z)$, $\sigma(z)$, and $\nu(z)$

$$\frac{p'}{\bar{p}} = \varphi(z)e^{-i\omega t} \; ; \qquad \frac{\rho'}{\bar{\rho}(z)} = \sigma(z)e^{-i\omega t} \; ; \qquad \frac{u'}{\bar{u}(z)} = \nu(z)e^{-i\omega t} \tag{6.192}$$

Then (6.191) becomes

$$\varphi(z) - \gamma\sigma(z) = \varepsilon e^{i\omega \int_{z_e}^{z} \frac{dz'}{\bar{u}}} \tag{6.193}$$

where ε is C_V^{-1} times the amplitude of the entropy oscillation.

With (6.192), equations (6.188) and (6.189) are now

$$\bar{u}\frac{d\nu}{dz} + \bar{u}\frac{d\sigma}{dz} - i\omega\sigma = 0 \tag{6.194}$$

$$\bar{u}\frac{d\nu}{dz} + \frac{\bar{a}^2}{\bar{u}}\frac{d\sigma}{dz} + \left(2\frac{d\bar{u}}{dz} - i\omega\right)\nu - (\gamma-1)\frac{d\bar{u}}{dz}\sigma = \varepsilon\left(\frac{d\bar{u}}{dz} - i\omega\frac{\bar{a}^2}{\gamma\bar{u}^2}\right)e^{i\omega \int_{z_e}^{z} \frac{dz'}{\bar{u}}} \tag{6.195}$$

Tsien (1952) first noticed that this pair of equations could be solved to give σ and ν in terms of a known function for the special case in which the mean velocity increases linearly with distance from the entrance plane. To simplify the discussion and results even further we will not account for entropy changes and set $\varepsilon = 0$.

To specify a linear velocity profile, take the slope to be constant, written as

$$\frac{d\bar{u}}{dz} = \frac{\bar{u}}{z} = \frac{\bar{a}_*}{z_*} = \frac{\bar{a}_* - \bar{u}_e}{(z_* - z_e)} \tag{6.196}$$

where $(\quad)_*$ denotes values at the throat and, as earlier, $(\quad)_e$ identifies values at the entrance.[35] Thus $z_* - z_e$ is the length of the subsonic section of the nozzle. Tsien introduced the new variable ζ,

$$\zeta = \left(\frac{z}{z_*}\right)^2 = \left(\frac{\bar{u}}{a_*}\right)^2 \tag{6.197}$$

The relation between the speed of sound and the Mach number,

$$\frac{T}{T_0} = 1 + \frac{\gamma-1}{2}M^2$$

may be used to give the formula

$$\left(\frac{\bar{a}}{\bar{a}_*}\right)^2 = \frac{\gamma+1}{2} - \frac{\gamma-1}{2}\zeta^2 \tag{6.198}$$

Finally define a dimensionless or "reduced" angular frequency β,

$$\beta = \frac{z_*\omega}{\bar{a}^*} = \frac{\omega(z_* - z_e)}{\bar{a}_* - \bar{u}_e} \tag{6.199}$$

Substitution of the preceding definitions and combination of (6.194) and (6.195) eventually produces the equation with which σ may be computed:

$$\zeta(1-\zeta)\frac{d^2\sigma}{d\zeta^2} - \left(2 - \frac{2i\beta}{\gamma+1}\right)\zeta\frac{d\sigma}{d\zeta} + i\beta\frac{2-i\beta}{2(\gamma+1)}\sigma = 0 \tag{6.200}$$

[34]Recall that we use the convention $e^{-i\omega t}$ whereas Crocco uses $e^{+i\omega t}$.

[35]Except M_N (not M_e) denotes the Mach number of the flow entering the nozzle.

The point $\zeta = 0$ lies upstream of the entrance to the nozzle, but $\zeta = 1$ is at the throat ($\bar{M} = \bar{M}_* = 1$). Hence we must choose the solution to (6.200) which is non-singular at $\zeta = 1$, known as the hypergeometric series (Morse and Feshbach 1953). Expanded in powers of $1 - \zeta$, the solution is

$$F(a, b, c; 1 - \zeta) = 1 + \frac{ab}{c}(1 - \zeta) + \frac{a(a+1)b(b+1)}{c(c+1)}\frac{(1-\zeta)^2}{2!} + \cdots \tag{6.201}$$

with

$$\begin{aligned} c &= a + b + 1 = 2\left(1 - \frac{2\beta}{\gamma + 1}\right) \\ ab &= \frac{-i\beta}{\gamma + 1}\left(1 - \frac{1\beta}{2}\right) \end{aligned} \tag{6.202a,b}$$

Crocco and Cheng (1956) noted that the convergence of (6.201) is slow for $1 - z_e$ near one (i.e. when z_e is small, as the case is for small Mach number at the nozzle entrance) and have given alternative representations for z_e small. Thus the problem of calculating the admittance function is solved, subject to the limitations of the analysis discussed above. Using the relation for isentropic flow assumed here, we find the admittance function for a nozzle[36]

$$A_N = -\frac{(\hat{\mathbf{u}} \cdot \hat{\mathbf{n}})/\bar{a}}{(\hat{p}/\gamma\bar{p})} = \frac{\hat{u}/\bar{a}}{\hat{\rho}/\bar{\rho}} = \bar{M}_N \frac{\nu_e}{\sigma_e} \tag{6.203}$$

where $\bar{M}_N$ stands for the Mach number of the average flow entering the nozzle.

A particularly important limit of (6.201) is that for very slow or "quasi-static" conditions, the value assumed for $\omega \to 0$ (i.e. $\beta \to 0$). This condition is equivalent to that existing in a "short" nozzle, that is when the wavelength of the oscillation is long compared with the length of the nozzle. Evidently the same result can therefore be obtained with at least two arguments. Under these conditions, the fluctuation of velocity at the nozzle entrance is in phase with the imposed pressure fluctuation. The admittance function for short nozzles was first obtained by Crocco (1953, p. 52, $\beta = 0$) and subsequently by several others, including Zinn (1972), the result being

$$A_N = \bar{M}_N \frac{\gamma - 1}{2} \tag{6.204}$$

This is of course the value of the nozzle admittance function for β(i.e. ω) $= 0$.

Figure 6.32 shows some results for realistic ranges of β and $\bar{M}_N$. For example, for a rocket having a nozzle entrance 15 cm long and with $\bar{a} = 1500$ m/s, $\beta = 0.3$ when $\omega = 3000s^{-1}$ ($f \approx 500s^{-1}$). This estimate shows that for practical purposes, since β is quite small, the approximation (6.204) is in fact quite good.

Experimental results have shown that for the conditions supposed, the theory worked out by Tsien and Crocco gives accurate results: The action of a choked exhaust nozzle on small amplitude sinusoidal oscillations may be assumed accurately known. Crocco, Monti and Grey (1961) reported the first test results, in which the velocity was measured with a hot wire. Data were obtained for relatively high values of β because the speed of sound in cold-flow test is much lower than the values in hot firings. Figures 6.33 and 6.34 show that their experimental results seem to agree quite well with the theory described above. However, the authors expressed some reservations since they were forced to apply significant adjustments to the raw data, owing in large part to inaccuracies in the results for the velocity fluctuations.

Bell (1972) has obtained the best data for the nozzle admittance function; his experimental results were included in the papers by Zinn, Bell, Daniel and Smith (1973) and by Bell, Daniel and Zinn (1973). The data were obtained using the method based on an impedance tube as recommended by Culick and

[36]Sometimes the density replaces the pressure, giving a quantity differing from (6.204) by a factor γ. Then (6.204), for example, becomes $\bar{M}_N(\gamma - 1)/2\gamma$.

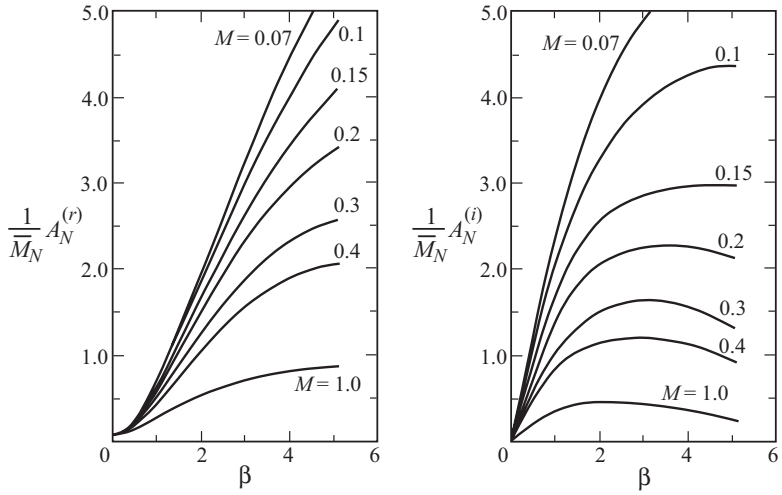

FIGURE 6.32. Numerical values for the admittance function of a nozzle exposed to isentropic oscillations, equation (6.203): (a) real part; (b) imaginary part. (Crocco and Cheng 1956)

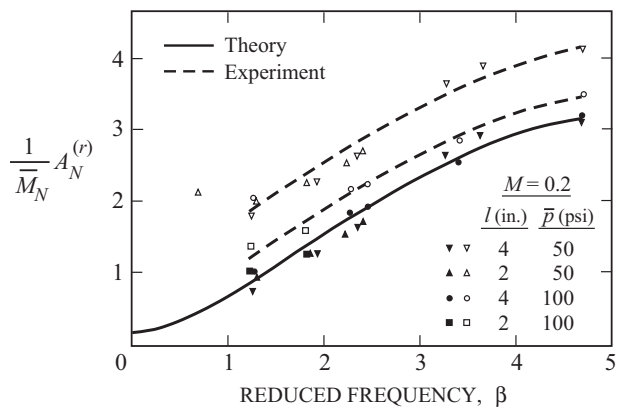

FIGURE 6.33. Results for the real part of the admittance function for a nozzle. Open symbols represent uncorrected data; filled symbols represent the same data corrected for closer agreement with Crocco's theory (Crocco, Monti, and Grey 1961).

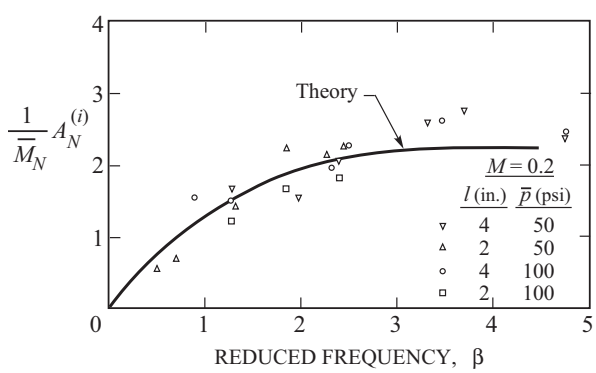

FIGURE 6.34. Results for the imaginary part of the admittance function for a nozzle (Crocco, Monti, and Grey 1961).

Dehority (1969).[37] Figures 6.35–6.37 show the experimental results and the predictions according to the theory described by Crocco and Sirignano (1967). The agreement with the theory is clearly quite good.[38] Results are shown for purely longitudinal modes, but Bell reported equally good agreement between theory and his data for the lowest longitudinal/tangential modes.[39]

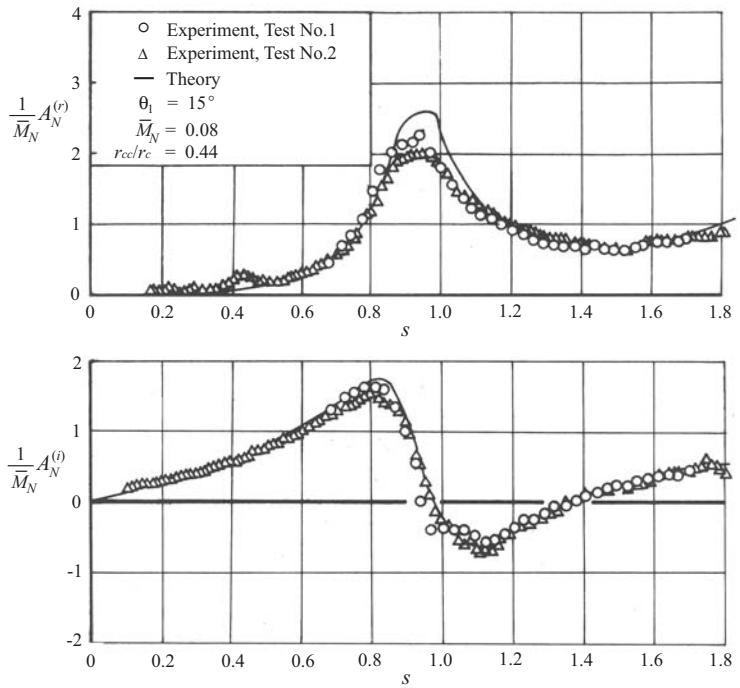

FIGURE 6.35. Comparison of the theoretical and experimental admittance results for nozzle 15-08-2.5, longitudinal modes (Bell 1972).

Some related data were taken in tests at the Naval Weapons Center (at that time the Naval Ordnance Test Station, usually called NOTS), reported by Buffum, Dehority, Slates and Price (1967); see also cited documents by the same authors. Those works are useful for a comparison of three methods of measuring the losses: the decay of pulses produced by small explosive charges; decay of steady oscillations; and properties of the resonance curve. The last seems to have been the best at that time although the results given are not useful for other applications.

[37]The general features of the method and its most effective realization, including best experimental procedure, have been described by Baum (1980).

[38]The independent variable is the dimensionless frequency, $s = \frac{\omega r_c}{\bar{a}}$, where r_c is the radius of the impedance tube; r_{cc} is the radius of the throat of the nozzle.

[39]Still not firmly established experimentally is the result predicted by the analyses (Culick 1961, Crocco and Sirignano 1967) that under some conditions, tangential modes are amplified by passage through a choked nozzle.

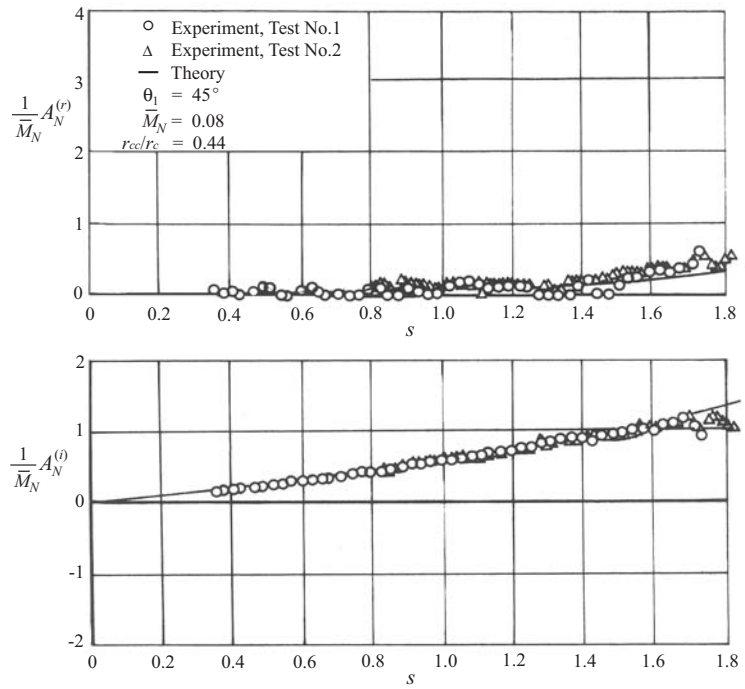

FIGURE 6.36. Comparison of the theoretical and experimental admittance results for nozzle 45-08-2.5, longitudinal modes (Bell 1972).

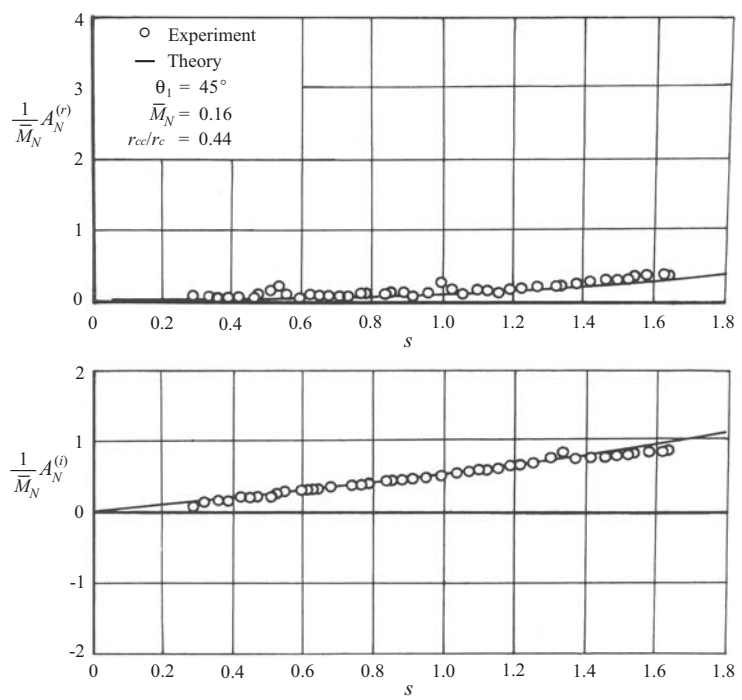

FIGURE 6.37. Comparison of the theoretical and experimental admittance results for nozzle 45-16-2.5, longitudinal modes (Bell 1972).

6.14.3. Attenuation of Acoustic Energy Due to Condensed Products of Combustion. Particularly in solid propellant rockets using metallized propellants, but in other systems as well, some of the combustion products are formed as liquid or solid particles. The viscous interactions between the particles and the gas may, under conditions, provide significant dissipation of energy. In the context of this chapter, that means that the corresponding contribution to α must be taken into account. It is often the case that the Reynolds number based on the particle diameter and the relative gas/particle velocity is outside the range for which Stokes' law—i.e. linear behavior—is a valid approximation. It is then necessary to use a more realistic nonlinear representation of the drag force. However, the linear approximation to attenuation tends in a sense to be conservative, so it is a good basis for an approximation. It is conservative in the sense that the curve of attenuation as a function frequency is broader, for a given particle size, for nonlinear behavior. Thus, over a frequency range centered at $\omega_n \tau = 1$, (Figure 6.38), the linear approximation is an over-estimate of the actual value one might expect would be the actual value.

In this section we discuss a contribution that is well-established as an important factor in the stability of solid propellant rockets, the energy loss and damping of acoustic waves caused by small-amplitude motions of small liquid droplets. By far the most important example is the attenuation of instabilities by liquid droplets of aluminum oxide (Al_2O_3) produced in the combustion of aluminized propellants.[40] The fact that (due to the high temperatures) the particles are liquid does not explicitly enter the following analysis. Internal motions of the droplet material are not accounted for.

The amount of damping provided by condensed material (liquid or solid) depends principally on three quantities: the mass fraction $C_m = \rho_\ell/\rho_g$ of condensed material; the size of the particles; and the frequency of the oscillations. Perhaps the most significant practical consequence of the analysis summarized here is the result that, for a given frequency, there is a particle size (diameter) for which the attenuation per particle is maximum. That conclusion has been confirmed in practice and is the basis for one important means of treating instabilities in solid propellant rockets.

Attenuation of sound by suspended particles in a gas was first treated theoretically more than 85 years ago. The modern theory began with the work of Epstein and Carhart (1953). A simplified analysis and experimental confirmation of the results have been provided by Temkin and Dobbins (1966)a,b. The calculations discussed here constitute an alternative method fitting naturally in the approximate analysis. Extensive work by Dehority and Kraeutle (1976) and by Kraeutle *et al.* (1976) has shown that this approach works in practice.

The linear gas/particle interactions arise from equations (A.34) and (A.49) written to first order in the fluctuations:

$$\begin{aligned} \delta\mathbf{F}'_l &= -\bar{\rho}_l \frac{\partial \delta \mathbf{u}'_l}{\partial t} \\ \delta Q'_l &= -\bar{\rho}_l C \frac{\partial \delta T'_l}{\partial t} \end{aligned} \tag{6.205a,b}$$

The parts of $\boldsymbol{\mathcal{F}}'$ and $\mathcal{P}'$ due to these terms only are found from the linearized forms of equations (A.68) and (A.70):

$$\begin{aligned} \boldsymbol{\mathcal{F}}'_l &= \delta\mathbf{F}'_l = -\bar{\rho}_l \frac{\partial \delta \mathbf{u}'_l}{\partial t} \\ \mathcal{P}' &= \frac{R}{C_V}\delta Q'_l = -\bar{\rho}_l R \frac{C}{C_V}\frac{\partial \delta T'_l}{\partial t} \end{aligned} \tag{6.206)a,b}$$

[40]The discussion in this section is a slightly revised form of Section IVD of the article by Culick and Yang (1992)

Thus, equations (6.93) and (6.94) give the contributions to the frequency shift and the growth constant:

$$(\omega - \omega_n)_l \equiv \delta\omega_l = \frac{-\bar{a}^2}{2\omega_n \bar{p} E_n^2} \left\{ \frac{k_n}{\bar{a}} \frac{R}{C_V} C\bar{\rho}_l \int \frac{1}{\eta_n} \left(\frac{\partial \delta T_l'}{\partial t} \right)^{(i)} \psi_n dV \right.$$
$$\left. -\bar{\rho}_l \int \frac{1}{\eta_n} \left(\frac{\partial \delta \mathbf{u}_l'}{\partial t} \right)^{(r)} \cdot \nabla \psi_n dV \right\} \tag{6.207}$$

$$\alpha_l = \frac{-\bar{a}^2}{2\omega_n \bar{p} E_n^2} \left\{ \frac{k_n}{\bar{a}} \frac{R}{C_V} C\bar{\rho}_l \int \frac{1}{\eta_n} \left(\frac{\partial \delta T_l'}{\partial t} \right)^{(r)} \psi_n dV \right.$$
$$\left. +\bar{\rho}_l \int \frac{1}{\eta_n} \left(\frac{\partial \delta \mathbf{u}_l'}{\partial t} \right)^{(i)} \cdot \nabla \psi_n dV \right\} \tag{6.208}$$

We have assumed, a good approximation in most practical cases, that the mass of particles per unit volume, ρ_l, and the mass fraction are nearly independent of position in the chamber and constant in time.

To find $\delta \mathbf{u}_l'$ and $\delta T_l'$, we treat the motions as locally one-dimensional and solve the problem of single particle motion, $\mathbf{u}_l'(t)$ and $T_l(t)$ being the velocity and temperature, respectively, of a particle located in a gas having oscillatory velocity $\mathbf{u}'(t)$ and $T'(t)$. Temperature gradients within a particle are ignored. See, for example, Rangel and Sirignano (1989) for a discussion of problems in which this assumption is not made. Moreover, for the following calculations we also ignore the effects of vaporization and combustion of the particles. In the absence of combustion, condensation or vaporization may cause increased attenuation of acoustic waves; the matter is addressed at the end of this section. We assume tentatively that the motions are such that the Reynolds number based on the relative speed, $|\mathbf{u}_l' - \mathbf{u}|$, is less than unity. The approximation of Stokes' flow then applies, and the equations of motion are

$$\frac{\mathrm{d}\mathbf{u}_l'}{\mathrm{d}t} = -\frac{18\mu}{\rho_s \sigma^2}(\mathbf{u}_l' - \mathbf{u})$$
$$\frac{\mathrm{d}T_l'}{\mathrm{d}t} = -\frac{12k}{\rho_s C \sigma^2}(T_l' - T)$$

where $\mathbf{u}_l'$ is the velocity in the same direction as $\mathbf{u}'$, and σ is the particle diameter. These equations can be rewritten as

$$\frac{\mathrm{d}\mathbf{u}_l'}{\mathrm{d}t} + \frac{1}{\tau_d}\delta\mathbf{u}_l' = -\frac{\mathrm{d}\mathbf{u}'}{\mathrm{d}t}$$
$$\frac{\mathrm{d}T_l'}{\mathrm{d}t} + \frac{1}{\tau_t}\delta T_l' = -\frac{\mathrm{d}T'}{\mathrm{d}t} \tag{6.208)a,b}$$

The relaxation times are

$$\tau_d = -\frac{\rho_s \sigma^2}{18\mu}$$
$$\tau_t = \left(\frac{3}{2} \frac{C\mu}{k} \right) \tau_d \tag{6.209)a,b}$$

With $\mathbf{u}' = (\dot{\eta}_n / \gamma k_n^2) \nabla \psi_n$ and $T'/\bar{T} = (\gamma - 1)\eta_n \psi_n / \gamma$, the steady-state solutions ($t \to \infty$) to equations (6.208)a,b are

$$\delta\mathbf{u}_l' = X_1(\eta_n - \tau_d \dot{\eta}_n) \frac{1}{\gamma k_n^2} \nabla \psi_n$$
$$\delta T_l' = -X_2 \left(\tau_t \eta_n + \frac{\dot{\eta}_n}{\omega_n^2} \right) \frac{\gamma - 1}{\gamma} \bar{T} \psi_n \tag{6.210)a,b}$$

Dependence on frequency and particle properties is contained chiefly in the two functions X_1 and X_2:

$$X_1 = \frac{\omega_n \Omega_d}{1+\omega_d^2}$$
$$X_2 = \frac{\omega_n \Omega_t}{1+\omega_t^2} \qquad (6.211)\text{a,b}$$

where $\Omega_d = \omega_n \tau_d$ and $\Omega_t = \omega_n \tau_t$. For use in equations (6.207) and (6.208), the time derivatives of equations (6.210)a,b are required. This produces terms containing $\dot{\eta}_n$ and $\ddot{\eta}_n$. To be consistent, we replace $\ddot{\eta}_n$ by $-\omega_n^2 \eta_n$ and, after setting $\eta_n = \hat{\eta}_n e^{i\omega_n t}$, we eventually find the results

$$\alpha_l = -\frac{1}{2}\frac{C_m}{1+C_m}\left[X_1 \frac{1}{E_n^2}\oiint \left(\frac{\nabla\psi_n}{k_n}\right)^2 dV + (\gamma-1)\frac{C}{C_p}X_2\right]$$
$$\delta\omega_l = \frac{1}{2}\frac{C_m}{1+C_m}\left[\Omega_d X_1 \frac{1}{E_n^2}\oiint \left(\frac{\nabla\psi_n}{k_n}\right)^2 dV + (\gamma-1)\frac{C}{C_p}\Omega_t X_2\right] \qquad (6.212)\text{a,b}$$

Equations (6.212)a,b, normalized to the angular frequency ω_n, are plotted in Figures 6.38 and 6.39 for longitudinal oscillations. The independent variable is $\omega_n \tau_d$, 2π times the ratio of the relaxation time for relative motion [see equation (6.137)a] to the period of the motion. According to equation (6.137)a, the dominant influence on the relaxation time is the particle diameter $\tau_d \sim \sigma^2$. For typical solid propellants and operating conditions, the diameters of particles may range from fractions of a micron to tens of microns. The results shown in the figures have been computed for longitudinal oscillations in a chamber of constant cross section, so $\psi_n = \cos k_n z = \cos(\pi n z/L)$. In this case, equations (6.212)a,b reduce to

$$\alpha_l = -\frac{1}{2}\frac{C_m}{1+C_m}\left[X_1 + (\gamma-1)\frac{C}{C_p}X_2\right]$$
$$\delta\omega_l = \frac{1}{2}\frac{C_m}{1+C_m}\left[\Omega_d X_1 + (\gamma-1)\frac{C}{C_p}\Omega_t X_2\right] \qquad (6.213)\text{a,b}$$

The most striking feature of the curves in Figure 6.38 is that, for a fixed value of mass loading C_m, the dimensionless attenuation constant has a maximum value. That is, according to the interpretation expressed by equation (6.96), the number of cycles of oscillation required to reduce the amplitude by $1/e$ is minimum. Thus, for a fixed frequency, there is a best value of relaxation time, that is, particle size, for obtaining maximum attenuation. This result has served as a successful practical guide to treating combustion instabilities in motors. Addition of inert particles having appropriate sizes, or altering the propellants in other ways to affect the sizes of particular produced, has reduced the amplitudes of oscillations in actual examples (e.g. Derr *et al.* 1979), discussed in Section 8.4.

If, as usually is the case, there is a distribution of particle sizes, (6.212)a,b become sums over the contributions from different sizes:

$$\alpha_\ell = -\frac{1}{2}\frac{C_m}{1+C_m}\sum_{s=1}^{m} K_s\left[x_{1s} + (\gamma-1)\frac{C}{C_p}x_{2s}\right]$$
$$\delta\omega_\ell = \frac{1}{2}\frac{C_m}{1+C_m}\sum_{s=1}^{m} K_s\left[\Omega_{ds}x_{1s} + (\gamma-1)\frac{C}{C_p}\Omega_{ts}x_{2s}\right] \qquad (6.214)\text{a,b}$$

The result (6.145)a was used by Dehority and Kraeutle (1976) to compute the damping for the experimentally determined distribution shown in Figure 6.40. These data were obtained as measured values for the residue produced in a T-burner firing. The process is extremely tedious and time-consuming. Details are given in the reference cited and other works. Table 6.5 is a list of the measured mass fractions used in

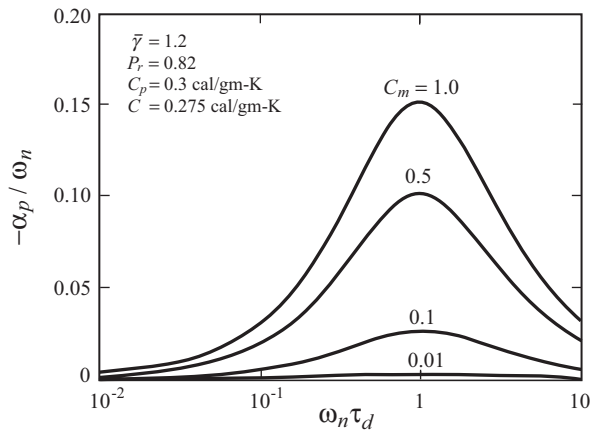

FIGURE 6.38. Attenuation of acoustic waves caused by small particles suspended in a gas (Culick and Yang 1992).

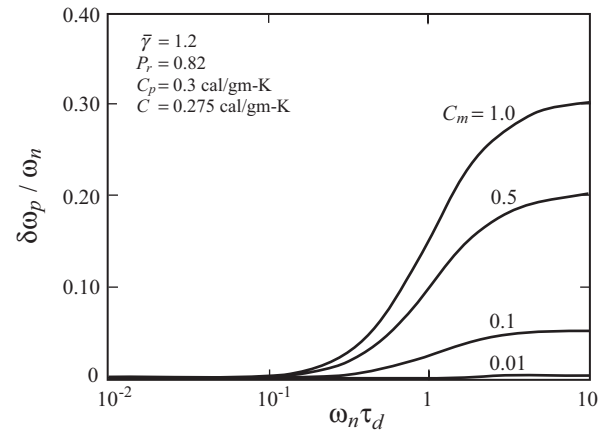

FIGURE 6.39. Frequency shift of acoustic oscillation caused by small particles suspended in a gas (Culick and Yang 1992).

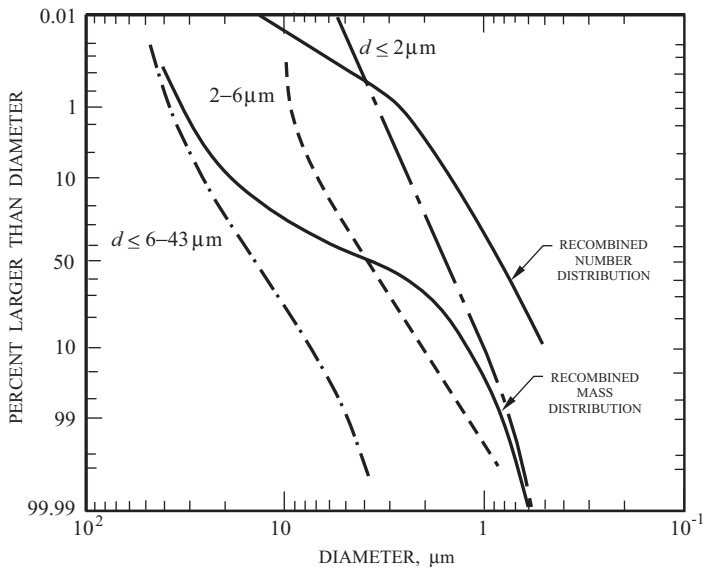

FIGURE 6.40. Mass distribution of subfractions of the combustion residue of NWC Mix No. 10. The total mass distribution was obtained by recombination of the distributions of subfractions. The total number distribution was calculated from the total mass distribution. (Dehority and Kraeutle 1976).

the preparation of Figure 6.40. The main parameter values used in the calculations of the particle damping are given in Table 6.6.

To check the validity of the theory over a realistic range of frequency, data were used from tests with T-burners of different lengths. The frequencies of the oscillations were about 290Hz, 640Hz and 1920Hz. Table 6.7 is a list of the attenuation coefficients computed for intervals of particle size varying from 0.4 μm to 3 μm.

TABLE 6.5. Mass Fractions of NWC Mix No. 10 Residue for Particles Smaller than 43 μm.

Diameter, μm	Residue in % of weight	Center of interval, μm	Interval, μm	% residue in interval	Mass fraction in interval
0.5	0.0				
0.9	1.9	0.7	0.4	1.9	0.016891
1.3	11.0	1.1	0.4	9.1	0.080899
1.7	24.0	1.5	0.4	13.0	0.115570
2.1	34.5	1.9	0.4	10.0	0.088900
2.5	40.3	2.3	0.4	6.0	0.053340
3.5	49.0	3.0	1.0	8.7	0.077343
4.5	54.4	4.0	1.0	5.4	0.048006
5.5	58.5	5.0	1.0	4.1	0.036449
6.5	61.6	6.0	1.0	3.1	0.027559
7.5	65.0	7.0	1.0	3.4	0.030226
8.5	68.0	8.0	1.0	3.0	0.026670
9.5	70.5	9.0	1.0	2.5	0.022225
10.5	73.0	10.0	1.0	2.5	0.022225
11.5	75.3	11.0	1.0	2.3	0.020447
12.5	77.5	12.0	1.0	2.2	0.019558
13.5	79.7	13.0	1.0	2.2	0.019558
14.5	81.8	14.0	1.0	2.1	0.018669
15.5	83.7	15.0	1.0	1.9	0.016891
16.5	85.4	16.0	1.0	1.7	0.015113
17.5	86.8	17.0	1.0	1.4	0.012446
18.5	88.2	18.0	1.0	1.4	0.012446
19.5	89.5	19.0	1.0	1.3	0.011557
20.5	90.7	20.0	1.0	1.2	0.010668
23.5	93.7	22.0	3.0	3.0	0.026670
26.5	96.0	25.0	3.0	2.3	0.020447
29.5	97.5	28.0	3.0	1.5	0.013335
32.5	98.6	31.0	3.0	1.1	0.009779
35.5	99.3	34.0	3.0	0.7	0.006223
38.5	99.7	37.0	3.0	0.4	0.003556
41.5	99.9	40.0	3.0	0.2	0.001778

TABLE 6.6. Parameters Used in the Particle Damping Calculations.

C	0.3396 cal/g°C
C_m	0.48 (obtained from propellant composition)
Pr	0.75
γ	1.2
ρ_l	3.0 g/cc
μ	0.00065 poise

The final results of this work are given in Table 6.8, the measured and calculated values of the attenuation coefficient for the three frequencies. The close agreement is actually vary surprising and is probably fortuitous. Nevertheless, it is really a testimony to two factors: the careful experimental work by Dr. Kraeutle[41] and the apparent accuracy of the approximate theory.

Figure 6.38 shows a strong dependence of the frequency shift on both particle mass loading and on $\omega_n \tau_d$ or, as reasoned earlier, on particle size. The behavior is better understood by recognizing that, in a fixed geometry (here a tube of length L), the wavelength is fixed so that, from the fundamental relation $a = f\lambda = \omega\lambda/2\pi$, a frequency shift is equivalent to a change in the speed of sound:

$$\frac{\delta\omega}{\omega} = \frac{\delta a}{a} \tag{6.215}$$

Note especially in Figure 6.39 that, as $\omega_n \tau_d$ approaches unity, when the attenuation constant is maximum, the change in the speed of sound is not a small perturbation if the particle mass loading is greater than 0.5. The mass loading as a function of aluminum content μ in the solid propellant is given by the formula

$$C_m = \frac{1.89\mu}{1 - 1.89\mu} \tag{6.216}$$

[41] Dr. Karl Kraeutle worked at the Naval Air Warfare Center for 40 years and produced many results of fundamental and practical value. He was widely known and highly respected for his dogged and precise experimental work on problems associated with solid propellants and hazardous materials. He suffered a premature death due to cancer in 2003.

TABLE 6.7. Damping Coefficients Measured, NWC Mix No. 10, for Particle Sizes Smaller than μm.

Center of interval, μm	Interval, μm	Damping ($\sec^{-1}$) for interval 290Hz	640Hz	1,920Hz
0.7	0.4	−0.01	−0.06	−0.56
1.1	0.4	−0.15	−0.73	−6.59
1.5	0.4	−0.40	−1.94	−17.44
1.9	0.4	−0.49	−2.39	−21.37
2.3	0.4	−0.43	−2.09	−18.53
3.0	1.0	−1.07	−5.14	−43.58
4.0	1.0	−1.17	−5.57	−41.68
5.0	1.0	−1.38	−6.37	−38.61
6.0	1.0	−1.48	−6.51	−30.06
7.0	1.0	−2.16	−8.82	−30.55
8.0	1.0	−2.41	−8.90	−23.64
9.0	1.0	−2.42	−7.95	−16.87
10.0	1.0	−2.80	−8.10	−14.36
11.0	1.0	−2.88	−7.29	−11.26
12.0	1.0	−2.99	−6.63	−9.23
13.0	1.0	−3.14	−6.19	−7.97
14.0	1.0	−3.07	−5.44	−6.62
15.0	1.0	−2.79	−4.51	−5.26
16.0	1.0	−2.46	−3.68	−4.15
17.0	1.0	−1.97	−2.76	−3.04
18.0	1.0	−1.90	−2.51	−2.72
19.0	1.0	−1.68	−2.13	−2.27
20.0	1.0	−1.48	−1.80	−1.89
22.0	3.0	−3.28	−3.78	−3.92
25.0	3.0	−2.09	−2.28	−2.33
28.0	3.0	−1.13	−1.20	−1.21
31.0	3.0	−0.69	−0.72	−0.73
34.0	3.0	−0.35	−0.35	−0.36
37.0	3.0	−0.17	−0.17	−0.17
40.0	3.0	−0.08	−0.08	−0.08

TABLE 6.8. Measured and Calculated Damping Coefficients for NWC Mix and 10.

NWC mix No.	Frequency, Hz	Measured damping ($\sec^{-1}$)	Calculated damping ($\sec^{-1}$)
10	290.7	−46.1	−48.52
10	640.6	−115.0	−116.09
10	1927.3	−364.2	−367.05

If the propellant contains 15% aluminum ($\mu = 0.15$), $C_m = 0.4$, substantial shifts in the speed of sound occur. That is why this effect of particles was included in the formulation of the conservation equations derived in Annex A and discussed further in Chapter 3. The speed of sound given by equation $\bar{a} = (\gamma RT)^{1/2} = \left[\frac{\gamma}{1+C_m}\left(\frac{p}{\rho_g}\right)\right]^{1/2}$, has the value implied by Figure 6.39 for $\omega_n\tau_d \to \infty$.

The dependence of the frequency shift on $\omega_n\tau_d$ may be interpreted as follows. According to equation (6.148)a, the relaxation time is proportional to the square of the particle diameter, and so $\omega_n\tau_d \sim \omega_n\sigma^2$. For low frequencies or small particles, $\omega_n\tau_d \to 0$; according to Figure 6.39, the frequency shift and change in the speed of sound, equation (6.215), vanish. In either case—slow unsteady motions with finite particle sizes or vanishingly small particles exposed to unsteady motions—the viscous losses in the flow about the particles become negligible. Hence, there can be no frequency shift, a result to be expected by analogy with the behavior of the resonant frequency of a classical mass/spring/dashpot system.

On the other hand, if the frequency is high enough, even for small particles, or if the particles are large, the viscous stresses cause substantial motions of the particles. When $\omega_n\tau_d$ is sufficiently small, the particles follow the gas motion very closely. The gas/particle mixture then behaves as a single fluid having density equal to the sum of the mass of gas and condensed material per unit volume, $\rho = \rho_g + \rho_\ell = \rho_g(1 + C_m)$,

but the compressibility is provided by the gas. Hence, the speed of sound assumes the equilibrium value, $\left[\frac{\gamma}{1+C_m}\left(\frac{p}{\rho_g}\right)\right]^{1/2}$ with mass-averaged values for the thermodynamic properties.

The preceding results rest crucially on the assumptions of Stokes' flow and rapid decay of transient motions so that equations (6.208)a,b apply. It is an easy calculation to show that the Reynolds number based on the relative velocity exceeds unity for realistic particle sizes ($1\mu - 10\mu$) even for quite modest amplitudes of oscillation. Hence, it appears that a nonlinear analysis of gas/particle interactions is required to cover conditions arising in practice. However, in all current applications, including the SSP program (Nickerson *et al.* 1983) the linear results are used. Dehority and Kraeutle (1976) based their experimental confirmations on the assumption of linear behavior, and it is likely that nonlinear effects cannot be detected within the experimental uncertainties.

Calculations of the attenuation constant including nonlinear effects have shown that the linear results tend to be conservative. That is, for a fixed frequency, increasing the amplitude of oscillation broadens the curves in Figure 6.38 and moves the peak to slightly larger particle size; the maximum value of the attenuation is practically constant with amplitude. Levine and Culick (1972, 1974) have produced some interesting results for the damping of nonlinear waves but with linear gas/particle interactions. The problem of nonlinear attenuation probably merits careful analysis, but the prospects for experimental verification are not especially promising at this time. Probably the best relevant reference for calculations is Korman and Micheli (1971).

6.15. Distributed Combustion

It may seem somewhat strange to identify 'distributed combustion' as a distinguished topic. All of the systems we have been discussing involve combustion distributed in space. In treatment of liquid rockets one must in fact take care to specify when the burning processes are idealized to be so rapid that they occur in thin sheets, in the limit having no volume. The early works at Princeton described in Sections 6.1 and 7.1 are well-known examples. Distributed combustion has therefore become a term and a subject referring virtually always to solid propellant rockets. The discussion in this chapter has illustrated some advantages of the realistic approximation that combustion is then confined to the boundary. This section is a brief essay on some problems arising with the presence of combustion distributed in space away from the surface.

In the context of an analysis based on spatial averaging, however, there is hardly any difference in the computational difficulties presented by processes concentrated or distributed in space. The important distinctions between combustion in a thin zone and distributed combustion are associated mainly with the modeling required: Attention is forcibly directed to the aspects of the subject where it will produce the greatest benefits.

Combustion processes in virtually all gas- and liquid-fueled systems are spread out in space and are logically referred to as distributed, except when approximated as isolated flame sheets. It is a matter of convention that the term 'distributed combustion' has come to refer to combustion within the volume of a solid rocket, removed from the boundary where most of the conversion solid $\longrightarrow$ products occurs. Moreover, at the usual chamber pressures, if distributed combustion occurs, it probably is primarily the oxidation of aluminum to aluminum oxide. That is the subject of this section.

The principal motivation to study distributed (sometimes referred to as 'residual') combustion has been the burning of aluminum. It's a subject which has received much attention, for several reasons, in connection with the formation of 'slag', relatively large collections or coalescences, of aluminum oxide (liquid Al_2O_3). So far as combustion instabilities are concerned, the central questions are directed to the dynamics. Particularly, do the dominant processes depend on frequency, or are they essentially quasi-static?

Although the idea that combustion of aluminum continues far from the primary burning surface of a metallized solid propellant, it had been considered mainly a matter of steady burning until the late 1970s. For example, in 1977 Geisler (1977) chaired a workshop on aluminum combustion in which the topic of residual combustion, reflected as distributed combustion in a chamber, received considerable attention. General characteristics of aluminum combustion, including behavior far from a propellant burning surface, was at that time a topic of fairly active research (e.g., see Derr *et al.* 1974, Micheli and Schmidt 1977, and a later comprehensive report by Price *et al.* 1982) which is especially interesting for its photographic evidence.

Beckstead (1987) first proposed that unsteady combustion of aluminum might not be negligible in the interpretation of T-burner data. His reasoning was based on unusually large values of the velocity-coupled response function inferred for metallized propellants, as much as ten times the values normally measured for the pressure-coupled response. The velocity-coupled T-burner has test grains on the lateral walls. Hence when a longitudinal mode is unstable, as suggested in Figure 6.41, the velocity fluctuation acts to 'scour' aluminum particles from the test propellant. Then the aluminum burns as it moves with the flow away from burning surface. Any fluctuations in the burning rate of the aluminum may contribute to the instability of waves in the chamber, but should not be attributed to the response of surface combustion.

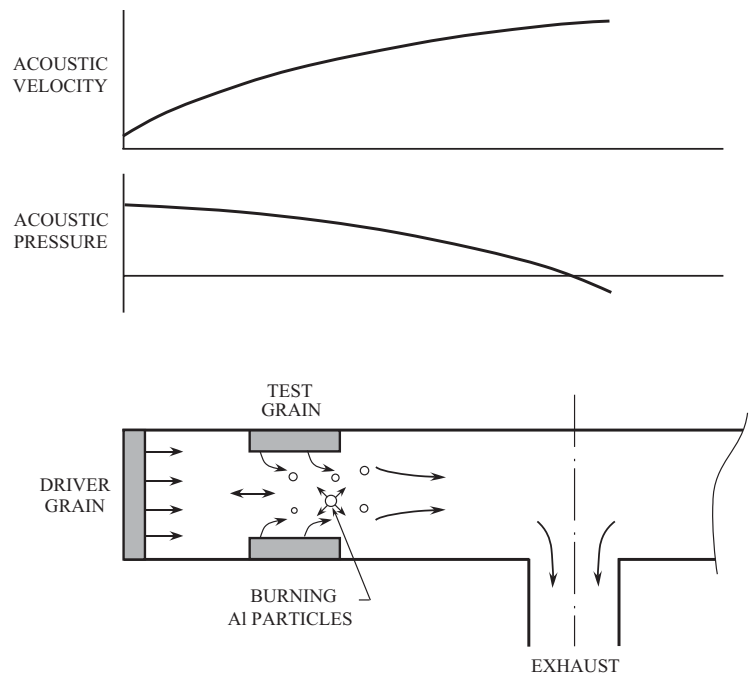

FIGURE 6.41. A possible explanation of increased growth rate due to distributed combustion of aluminum in a T-burner.

Consequently, the distributed combustion of aluminum could conceivably give falsely increased values of the surface response if the traditional interpretation is used. This idea seems not to have been pursued further. There have been other, isolated and brief, speculations concerning the possible importance of distributed combustion of aluminum in laboratory test devices but no incontrovertible evidence is available and the matter remains open.

The term involving combustion in the volume of a chamber is explicit in the general equations developed in Annex A and Chapter 3. Formally, then, it is quite easy in a linear analysis to treat distributed combustion. Beckstead and Brooks (1990) noted that the Standard Stability Program (SSP, Nickerson *et al.* 1984) contains the term, therefore providing a means of investigating the possible effects of distributed combustion on

stability. They had only an elementary model of the combustion processes so the results are probably too over-simplified to be of great value. However, the strategy is correct and merits further development.

Professor Beckstead and his students reported some interesting work based on use of a Rijke tube to investigate combustion of aluminum under unsteady conditions. Measurements of distributed combustion were carried out by Braithwaite *et al.* (1984) and Beckstead *et al.* (1985). Results of experimental work with the Rijke tube were summarized by Finlinson *et al.* (1987) and Raun and Beckstead (1993); a useful general review of Rijke tubes was provided by Raun *et al.* (1993). The main final results of the program are summarized in the paper by Brooks and Beckstead (1995) in which they give a good list of references. Much of the paper is devoted to some aspects of the steady combustion of aluminum and is not of immediate interest here. So far as the unsteady behavior is concerned, perhaps the main conclusion in the present context is that the effects of aluminum combustion on acoustics are indirect, in the words of the authors, "... a significant part of the acoustic growth with the addition of aluminum is due strictly to the change in the gas temperature profile." The effects observed are therefore, apparently, specific to the device. It does not seem possible to draw any conclusions or guidelines generally helpful to understanding the role of aluminum combustion in problems of unsteady combustion in solid propellant rockets.

In contrast to the situation in the U.S., there was a significant effort in France devoted to distributed combustion of aluminum from the mid-1990s to 2002. As true of much of the French work on unsteady behavior in solid propellant rockets in the 1990s and later, motivation was related to significant difficulties associated with an instability of the fundamental longitudinal mode in the Ariane 5 booster motor (P230). The program devoted to two-phase flow in that motor apparently began with the doctoral thesis by Dupays (1996), who remained a central figure in the work until it ended in ∼2002. Work on distributed combustion was a logical development in the broader program formed to treat problems in the Ariane motor P230.

Early concern with oscillations in the Ariane 5 led to the integrated effort with the broader program ASSM, Aerodynamics of Segmented Solid Motors. The Pressure Oscillations Program (POP) has been devoted to obtaining numerical and experimental results for subscale tests ($1/15^{th}$ scale) of the P230. Much effort has been appended on validating numerical tools for predicting the frequencies and amplitudes of oscillations. Fabignon *et al.* (2003) gave a very informative overview of the principal results for oscillations studied in ASSM and POP. A general view of the three-segment motor in question is shown in Figure 6.42.

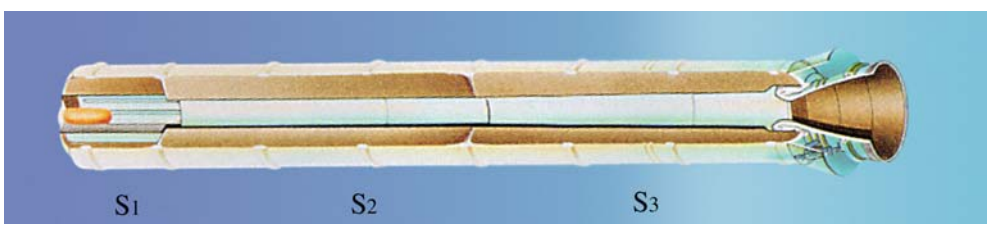

FIGURE 6.42. General view of the Ariane 5 strap-on booster motor P230 (Fabignon *et al.* 2003).

Evidence of a serious problem is reproduced in Figure 6.43, based on measurements taken during static qualification tests of the full-scale motor performed sometime in 1993–1995. The maximum amplitude of the oscillatory pressure is about 0.5% of the mean pressure but the thrust oscillation has maximum amplitude 5% which causes practical problems due to oscillatory accelerations. That is the main reason that the programs ASSM and POP have existed.[42] Recall that the propellant in the Ariane 5 contains 18% aluminum. Vortex shedding leads to interactions between the vortices and either the internal structural surfaces of the motor, or the mean flow field. There are two potentially troublesome consequences: Acoustic waves may be excited and sustained; and the accompanying fluctuations of thrust are liable to be unacceptably large.

[42]The greater thrust oscillations, for roughly the same amplitude of pressure oscillations, in the Ariane 5 than in the Shuttle, are due to geometrical and phase relations (Vuillot and Casalis 2002).

Already by the early 1990s, subscale firings of motors related to the P230 configuration had caused concern about the prospects for oscillations in the full-scale motor. The possible amplitudes were of course unknown, but more worrisome for the program, as were the causes. For the range of low frequencies characterizing the first few longitudinal modes, weak pressure and velocity-coupled driving (nearly quasi-steady), combined with the large damping associated with the nozzle and convective flow acoustic losses, to give stable modes according to widely accepted procedures based on the ideas developed in this chapter. However, known experience with the Shuttle SRMs and the Titan had shown that vortex shedding in segmented motors could drive the fundamental mode to relatively low amplitudes. (See discussion in Sections 1.3.3, 2.2.7, and 6.12.1. The process of vortex shedding is not included in the systematic treatment of unsteady motions based on the ideas and equations developed in the framework suggested by classical acoustics.

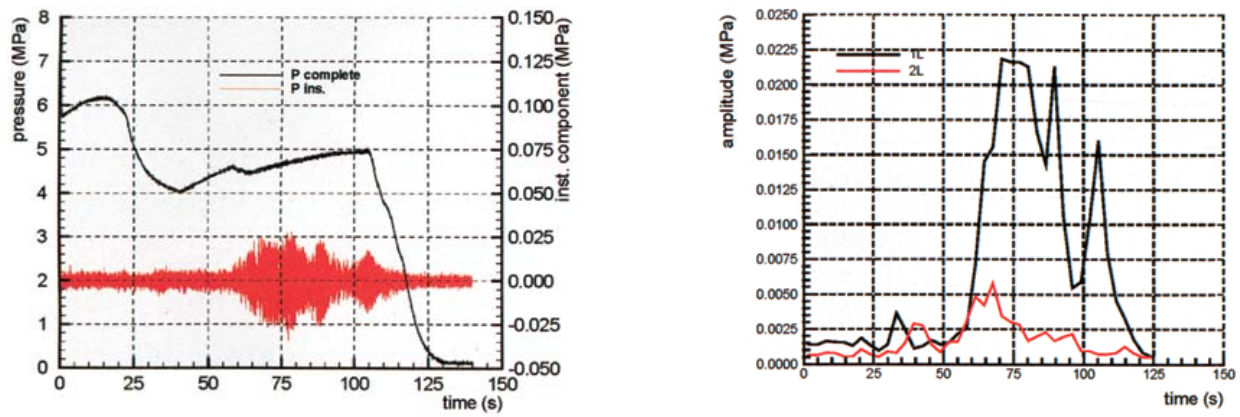

FIGURE 6.43. Results for the unsteady pressure measured in a static test firing of the Ariane 5, P230 motor (Fabignon *et al.* 2003).

We have already discussed the developments beginning with the suggestion by Flandro and Jacobs (1973) followed by the sequence of analytical and experimental works establishing the importance of the process in particular cases (Dunlap and Brown 1981, Dotson *et al.* 1997) and in general (Flandro 1995, Vuillot 1995). Vortex shedding from edges exposed as propellant burned away from inhibitor material installed between segments in the Shuttle SRM was confirmed in the 1980s as the source of low-level oscillations (Blomshield 2001, Blomshield and Mathis 1993). Reproducibly present during a predictable interval of every firing, the oscillations have never become a practical problem.

It was therefore logical to investigate vortex shedding as a possible, if not likely, cause of oscillations in the Ariane 5 booster motor. The first report of this cause was the paper by Scippa, Pascal and Zanier (1994). For the next eight years, researchers at ONERA especially, but at several other organizations in France as well, collaborated in a broadly based program directed to solving the problem of vortex shedding. The immediate motivation of course came from the Ariane 5; the research has, however, been sufficiently general to be of value much more generally. Progress in understanding the phenomenon of vortex shedding, particularly the discovery of parietal vortex shedding, has been discussed in Section 6.12.1.

As noted above, the work was coordinated in the ASSM program which began with definition of two phases (Fabignon *et al.* 2003):

(1) demonstration of numerical tools to predict instabilities excited and sustained by vortex shedding;
(2) development of physical models including the propellant combustion response with two-phase flow accounted for.

The second item bears directly on the subject of distributed combustion. A report of results obtained in the first half of the program was published by Dupays *et al.* (2000). Various aspects of two-phase flows, with emphasis on slag accumulation and, relevant here, interactions associated with acoustic oscillations as well as vortex shedding. It was in this work that, based on earlier results obtained by Dupays and Vuillot (1998), the suggestion was made that distributed combustion is potentially an important contribution to instabilities.

Subsequent calculations by Lupoglazoff *et al.* (2000) showed that with distributed combustion accounted for, oscillations in the Ariane 5 boosters seem to be amplified by combustion of small aluminum drops and attenuated by combustion of large drops ($> 125\mu$m). The situation is in fact more complicated than this simple conclusion suggests. Simulations were carried out for the full-scale P230 motor with a rough approximation to the particle size distribution and combustion. An important factor is interaction between parietal vortex shedding and vortices shed from the vicinity of the joint between segments. Figure 6.44 is a sketch of the grain geometry used in the simulations. It is an interesting example of how far simulations have progressed in treating realistic configurations. Compare Figure 6.44 with the actual shape shown in Figure 6.42; there is little difference. The paper by Lupoglazoff *et al.* is really a progress report, but their conclusion that distributed combustion was essential for successful simulation of unsteady flow in the Ariane 5 must be taken into account in formulating simulations for other large boosters.

FIGURE 6.44. Shape of the grain used in simulations of two-phase unsteady flow in the Ariane 5, P230 motor (Lupoglazoff *et al.* 2000).